COMPUTATIONAL MODELING OF INFLAMATORY MEDIATORS IN ACUTE ILLNESS: FROM NETWORKS TO MECHANISMS

by

Nabil Azhar

BS, University of California, Berkeley, 2007

Submitted to the Graduate Faculty of

School of Medicine in partial fulfillment

of the requirements for the degree of

Doctor of Philosophy

University of Pittsburgh

2014

UNIVERSITY OF PITTSBURGH

SCHOOL OF MEDICINE

This dissertation was presented

by

Nabil Azhar

It was defended on

July 21, 2014

and approved by

James Faeder, PhD, Associate Professor, University of Pittsburgh Department of Computational and Systems Biology

Greg Constantine, PhD, Professor, University of Pittsburgh Department of Mathematics

Seyoung Kim, PhD, Assistant Professor, Carnegie Mellon University Department of Computational Biology

Ioannis Androulakis, PhD, Professor, Rutgers University Department of Biomedical Engineering

Dissertation Advisor: Yoram Vodovotz, PhD, Professor, University of Pittsburgh Department of Surgery

COMPUTATIONAL MODELING OF INFLAMMATORY MEDIATORS IN ACUTE ILLNESS: FROM NETWORKS TO MECHANISMS

Nabil Azhar,

University of Pittsburgh, 2014

The acute inflammatory response is a complex defense mechanism that has evolved to respond rapidly to injury, infection, and other disruptions in homeostasis. The complex role of inflammation in health and disease has made it difficult to understand comprehensively. With the advent of high throughput technologies and the growth of systems biology, there has been an unprecedented amount of data and –omics analysis aimed at uncovering this complexity. However, there still remains a shortage of translational insights for acute inflammatory diseases from these studies. In this dissertation, we employ a comprehensive systems approach in order to study the coordination of inflammation and identify key control mechanisms, and how these map onto clinical outcomes. This process begins with collection of high-dimensional time course data of inflammatory mediators, followed by data-driven modeling and network inference that finally informs mechanistic computational models for prediction and analysis. In patients with pediatric acute liver failure (PALF), we inferred inflammatory networks and identified key differences between patients that were survivors versus non-survivors when other analyses proved inconclusive. We showed that inflammatory networks can be used both as biomarkers and to generate mechanistic hypotheses for this poorly understood disease. In experimental models of trauma as well as in human trauma patients, we identify a conserved central network motif of cross-regulating chemokines. We develop a logical model based on this hypothesized network, which is able to capture both inflammatory trajectory and clinical outcome differences among

patients with differing injury severity. These studies suggest that the hypothesized cross-regulatory interactions among chemokines MIG, IP-10 and MCP-1 represents an important point of control regulating the progression of acute inflammation. We propose that further analysis and validation of this hypothesis will require targeted perturbation studies in cells and animals with iterative rounds of mechanistic model refinement. We explore an example of such a study focused on the anti-inflammatory effects of NAD^+, wherein we characterize a signaling pathway that gives rise to a complex dose and time dependent induction of TGF-β1.

TABLE OF CONTENTS

LIST OF TABLES

LIST OF FIGURES

1.0 INTRODUCTION

1.1 INFLAMMATION BACKGROUND

Inflammation is an essential process in maintaining health and responding to disease. Acute inflammation is driven largely by the innate immune system, which not only serves as the first line of defense against invading pathogens but also functions to resolve tissue damage and restore homeostasis upon a variety of inflammatory conditions including sepsis, trauma, wound-healing, and many more. Dysregulated systemic inflammation also plays a significant role in the pathophysiology of other diseases that are not primarily attributed to innate immunity, such as cancer and diabetes. Although its diseases are varied, the core architecture of the inflammatory response to biological stress is highly conserved (1). An infection or tissue injury/damage triggers an initially local cascade of events mediated by an array of cells (e.g. macrophages, neutrophils, dendritic cells, lymphocytes, etc.) and molecules (cytokines, free radicals, and damage-associated molecular pattern molecules [DAMP's]) that locate invading pathogens or stressed/damaged tissue, alert and recruit other cells and molecules, eliminate the offending agents and finally restore

the body to equilibrium (2). When dysregulated or over-exuberant, inflammation can be discerned in the systemic circulation in the form of altered levels of inflammatory cells and molecular mediators. Thus, querying the serum levels of these mediators after an inflammatory stimulus can provide information regarding pathophysiology.

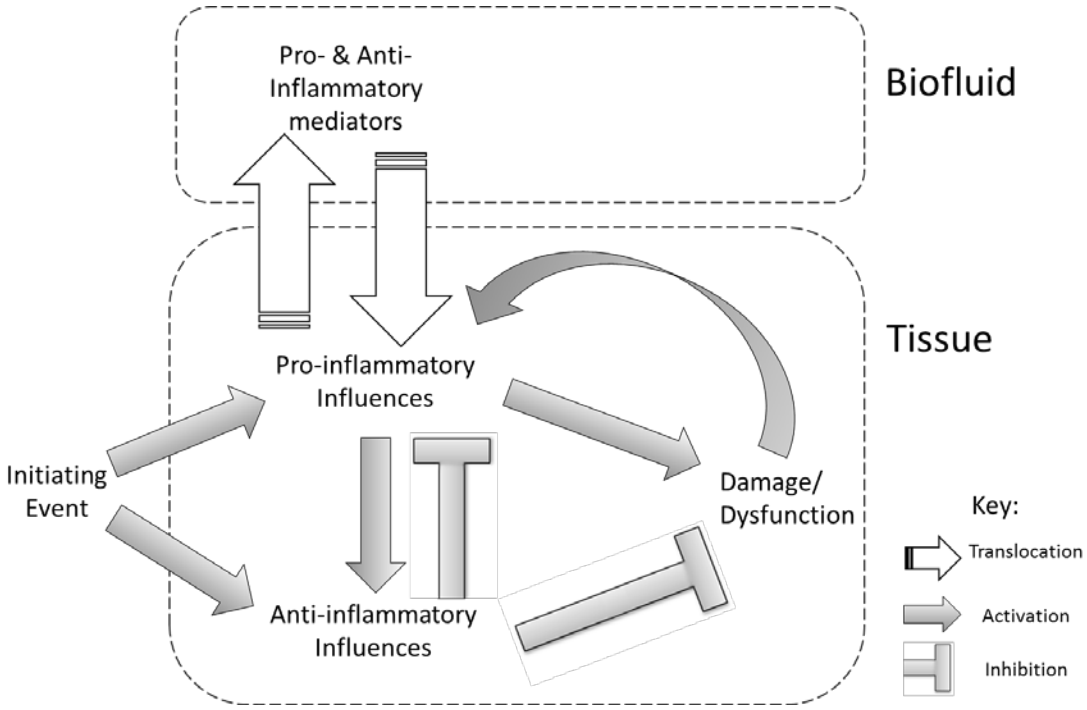

Figure 1.1 Complex structure of the innate immune response to biological stress.
Following an initiating event (e.g. trauma, hemorrhage, infection), both pro- and anti-inflammatory influences (e.g. chemokines, cytokines, lipid products, and free radicals) are elaborated, leading to tissue damage or dysfunction. These stressed tissues elaborate DAMPs, which further propagate innate immune mechanisms. When the pro-inflammatory mediators exceed defined thresholds, both pro- and anti-inflammatory mediators spill over into the blood and may cause inflammation to feedback and spread systemically to other organs as well.

In sepsis and trauma, this response is concomitant with physiologic manifestations including changes in heart rate and body temperature, responses that act in a concerted fashion in order to help optimize host defense while minimizing tissue damage. Indeed, although a well regulated inflammatory response is essential for proper healing and host defense, an overly

exuberant response can become self-perpetuating and lead to organ dysfunction and death (3, 4). These vastly different outcomes can be explained by the high-level architecture of the immune response, which includes a positive feedback loop from inflammation →damage/dysfunction → inflammation that can drive pathophysiology in inflammatory diseases (Fig 1.1).

The detrimental effects of self-sustaining inflammation are likely responsible for the general perception of inflammation as an inherently harmful process (5, 6). However, in addition to the aforementioned beneficial roles of inflammation in the resolution of tissue injury, recent studies suggest that morbidity and mortality are worse in animals with low levels of early pro-inflammatory signals (7). The emerging view of inflammation is indeed more nuanced, casting inflammation as a highly coordinated communication network that allows the body to sense and respond to challenges and subsequently restore homeostasis(8, 9).

The current paradigm for acute inflammation, based in large part on studies in response to trauma, hemorrhage, or infection, involves a dynamic cascade of cellular and molecular events. Innate immune cells such as mast cells, neutrophils, and macrophages are activated directly by bacterial endotoxin or indirectly by various stimuli elicited systemically upon trauma and hemorrhage (10-13), including the release of cytokines, chemokines, and DAMPs (Fig. 1)(14-16). These stimuli enter the systemic circulation and activate circulating monocytes and neutrophils (17), which subsequently migrate to compromised tissue by following along a chemoattractant gradient induced at the site of injury/infection (18). Activated macrophages and neutrophils produce and secrete effectors that activate a variety of immune cells (including further activating themselves) as well as non-immune cells such as endothelial cells. Both DAMPs and pro-inflammatory cytokines—primary among them tumor necrosis factor-α (TNF-α) (19-25)—

promote immune cell activation and affect important physiological functions that feedback positively to promote further production of inflammatory mediators. This behavior may lead to inflammatory tipping points – and concomitant spillover of inflammatory mediators into the blood – indicative of cascading system failure that occurs at multiple scales and across multiple compartments (26) (Fig. 1.1). In turn, dysregulated inflammation in the blood may itself become a driver of further inflammation in other tissues.

As evidenced by the preceding description, inflammation, like most biological systems, is a highly nonlinear system with multiple feedback loops (Fig 1.1). Positive feedback loops allow rapid ramping up of a response to biological stress, while the negative feedback works to suppress inflammation and restore homeostasis once the threat (infection, damaged tissue, etc.) has been eliminated. We suggest that, as has likely occurred in many other complex biological systems (27), inflammation has evolved to be robust to a broad range of perturbations but at a cost of fragility in key control nodes that may account for the tipping point behavior described above (27) (Fig. 1.1). Failure at these points can lead to disease; therefore, characterizing these failure modes, and especially the tipping point phenotype, is paramount for the development of effective therapeutic interventions (26). Another property of a complex nonlinear system is the ability to exhibit vastly different behaviors that depend on initial conditions and parameters (i.e. strengths and rates of interactions of components)(28). This heterogeneity, which recapitulates the clinical observation of patient-to-patient variability, complicates the prediction of individual patient outcomes using the current suite of statistically-based tools (15, 26). Among the possible reasons for this observed heterogeneity, one key factor may be that while there are several experimentally well-established mechanisms of interactions between inflammatory mediators, many mediators have unknown

mechanisms, or differing actions based on context and timing (29). The complex, context-dependent and individual-specific nature of acute inflammation has made it difficult to modulate.

To address the aforementioned challenges, we propose to use computational modeling to infer networks of interactions among inflammatory mediators directly from data, using an approach that can capture the differences and similarities in context and timing of interactions. These networks are then correlated with particular clinical outcomes to suggest the role of inflammation/inflammatory networks in leading to different outcomes. We gain further insight into the functional roles of these networks by constructing mechanistic models of inflammation that can be tested and whose properties can be studied in terms of the kinds of behaviors they may exhibit. Throughout this process, we seek to infer clinically-relevant features of the inflammatory response that were previously inaccessible. As described below, a systems approach to inflammation can be useful, indeed necessary, to explain the behavior of the innate immune response in individual patients to various biological conditions and ultimately allow for the modulation of this response in pathological conditions.

1.2 COMPUTATIONAL MODELS OF INFLAMMATION

Systems biology approaches span a broad range of techniques, and can be categorized roughly into correlative or causative approaches, with focus on either learning basic principles of system organization and function (30-32) or building predictive computational models (30, 33). Although there is overlap between these areas, most efforts at elucidating biological mechanisms from high-dimensional data have traditionally focused on particular points along this spectrum of

computational approaches. We suggest that gleaning translationally-relevant insights into the inflammatory response and its interconnected (patho)physiology will require the successful navigation of this spectrum, in a logical progression from data to models to understanding and prediction (26)(Fig 1.2).

Correlative approaches include regression techniques that build models predictive within the conditions of the data they were trained on (34). Although these methods do not provide detailed mechanistic insight, these approaches can be used to understand abstract features of the response, such as the presence of nonlinearities and the order of the response. The main drawback of this class of models is that they are often lack mechanistic insight, and can be over-fit to the data on which they were trained. A less-utilized data-driven method is Principal Component Analysis (PCA), which reduces a high-dimensional dataset into a few principal components that account for much of the observed variance in the data. When applied to time-series data, the variables (genes/proteins/etc.) that constitute these principal components may be interpreted as the principal drivers of the observed response and can give some mechanistic insights into the underlying process (35). In the setting of inflammation, correlative approaches such as PCA may facilitate the development of diagnostics by analyzing the cytokine milieu in the blood resulting from inflammatory spillover, in order to identify the health state of individuals and possibly inform patient-specific interventions (15). While these methods correlate gene/protein levels to phenotype and can suggest relevant molecular players involved in a given inflammatory process, these methods do not provide much information about how the genes/proteins interact with each other (35).

In order to better discern organizational aspects of interacting networks of mediators, such as co-regulation or auto-induction, a variety of methods have been developed. Hierarchical clustering and Bayesian methods use high-throughput genomic or proteomic data of several time-points and/or conditions to correlate gene expression patterns with function and infer regulatory networks of correlated genes. Several developments in these methods over the last two decades have yielded more informative networks that can be more easily translated into mechanistic models. Among these methods, Dynamic Bayesian Networks (DBNs) are particularly suited for inferring directed (causative) networks of interactions based on the probabilistic measure of how well the network can explain observed data. DBNs can be supplemented by additional experimental evidence and expert knowledge to hypothesize mechanistic models (Fig. 1.2).

Mechanistic models are derived from more detailed biological and physical descriptions of a system have a rich set of tools for both analysis and simulation. These models, based on causative interactions, can be constructed as ordinary differential equations (ODEs), rules-based models (RBMs), and agent-based models (ABMs) among other methods (including hybrid methods), and have the advantage of potentially being predictive outside the range of conditions/time-points that they were calibrated on. Although it is often difficult to parameterize such models, they can unveil emergent phenomena that not immediately obvious from the interactions that are encoded in the model.

There are several analytic tools, especially for ODE models, that have been developed and used to uncover the organizational principles of networks (or sub-networks), the properties that explain the dynamics and robustness/sensitivity of a given complex system, and, perhaps most importantly, the critical points of control in the system (32). These tools are particularly important

in order to help define the complex interplay between the inflammatory mediators in the blood and tissues. Tools from dynamical systems theory allow identification of the possible steady state(s) of a system as well as the kinetics of the system's time evolution. These tools have been used extensively to explain (or predict, depending on the context) diverse behaviors such as bistability, hysteresis, and oscillations in a variety of biological systems (36). Bifurcation diagrams, in particular, can be used to map out the effects of a particular parameter on the possible steady state behaviors of a system, and to indicate the transition from a healthy steady state to a pathological one(37-39). The relative importance of parameters can also be quantified by calculating the change in the model output in response to changes in the parameter values using sensitivity analysis (32, 40). These methods work in a complementary fashion to identify the key points that can be modulated to change the behavior of a system (Fig. 1.2).

While we wish to navigate through process of data to data-driven model to mechanistic model to prediction and understanding of the innate immune response, we seek to put it in the perspective of translational applications with a focus on clinical and pre-clinical settings. Much of the work in systems biology has understandably been in simpler, well-studied model organisms, but even among studies focused on pre-clinical science, there has been an overall lack of translation to the clinical arena. The studies in this dissertation follow the framework of Translational Systems Biology, which focuses on translational insights for novel diagnostic or therapeutic purposes and predictive mathematical models that can inform *in silico* clinical trials (41, 42).

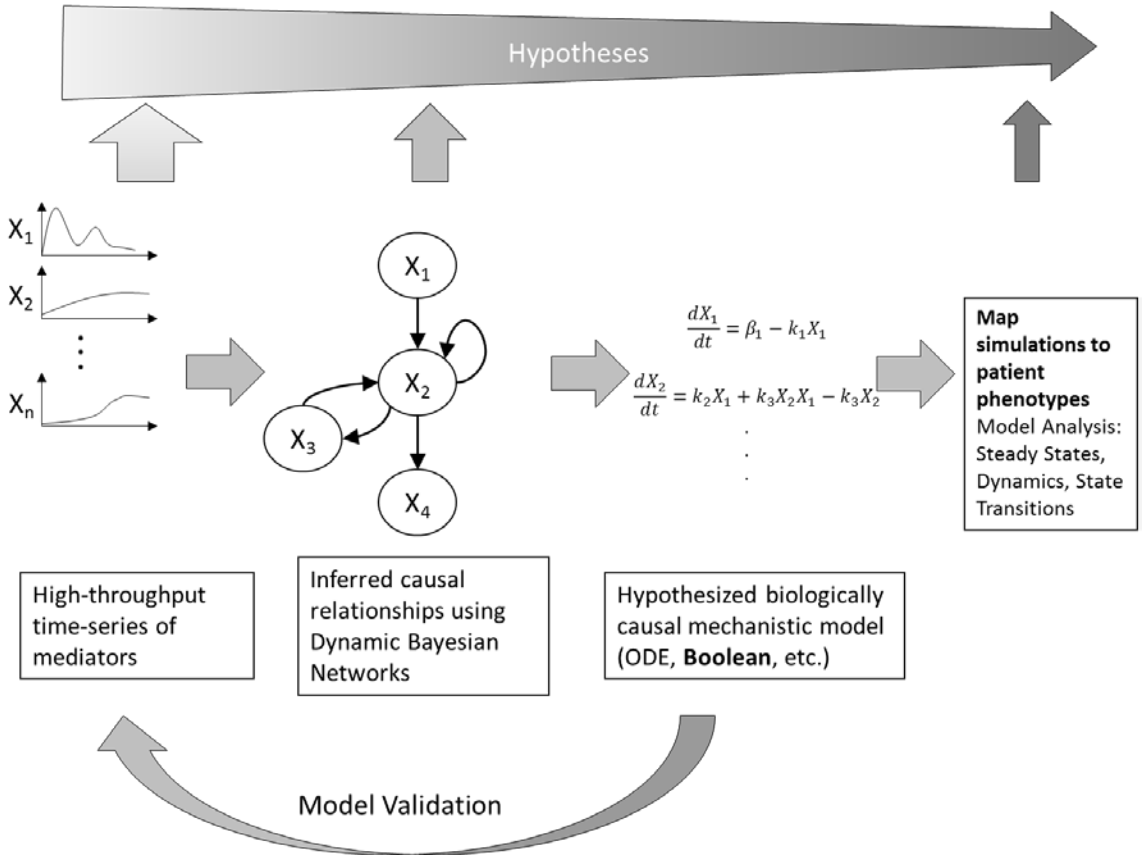

Figure 1.2 Overview of workflow for integrating data-driven and mechanistic modeling.
Multiplexed timecourse data is measured and causal interactions are inferred by Dynamic Bayesian Networks. Inferred network topology forms the basis of mechanistic equation-based models that can be simulated to compare to experimental/clinical data, suggest diagnostic initial conditions, and analyzed and validated with further experiments. Along the path, we generate more focused hypotheses, from associating dynamic patterns of inflammatory mediators with phenotype, to hypothesizing functional roles for particular interactions in the inflammatory network.

1.3 OVERVIEW AND CONTRIBUTIONS

As outlined in the preceding sections, an integrated computational and experimental approach may prove essential in deciphering the complexity of the acute inflammatory response. Current technology allows the simultaneous measurement of a multitude of inflammatory parameters including cells, (molecular) inflammatory mediators, and physiologic parameters. The

challenge lies in obtaining mechanistic insight from often highly variable, multidimensional data. In this dissertation, we address this challenge by following the workflow outlined in Figure 1.2. We first measure multiple inflammatory mediators across time in order to query the dynamics of the overall innate immune response. A key feature of our data is measurement at multiple time points early in the response to an insult (e.g. within first 24 hours after traumatic injury). We hypothesize that the control points that dictate final system behavior operate within this critical period. Indeed, we see that the greatest variations in concentrations of inflammatory mediators occur within this period, indicating that it contains the richest dynamics.

In chapter 2, we use the aforementioned time course data to first infer causal relationships among inflammatory mediators using Dynamic Bayesian Networks (DBNs, step 2 in Figure 1.2). To account for the nonlinear and time-dependent nature of inflammatory mediator interaction, we use a non-linear generalization of standard DBNs, as described by Grzegorczyk & Husmeier (43). The parameters indicating strengths of interaction are integrated out in their algorithm in order to efficiently learn a nonlinear DBN. We develop a method of estimating these parameters post hoc using linear regression, after the network inference. Thus we provide a valuable tool to quickly and agnostically learn whether interactions are stimulatory or inhibitory, which is essential information for biological processes. We apply the aforementioned network inference algorithm to infer differential networks of inflammation in Pediatric Acute Liver Failure patients that were grouped according to survival outcomes in section 2.3. Network inference proved invaluable, as other statistical techniques were unable to differentiate the inflammatory response among spontaneous survivors, liver transplant recipient survivors, and non-survivors. In Section 2.4, we analyze inflammatory networks in Trauma and Hemorrhagic Shock (T/HS), comparing results from a mouse model with those from human trauma patients. We observe key differences between

the case of trauma with and without hemorrhagic shock that suggest mechanistic differences in the progression of inflammation in these settings. After accumulating results from various settings spanning cell, animal, and human acute inflammation, we hypothesize a conserved network module comprising of cross-regulating chemokines, which we term “chemokine switching motif”, and hypothesize that this may drive differential inflammatory trajectories.

While network inference can help hypothesize important interactions in the inflammatory response, we sought to further investigate the functional principles and behaviors that are associated with these networks by constructing mechanistic equation based models in Chapter 3. In Section 3.1, we develop a logical model based on the conserved chemokine network motif observed in the DBNs. The model was calibrated to capture the differences in mean inflammatory trajectory for populations of patients who were injured with moderate or severe injury. Although the model was fit to mean data, it was able to capture differences in the trajectories of subpopulations of patients. We map out the dynamical behavior of the model for all possible starting conditions and find that differences in the time for the model to reach steady state between moderate and severe injury simulations match closely with clinically observed patient discharge - a novel way to link modeling results to relevant clinically observed phenomena. Taken together, these studies suggest that the inferred chemokine switching motif comprising of MIG, IP-10 and MCP-1 may represent a control strategy that regulates the progression of acute inflammation. Further analysis and validation of this hypothesis will require targeted perturbation studies in cells and animals with iterative rounds of mechanistic model refinement. In section 3.2, we describe such a study wherein we characterize a signaling pathway that gives rise to a complex dose and time dependent induction of TGF-β1 by NAD^+, a potent anti-inflammatory mediator. To summarize, the major contributions of this dissertation are:

- Establishing a protocol for gaining mechanistic insight from multidimensional data through a rational progression from data-driven to mechanistic modeling (Figure 1.2)
- Establishing network inference as a tool to generate quasi-mechanistic hypotheses regarding differences in inflammation between disease phenotypes/clinical outcomes
- Estimating the parameters of the DBNs inferred from Grzegorczyk & Husmeier's method post hoc using multiple linear regression
- Showing that patients suffering from Pediatric Acute Liver Failure have distinct networks of inflammation associated with survival, non-survival, and liver transplantation
- Showing that inflammatory networks in human trauma are driven primarily by chemokines MIG and MCP-1, with a greater role for MCP-1 in patients that also have hemorrhage. Showing analogous results for a mouse model of trauma/hemorrhage for the chemokines IP-10 and MIG.
- Developing a logical model of the inferred chemokine switching motif and showing that this model can capture differences in the inflammatory dynamics of subpopulations of trauma patients and map model behavior onto patient discharge
- Identifying the signaling pathway that leads to the complex induction of TGF-β1 by NAD^+ by combined computational modeling and experiments

2.0 NETWORKS OF INFLAMMATORY MEDIATORS IN ACUTE INFLAMMATION

Many data-driven methods help to identify which mediators are central for a particular process and can help discriminate between groups. Previous studies of inflammatory mediators in Trauma/Hemorrhagic Shock (T/HS) have identified such mediators (44). Network inference can suggest how these inflammatory mediators may interact, providing us with another dimension to compare groups and generate hypotheses, and giving insight into the architecture of the inflammatory response. Indeed, when other statistical test and data-driven methods were unable to adequately distinguish survivors from non-survivors in transplant recipients of patients with Pediatric Acute Liver Failure (PALF), DBNs inferred for each group showed clear differences in their inflammatory networks (45) (Section 2.3). Based on our preliminary results, we have hypothesized a potential core structure of interaction among inflammatory mediators that may play a role in determining the trajectory of the innate immune response, and whether it leads to a healthy, self-resolving state or an over-exuberant and self-maintaining elevated pro-inflammatory state. We have demonstrated that we can infer dynamic networks of inflammatory mediators in T/HS.

2.1 BACKGROUND

Network inference in biology has been an intense area of study since the advent of high throughput biological data. Biological processes are characterized by the interaction among biomolecules. These interactions can be studied either by direct measurement of binding, observing phenotypic changes by targeted perturbations, large scale changes in expression after perturbations, or by analyzing the time courses of the various genes/proteins. The last two are particularly powerful as they consider the systemic level rather than a reductionist approach. Although network inference methods were originally used to learn gene regulatory pathways from microarray data, advancements over the last decade have facilitated their use in investigating proteomic interactions, signaling pathways, and integrating heterogeneous biological data (46). Bayesian methods in particular have been useful for the latter, as they frame the problem in a probabilistic context and allow integration of diverse datasets. However, the majority of studies on inflammation measure the transcriptional response at a genome-wide level to correlate sets of genes with different phenotypes (47-49), including those focused on cytokines (50). Proteomic studies have been limited to correlative approaches or focused on cytokine signaling within single cells (51, 52). Inflammatory mediators function primarily to the recruit and/or activate cells to change both their expression and secretion profiles. Therefore, we hypothesize that measuring protein concentrations at the bulk (tissue/blood) level as opposed to gene expression or signaling within single cells is more relevant in discerning the interaction among these mediators across cells. We choose to measure inflammatory mediators in the blood because it is an easily accessible compartment for obtaining serial samples, especially in human patients. Unlike the aforementioned

studies, this allows us to capture the coordination of the response across multiple tissues and cell types. These interactions are not necessarily direct protein-protein or gene-gene interactions, but they provide an idea of how inflammatory mediators eventually influence each other at the protein level, which is generally their functionally active form (in the context of inflammatory trajectories)

Dynamic Bayesian Networks (DBNs) are particularly suited for inferring directed networks of interactions. By allowing edges (interactions) from nodes in one time point towards nodes in the following time point, DBNs can represent feedback loops, which are lacking in standard Bayesian networks. The general method to learn DBNs involves iterating through the process of i) proposing a candidate graph (network) structure, ii) given the graph and experimental data, finding the best conditional probabilities for each node, and iii) scoring the candidate network based on i) and ii). To discuss the method in more detail, we follow the approach from Markowetz & Spang's review (46), beginning with the simplest case that utilizes statistical correlations between variables to infer connections, and then introduce graphical modeling methods that account for the possible influence of other variables when inferring connections between two given variables.

2.1.1 Coexpression Networks and Conditional Independence

A simple way of inferring that two genes/proteins interact or are functionally related is to use the guilt-by-association principle. That is, if the similarity of their expression profiles is above a threshold, they are considered to be connected. Similarity can be measured by common statistical tests, such as Pearson's correlation, or by more sophisticated non-linear similarity measures like mutual information or non-linear kernel functions (46). However, although 0 correlation

corresponds to statistical independence, high correlation is still a weak criterion for statistical dependence. High correlation may occur by chance, depending on the size of the data. Moreover, correlation cannot distinguish between direct and indirect dependences, as it is measured by pairwise tests that do not account for the possible influence of other variables in the network. One way to resolve this uncertainty is to use the concept of conditional independence.

If X, Y, and Z are random variables then X is conditionally independent of Y given Z if and only if

$$P(X = x, Y = y \mid Z = z) = P(X = x \mid Z = z)P(Y = y \mid Z = z)$$

Or equivalently,

$$(X = x \mid Y = y, Z = z) = P(X = x \mid Z = z)$$

In other words, given that we know the value of Z, knowing the value of Y gives no new information and is irrelevant for explaining the value of X. Conversely, any correlation between X and Y can be fully explained by the variable Z. Thus, considering conditional independence allows us to differentiate between direct and indirect relationships by asking whether the correlation between two variables can be explained by a third variable (or set of variables). A powerful way to encode and manage conditional independencies is to use graphical models.

2.1.2 Graphical Models

In probabilistic graphical models(53-55), variables are represented as nodes and their relationships are represented by directed edges. They provide a compact representation of the joint probability distribution (JPD) of a set of variables by utilizing conditional independencies to factorize the JPD. Graphical models may be undirected (i.e. Markov Random Fields) or directed (i.e. Bayesian

Networks). Undirected graphical models consider whether the correlation between two variables can be explained by all other variables in the network. In other words, Z from the preceding discussion now represents the set of all other variables. In the Gaussian setting, assuming that the covariance matrix $\sum$ is invertible, we can define $K = \sum^{-1}$ as the precision matrix, and the value $-k_{ij}/\sqrt{k_{ii}k_{ij}}$ as the partial correlation coefficient between variables *i* and *j*. Then, $k_{ij} = 0$ means that variables *i* and *j* are conditionally independent given the rest of the variables. Thus, a Gaussian Graphical Model (GGM) can be defined whose edges are defined by non-zero partial correlation coefficients(55). This graph represents the correlation between variables after accounting for all other variables in the model. However, these models suffer from insufficient data for inference, as the number of observations/samples has to be much larger than the number of variables, which is rarely the case for biological data. Moreover, they do only consider the set of all other variables when calculating conditional independence, although there may be only specific subsets that lead to conditional independence between genes.

Directed graphical models consider whether two variables are conditionally independent given all possible subsets of other variables. An added benefit of directed graphical models is that the regulatory relationships among the variables are clear to see in the graphical representation. Specifically, an edge from X to Y in the graph means that Y is conditionally independent of its non-descendants, given X. In other words, the probability distribution of node Y can be specified by knowing the value of its parent node X, regardless of the values of other nodes in the graph. This dependency relationship can be loosely interpreted as X "causes" Y. This a stronger criterion for inferring causality than correlative methods, as in addition to specifying direction, an edge in a Bayesian Network (BN) means that no other subset of variables can explain the correlation

between the parent and child nodes (46). It is important to note however that, in order for efficient inference, the structure of the graph must be acyclical (53, 56).

2.1.3 Bayesian Networks

To fully define a BN, we need to specify both a graph structure and corresponding parameters for the conditional probabilities. In the simplest, discrete variable case, the probability distributions are presented in conditional probability tables. For each state of the parent variable, the probability of the child variable being in one of its possible states can be calculated by observing the frequency of its occurrence in a training data set. In the case of biological data, which is often composed of continuous-valued concentration or expression levels, it is more appropriate to use continuous variables. Instead of tables, conditional probability densities, such as Gaussian distributions, are used to model the relationship between connected nodes(54, 56). For instance, Y is normally distributed with a particular mean and variance when $X=x$, i.e. $P(Y|X) \sim N(B_0 + B_1(X=x), \sigma^2)$. Similar to the discrete case, the parameters (the mean and variance of the Gaussian) would be estimated from a training dataset. In Gaussian Bayesian Networks, the distribution of each variable is a Gaussian distribution with a mean and variance defined by a linear combination of the parent variables.

There are two classes of algorithms for learning the structure of BNs: *constraint-based* algorithms and *score-based* algorithms(54, 55). Constraint-based algorithms, which require the testing of conditional dependence between node pairs, given every possible subset of other nodes, are generally computationally infeasible for the number of variables modeled in biological studies

(46). Score-based methods avoid this problem by posing the structure learning task as an optimization problem. A scoring metric is first defined for evaluating how well a particular model (structure) fits to the data. The goal then is to find the maximum-scoring structure(s) by searching through the discrete space of possible structures. The simplest scoring metric is the Maximum Likelihood estimate – however, this score suffers from overfitting as it increases with the number of parameters and edges in a graph. Regularization parameters may be added to ML scores, but the full Bayesian approach is preferred because of its built-in regularization. This score is defined by the posterior probability of observing the model structure, G, given the data, D:

$$P(G|D) = \frac{P(D|G)P(G)}{P(D)}$$

The denominator is the same for all models and thus does not need to be computed when comparing model scores. The key component of Bayesian scoring metrics is the marginal likelihood, which is averaged over parameters of local probability distributions i.e. the parameters are integrated out.

$$P(D|G) = \int_{\theta} P(D|G,\theta)P(\theta|G)d\theta$$

The marginal likelihood can be computed analytically, depending on the choice of local probability distributions and corresponding conjugate priors. Structure priors, P(G), may be chosen to incorporate prior biological knowledge or focus on specific types of interactions.

The space of all possible graph structures is super-exponential in the number of nodes, therefore we must use some heuristics to search through this space. One class of heuristics is based on Markov Chain Monte Carlo. In this method, we start with some network and make a local

perturbation (i.e. add/delete/invert one edge) and accept the new structure with some acceptance criterion (such as the Metropolis-Hastings acceptance criterion).

2.1.4 Dynamic Bayesian Networks

A major restriction of Bayesian Networks is that cyclical loops in the graph are not allowed. However, feedback is an essential feature of biological networks and therefore important to model when inferring networks of interactions among biological agents. Dynamic Bayesian Networks (DBNs) allow for inference of feedback by indexing the variables by discrete timepoints, in effect unrolling the network in time (Figure 2.1)(57). Generally, each time slice contains an instance of the variables being modeled ($X_1 \ldots X_n$) and edges are drawn from parent nodes at time *t* to the nodes they influence at time *t+1*. More generalized cases that allow edges within a time slice or between time slices of distance greater than 1 may also be constructed.

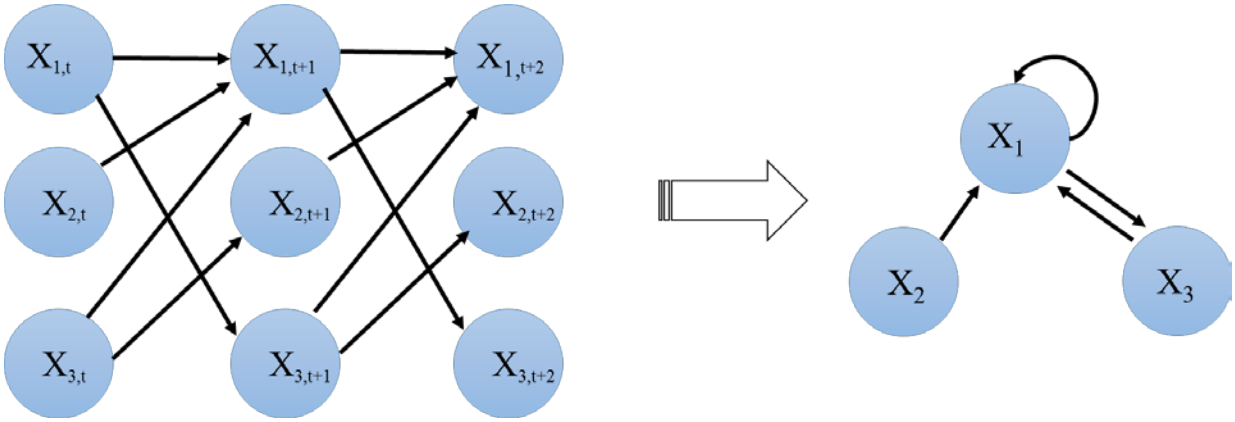

Figure 2.1 Dynamic Bayesian Network.

2.2 NETWORK INFERENCE METHODOLOGY

2.2.1 Grzegorcyk & Husmeier's changepoint BGe DBN algorithm

We use the Matlab code provided by Grzegorczyk et al for their algorithm, described in detail in (43). Briefly, we have a set of variables (nodes) that represent the different inflammatory mediators in our model, $X_1,\ldots X_N$ and a directed graph (network) structure G that describes the interactions between them. The parent set of each node X_n, denoted by $\pi_n(G)$, is the set of nodes that influences the value of node X_n. Intra-timepoint interactions are not considered, as parent node sets for Xn are only considered from $X_{1,t-1},\ldots X_{N,t-1}$. The model proposed by Grzegorczyk et al is a non-stationary generalization of the Bayesian Gaussian with score equivalence (BGe) model (58) and is essentially a node-specific mixture of BGe models. The marginal likelihood is given by:

$$P(D|G,\boldsymbol{V},\boldsymbol{K},\boldsymbol{\theta}) = \prod_{n=1}^{N}\prod_{t=2}^{m}\prod_{k=1}^{\kappa_n}\psi\left(D_n^{\pi_n}\left[t,\boldsymbol{\theta_n^k}\right]\right)^{\delta_{\boldsymbol{V}n(t),k}}$$

$$\psi\left(D_n^{\pi_n}\left[t,\boldsymbol{\theta_n^k}\right]\right)^{\delta_{\boldsymbol{V}n(t),k}} = P\left(X_n(t) = D_{n,t}|\pi_n(t-1) = D_{(\pi_n,t-1)},\boldsymbol{\theta_n^k}\right) \quad (1)$$

Where D is the time course data, $\delta_{\boldsymbol{V}n(t),k}$ is the Kronecker delta, V is a matrix of latent variables that indicate which mixture component a data point has been generated by, and K = (κ1,…κn) is the vector of mixture components (see (43) and corresponding supplementary information for more details). The data points are assigned to mixture components by a discrete changepoint process. The vector V_n thus divides the data for each node into different time segments (between

changepoints), each pertaining to a separate BGe model with parameters θ_n^k, resulting in a model with non-stationary parameters. This allocation scheme provides the approximation of a nonlinear regulation process by a piecewise linear process. The marginal likelihood conditioned on the latent variables is then given by

$$P(D|G,\boldsymbol{V},\boldsymbol{K}) = \int P(D|G,\boldsymbol{V},\boldsymbol{K},\boldsymbol{\theta})\,P(\boldsymbol{\theta})d\boldsymbol{\theta} = \prod_{n=1}^{N} \Psi^*\left(D_n^{\pi_n}[\kappa_n,\boldsymbol{V_n}]\right) \quad (2)$$

$$\Psi^*\left(D_n^{\pi_n}[\kappa_n,\boldsymbol{V_n}]\right) = \prod_{k=1}^{\kappa_n} \Psi\left(D_n^{\pi_n}[k,\boldsymbol{V_n}]\right) \quad (3)$$

$$\Psi\left(D_n^{\pi_n}[k_n,\boldsymbol{V_n}]\right) = \int \prod_{t=2}^{m} P\left(X_n(t) = D_{n,t}|\pi_n(t-1) = D_{(\pi_n,t-1)},\boldsymbol{\theta_n^k}\right) P\left(\boldsymbol{\theta_n^k}|\pi_n\right)d\boldsymbol{\theta}$$

Equation 3 is the local changepoint BGe (cpBGe) score for node X_n, and has a closed-form solution (43). Changepoints are sampled from a point process prior using dynamic programming, and graphs are sampled by sampling parent node sets (restricted to a maximum of three parents per node) for each node directly from a Boltzmann posterior distribution based on the cpBGe score. The marginal edge posterior probabilities can be estimated simply by computing the frequency of existence of an edge from node x_i to node x_j in the sampled networks and dividing by the number of samples. For our studies, graphs are inferred in one of two ways: 1) using a single time course of the mean values for each variable and 2) individually for each sample (e.g. each patient), and the marginal edge probabilities are averaged to give a final consensus graph structure for the group. We include only edges (interactions) that have an averaged edge probability > 0.5 in the consensus

network, although this threshold can be adjusted to give sparser or denser networks. The authors measure the performance of this algorithm on synthetic computationally simulated data (i.e. data generated from a deterministic model with Gaussian noise) as well as synthetic biological data (expression levels from a synthetic gene circuit in yeast) and show that it outperforms TSNI (59) and Banjo (60), two popular network inference methods.

2.2.1.1 Computing Influence Scores for Directed Edges

The output of the aforementioned algorithm is a final graph structure indicating the interactions, as well as the node-specific changepoint set indicating time segments across which the interaction parameters vary. Because interactions within a particular time segment are modeled as linear combinations of parent nodes, we will compute the coefficients of influence of each parent node on a child node by multiple linear regression within that time segment. The overall influence score will be computed by determining the duration of positive or negative coefficient time segments. That is, the score for edge from node *x* to node *y* is given by

$$S_{x,y} = \sum_{c=2}^{C} sign(\beta_c) * (t_c - t_{c-1})$$

Where β_c is the coefficient of linear regression of *y* on *x* (multiple linear regression if y has multiple parents), *C* is the total number of changepoints, and t_c is the time corresponding to the c^{th} changepoint. As a test case, we generated simulated data with Gaussian noise to see if we could correctly infer the interactions as well as the label of positive or negative. Data were generated according to the following equations:

$$X_1(t) = \begin{cases} 1 + \varepsilon, & 2 \le t \le 10 \\ -1 + \varepsilon, & 11 \le t \le 20 \end{cases}$$

$$X_2(t) = \begin{cases} -3X_1(t-1) + 0.3 * \varepsilon, & 2 \le t \le 10 \\ -X_1(t-1) + 0.3 * \varepsilon, & 11 \le t \le 20 \end{cases}$$

$$X_2(t) = \begin{cases} 2X_1(t-1) + 0.3 * \varepsilon, & 2 \le t \le 6 \\ -2X_1(t-1) + 0.3 * \varepsilon, & 7 \le t \le 15 \\ 2X_1(t-1) + 0.3 * \varepsilon, & 16 \le t \le 20 \end{cases}$$

Where ε is a random number drawn from the standard normal distribution. The value at the first time point for each variable is also drawn from a standard normal. In this case, we have a common changepoint for X_1 and X_2 at t =10, whereas X_2 has two changepoints at t=6 and t=15. The output of the DBN inference algorithm is depicted in Figure 2.2.

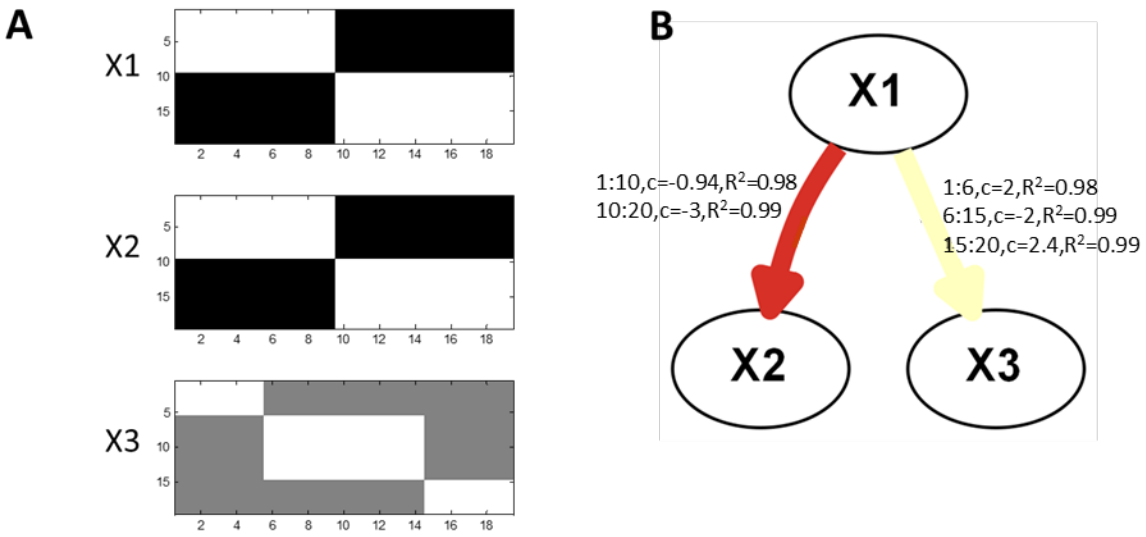

Figure 2.2 A Co-allocation matrices for each variable showing posterior probability of two time points being assigned to same mixture component. B. Final graph structure inferred for simulated data with inferred correlation coefficient for each time segment.

Figure 2.2A depicts the co-allocation matrices for each variable, showing the marginal posterior probability of two time points being assigned to the same mixture component from 0 (black) to 1 (white). The boundaries of white boxes indicate the location of changepoints, with time segments between changepoints. The final graph structure is color coded with red-yellow-green color scheme depending on whether the influence score is positive, neutral or negative (Figure 2.2B). The edges are also labeled with the correlation coefficient and R^2 for each time segment. The information about influence scores and segmentations will be used to guide future studies. For the studies in this thesis, we report only the final graph structure.

2.3 UNIQUE DYNAMIC NETWORKS ASSOCIATED WITH DEATH AND SPONTANEOUS SURVIVAL IN PEDIATRIC ACUTE LIVER FAILURE

This section is edited from a paper published in PLoS ONE (45). In this work, Dynamic Bayesian Networks are used to infer inflammatory networks for patients with pediatric acute liver failure (PALF). Although raw inflammatory mediators assessed over time could not distinguish among patient outcomes, DBN analysis revealed distinct interferon-gamma-related networks that distinguished spontaneous survivors (SS) from those who died (NS). The network identified in liver transplant recipients (LTx) pre-transplant was more like that seen in spontaneous survivors than in those who died, a finding supported by PCA. My role in this study was to implement and interpret the network analysis of inflammatory mediator profiles in PALF patients.

2.3.1 Introduction

Pediatric acute liver failure (PALF) is a complex, catastrophic, rapidly evolving clinical syndrome (61). Like all complex diseases, the clinical trajectory of PALF is dynamic and non-linear. Its course reflects a complex interaction among the child's clinical condition, response to supportive care, disease severity, potential for recovery, and availability of a suitable organ if liver transplantation (LTx) is believed to be life-saving (62). Yet, LTx is irreversible and impacts both society, in terms of organ allocation, as well as the individual patient and family coping with life-long immunosuppression and monitoring. Identification of patients likely to survive or die or whose condition would not benefit from LTx is necessary to inform LTx decisions.

Outcomes in PALF vary both between and among diagnostic categories, yet LTx occurs more commonly among those patients with an indeterminate diagnosis (63) . Recent data suggest immune or inflammatory dysregulation occurs in the setting of acute liver failure (ALF). For example, patients with acute liver failure (ALF) have increased risk for bacterial and fungal infections (64), aplastic anemia (65, 66), and impaired cell-mediated and humoral immunity (64). Moreover, evidence of immune-inflammatory activation, characterized by marked elevation of soluble interleukin-2 receptor alpha (sIL-2R α), was identified in PALF (67). These observations led us to hypothesize that immune or inflammatory dysregulation is present in PALF.

Acute inflammation elicits interrelated immune, inflammatory, neuronal, and physiological responses that can lead to severe organ dysfunction and death (2). The complexity of the inflammatory response has stymied attempts at therapeutic modulation of acute inflammation. Computational modeling of complex systems is emerging as an approach to address

the plethora of known and unknown interactions among biologic pathways (32), including those pathways operant in inflammation (9). Recently, we used computational algorithms to assess multiple circulating inflammatory mediators coupled to dynamic network analyses to suggest both drivers and markers of inflammation in the setting of experimental trauma/hemorrhage in mice (44). This methodology allowed us to identify unique cytokine interactions between mice undergoing trauma/hemorrhage compared to those who underwent sham intravenous cannulation procedure alone (44).

Our goal in the present study was to apply a similar methodology to PALF. Identification of immune/inflammatory networks will likely reflect dynamic changes in the inflammatory response and could lead to opportunities for directed therapeutic intervention, enhance liver transplant decisions, and improve patient outcomes.

2.3.2 Methods

2.3.2.1 PALF participants

This was a cohort study conducted through the Pediatric Acute Liver Failure Consortia (PALF; National Institutes of Health/National Institutes of Diabetes, Digestive, and Kidney Disease: 5U01 DK072146). Patients less than 18 years of age were eligible for enrollment into the PALF registry if they met the following entry criteria: 1) no known evidence of chronic liver disease, 2) biochemical evidence of acute liver injury, and 3) hepatic-based coagulopathy (not corrected with vitamin K) defined as a prothrombin time (PT) $\geq$ 15 seconds or international normalized ratio (INR) $\geq$ 1.5 in the presence of clinical hepatic encephalopathy (HE), or a PT $\geq$ 20 seconds or INR

≥ 2.0 regardless of the presence or absence of HE. During the period of this study, the PALF study group consisted of 22 pediatric sites: 19 centers in the United States, one in Canada, and two in the United Kingdom. Patient enrollment began in December 1999. The study was approved by the Institutional Review Boards from all of the participating institutions, and the NIH provided a Certificate of Confidentiality to the study. Written informed consent was obtained from the parents or guardians of the children in the study.

After enrollment into the PALF cohort, demographic and clinical data were recorded daily for up to seven days. Diagnostic evaluation and medical management were under the direction of the attending physician at each participating institution, and were consistent with the standard of care at each site. A final diagnosis for the cause of PALF was assigned by the primary physician at each study site as summarized previously (61). 21-day outcomes were recorded as death without transplantation, LTx, or survival without LTx. A single daily serum sample was scheduled to be collected with the first morning blood draw following enrollment and daily for up to seven days, or until death, LTx, or discharge from hospital. The serum sample was divided into 250 µL or 500 µL aliquots, promptly frozen at -80ºC at the enrollment site and later batch-shipped to the research bio-repository long-term storage. The frequency and volume of serum that could be collected for research purposes was dependent upon patient weight, hemoglobin, and the daily volume of blood required for diagnosis and patient management. Given these patient safety restrictions, research samples were not available at all potential time points for all PALF cohort participants.

A study cohort for this analysis was selected from the PALF cohort. We identified a convenience sample of participants to serve as the study cohort. Participants in the study cohort

were to have at least 3 daily samples with at least 100 μL of serum. From those participants, the study cohort was further prioritized to capture those with the most samples available between study entry and outcome, and to recapitulate the diversity of age, diagnosis and outcome throughout the PALFSG as a whole.

2.3.2.2 Assays of inflammatory mediators

We chose chemokines, cytokines, and reactive nitrogen oxide species that serve generally or specifically as biomarkers for various phases of the complex inflammatory response. Cytokines and chemokines (eotaxin, granulocyte-macrophage colony stimulating factor [GM-CSF], interferon [IFN]-α2, IFN-γ, interleukin [IL]-1β, IL-1 receptor antagonist [IL-1ra], IL-2, soluble IL-2 receptor α chain [sIL-2rα], IL-4, IL-5, IL-6, IL-7, IL-8, IL-10, IL-12p40, IL-12p70, IL-13, IL-15, IL-17, IFN-γ-inducible protein of 10 kDa [IP-10; CXCL10], monocyte chemotactic protein-1 [MCP-1; CCL2], monokine induced by γ-interferon [MIG; CXCL9], macrophage inflammatory protein [MIP]-1α, MIP-1β, and tumor necrosis factor [TNF]-α) were assayed using a Luminex™ 100 IS apparatus (Luminex™, Austin, TX) using specific beadsets (Millipore, Billerica, MA). The nitric oxide reaction products NO_2^- + NO_3^- were assayed using the nitrate reductase method (Cayman Chemical, Ann Arbor, MI).

2.3.2.3 Statistical analyses

Patients' gender and coma grade at enrollment are reported as percentages. Outcomes are reported at 21 days. Age at enrollment is reported as medians (25^{th} and 75^{th} percentiles). Pearson chi-square tests were used to test differences in proportions between those patients in this inflammatory study

and those not in this study, but in the PALF registry cohort. Wilcoxon Rank-sums tests were used to test for differences in distributions of age between the two groups. P-values less than 0.05 were used to determine statistical significance.

2.3.2.4 Patient-Specific Principal Component Analysis (PCA)

Principal Component Analysis is a statistical method to reduce the dimensionality of data by finding new axes, or components, along which the variables exhibit the greatest variance or response (68, 69). This analysis identified subsets of mediators that most strongly correlated with the inflammatory response trajectory of an individual patient using at least 3 samples for each patient. A PCA score was then calculated for each cytokine, summarizing the relative degree to which that cytokine contributed to the inflammatory response for that patient over time. The PCA scores were used to group participants using hierarchical clustering as described below. Resultant patient sub-groups were then cross-correlated with clinical outcomes: spontaneous survivor (SS), non-survivor with native liver (NS), or received LTx (LTx). This method was unbiased in that all the patients' data were subjected to PCA independent of outcome groups.

2.3.2.5 Hierarchical clustering analysis

This analysis highlighted the natural variability, as well as any overlap, in inflammatory mediators from among SS, NS, and LTx PALF participants. The details of this analysis are provided in the *Appendix A.2*. The calculation is performed by using the Bioinformatics Toolbox in Matlab® 7.6.0, and the code for this algorithm and an explanation of its use in the context of experimental

trauma/hemorrhagic shock has been made available publicly (44). This method is unbiased, and so the segregation of post-PCA data by hierarchical clustering was likewise unbiased.

2.3.2.6 Dynamic Bayesian Network Analysis

This analysis delineated the connectivity among circulating inflammatory mediators as a function of time, thereby describing a possible biomarker signature as well suggesting possible mechanisms by which the progression of the inflammatory response differs based on patient sub-group. In this analysis, time courses of unprocessed cytokine measurements (e.g., measurements were not converted to PCA or to fold change over baseline, or normalized in any other way) from each experiment were used as input for a Dynamic Bayesian Network (DBN) inference algorithm, implemented in Matlab® as described in Section 2.2 (43).

2.3.3 Results

2.3.3.1 PALF participants

There were 986 participants enrolled in PALF at the time of this analysis. We identified 49 PALF participants that met criteria for our convenience sample. Demographics of the 49 participants included in this analysis are presented in Table 2.1. All participants had at least 3 and not more than 7 samples for analysis. The median number of samples per patient was 4 (25^{th} and 75^{th} percentiles were 3 and 6, respectively). The number of participants with samples tested was 18 with 3 samples, 12 with 4, 6 with 5, 7 with 6 and 6 with 7 samples analyzed. 15 participants had available samples on each day from enrollment to outcome or over 7 days from enrollment. For

the remainder with at least one missing sample, 3 participants had 4 missing samples, 4 participants had 3 missing samples, 12 participants had 2 missing samples, and 15 participants had only one missing sample.

Table 2.1 Demographics, final diagnosis and outcomes of the Study Cohort

	Study Cohort (n=49)
	N (%)
Age at enrollment (years)	
Median	7.9
25%, 75%	1.1, 15.1
Male	25 (51.0)
Diagnosis	
APAP toxicity	8 (16.3)
Autoimmune hepatitis	5 (10.2)
Viral infection	3 (6.1)
Indeterminate	26 (53.1)
Other diagnoses	7 (14.3)
Coma grade at enrollment	
Not assessable	3
0-I	36 (78.3)
II-IV	10 (21.7)
21-day outcome	
Alive without LT	27 (55.1)
LT	15 (30.6)
Died without LT	7 (14.3)

2.3.3.2 Variability of circulating inflammatory mediators in PALF participants.

Plotting individual cytokine trajectories grouped by outcome did not reveal any obvious patterns or characteristic properties. (See *Appendix A* Figs. A1.1-A1.3). Hierarchical clustering was then used to segregate the cytokine data based on similar dynamic patterns to determine if participants with similar outcomes naturally clustered together based on their cytokine values, but concluded that unsupervised clustering of raw cytokine measurements was incapable of predicting clinical

outcomes for these participants (see *Appendix A.2*). Indeed, the time courses of the 26 measured mediators were highly variable (Fig. 2.3; *Appendix A* Figs. A1.1-A1.3), and standard statistical analyses could not segregate among SS, NS, or LTx PALF participants (data not shown).

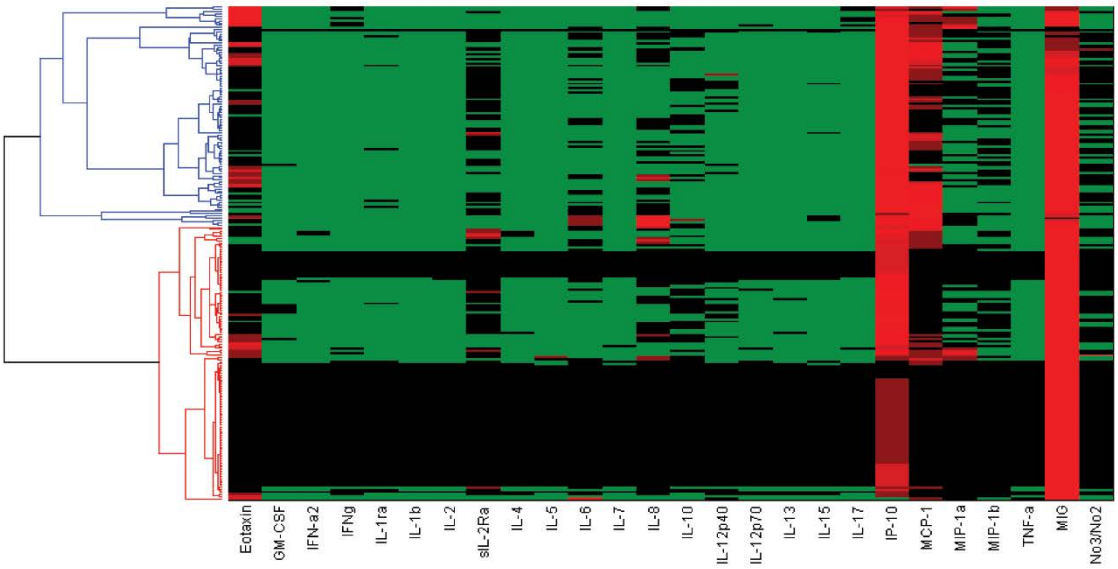

Figure 2.3 Hierarchical clustering of raw circulating inflammatory mediator data in PALF patients. Circulating inflammatory mediators in PALF spontaneous survivors, non-survivors, and LTx recipients were determined as described in the Section 2.4.3.2. Unsupervised hierarchical clustering was performed as described in the Materials and Methods

2.3.3.3 Patient-Specific PCA separates some NS from SS and transplanted participants.

We next utilized PCA to determine those circulating inflammatory mediators that dominated the overall patient-specific, time-dependent inflammatory profiles of the study cohort. We then performed hierarchical clustering on these individual inflammatory patterns and found that the participants segregated naturally into seven clusters (Fig. 2.4A). The first two of these clusters contained only survivors (Fig. 2.4B), suggesting that the inflammatory signature common to the participants in those clusters might be characteristic, and perhaps predictive, of spontaneous

survival. We note that the PCA and clustering analyses are both unsupervised methods, and thus the algorithm was blinded with regard to outcome groups. After the clustering was performed, cluster assignments were cross-referenced to outcomes.

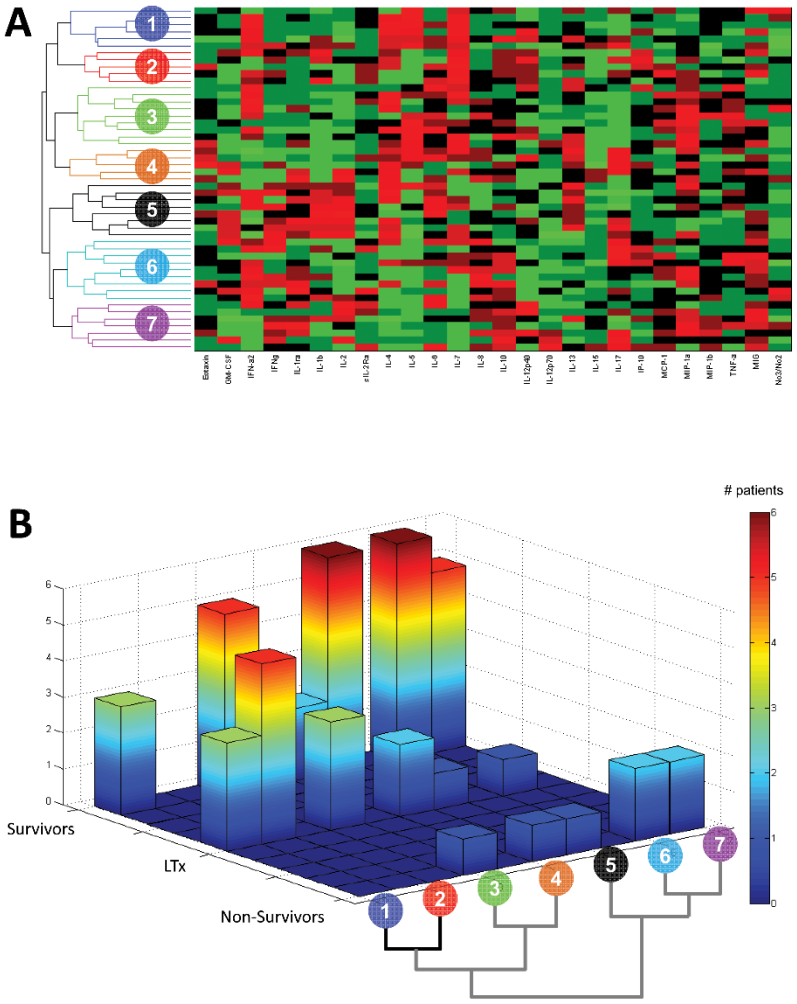

Figure 2.4 Hierarchical clustering of patient-specific PCA ("inflammation barcodes") in PALF patients.
The data from Figure 2.5 were subjected to patient-specific PCA (generating an "inflammation barcode") followed by unsupervised hierarchical clustering as described in the Materials and Methods. Panel A: hierarchical clustering results, suggesting 7 distinct patient sub-groups. Panel B: Comparison of PALF sub-groups to "inflammation barcode"-defined sub-groups. Color spectrum bar represent the number of PALF patients.

2.3.3.4 Dynamic Bayesian Network analysis segregates PALF patient sub-groups.

The PCA/hierarchical clustering analysis suggested common inflammatory signatures may be associated with clinical outcomes in the study cohort. We hypothesized that these inflammatory patterns could reflect dynamic inflammation networks that identify key inflammatory mechanisms in PALF. We therefore utilized Dynamic Bayesian Network (DBN) inference to determine if such networks could be discerned from the time courses of circulating inflammatory mediators in PALF participants. Results of this analysis on each of the three PALF sub-groups are shown in Fig. 2.5. Though the data were segregated by outcome group before being subjected to DBN inference, we note that the algorithm makes no assumptions about the connectivity of the network in any of the outcome groups.

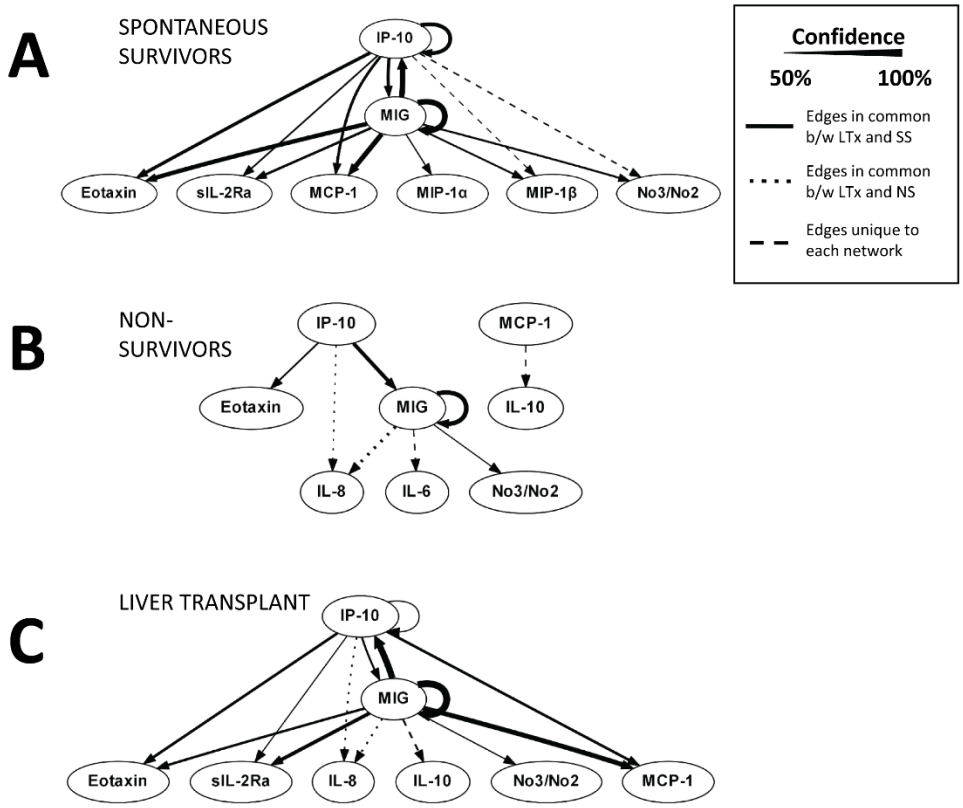

Figure 2.5 Dynamic Bayesian Network analysis of inflammatory mediator data in PALF patients.

The data from Figure 2.5 were subjected to DBN analysis. Inflammatory mediators are shown as nodes, and the arrows connecting them suggest an influence of one mediator on the one(s) to which it is connected. The arrows do not distinguish positive from negative influences of one mediator on another.

For SS: the DBN pattern suggested a network regulated via switching between the chemokines MIG/CXCL9 and IP-10/CXCL10, each of which drives its own expression and leads to the downstream production of eotaxin, sIL-2rα, MCP-1, MIP-1α, MIP-1β, and nitric oxide. In contrast, for NS: the DBN analysis suggested a primary network driven by the self-maintaining behavior of MIG/CXCL9, leading predominantly to the production of IL-6, IL-8, and nitric oxide. IP-10/CXCL10 was still present and driving eotaxin in this DBN, but without increasing its own production. A separate network consisting of MCP-1 driving IL-10 was also evident. For LTx: the DBN suggested a network very similar to that of spontaneous survivors, namely the apparent MIG/CXCL9 – IP10/CXCL10 switching with self-sustaining behavior and downstream production of eotaxin, sIL-2rα, IL-8, IL-10, MCP-1, and nitric oxide. To support the idea that the differences between groups did not arise by chance, we repeated the DBN analysis on a random grouping of the data and observed that the networks contained no major differences, with the core module of IP10/CXCL10 and MIG/CXCL9 cross-regulation and self-feedback being retained in all networks (Figure 2.6).

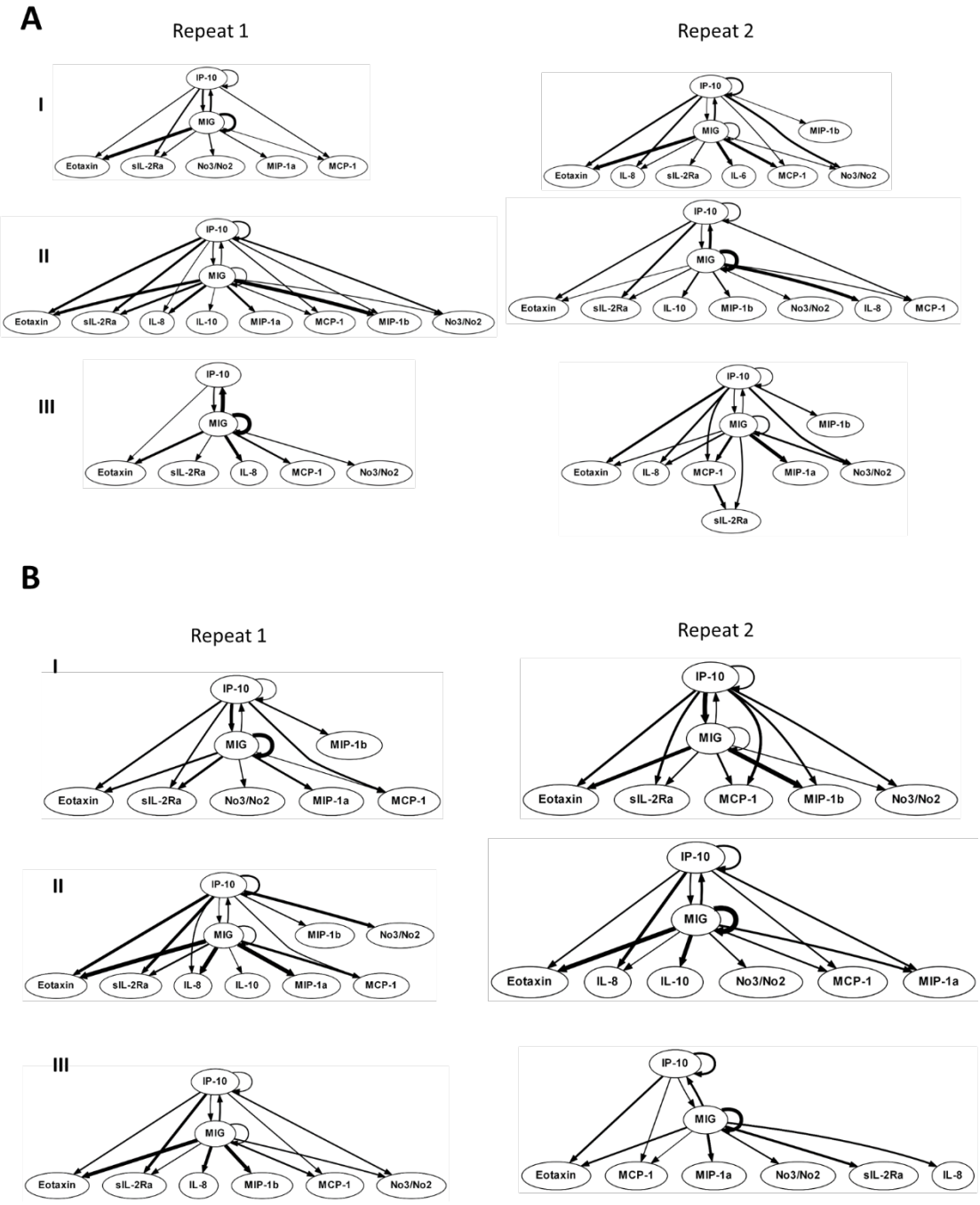

Figure 2.6 DBN results from randomized outcome groups.

Patients were grouped randomly into three groups of sizes of 27, 15, and 7 while maintaining approximately the same percentage of SS (55%):NS (14%):LTx (31%) in each group (panel A) or allowing the percentages to vary (panel B)**.** DBNs were inferred on each group and showed no major differences, with the core module of IP-10 and MIG self-feedback and cross-regulation being observed in all networks**.** Groups I, II, and III have 15, 27, and 7 patients respectively

2.3.4 Discussion

The search for biomarkers in liver diseases has been fraught with difficulty. Putative biomarkers identified in small studies are often not sufficiently disease-specific, not tied mechanistically to a given disease, and non-reproducible in larger studies. Even those that are reproducible are frequently limited in their value to the most severe or advanced stages of disease (70-72). Recent studies have emphasized the need for studying multiple inflammatory biomarkers combined with informatics/computational techniques as a key part of the interpretation of biomarker data (15, 73-75). This pilot study examines the use of novel analytic methods that may account for the dynamic complexity of the inflammatory response in PALF.

Analysis of raw circulating inflammatory mediator data in a convenience sample of PALF participants demonstrated a high degree of patient-to-patient variability. In contrast, when data underwent patient-specific PCA followed by unsupervised hierarchical clustering in a blinded fashion, seven distinct patient clusters were identified and some clusters contained only spontaneous survivors and LTx. This suggests that dynamic aspects of inflammation may be associated with patient-specific clinical outcomes. Finally, using DBN inference, cytokine networks associated with SS differed from those associated with NS. The cytokine network associated with LTx had characteristics more similar to SS than NS.

In a previous study on experimental trauma/hemorrhagic shock in genetically identical mice, we observed a high degree of variability in the raw circulating mediator data, but could identify distinct principal inflammatory drivers in animals receiving hemorrhagic shock from those subjected to sham cannulation (44). In the present study, we affirm that the inflammatory response

of a diverse cohort of PALF participants is highly variable (76-78) and that PCA could segregate inflammation patterns associated with different outcomes.

The inflammatory response can take two potential paths: (1) resolvable inflammation, in which the initial inflammatory response is harnessed by negative feedback that drives resolution, healing, and regeneration; or (2) unresolvable inflammation, which occurs when negative feedback is insufficient, a positive feedback loop of inflammation goes unchecked, and inflammation begets cellular damage and destruction which begets further inflammation (9, 14, 26, 79, 80). Positive and negative inflammatory feedback with regard to ultimate health status of the patient might be mapped onto pro- and anti-inflammatory mediators in some contexts, but not in others. Furthermore, any given mediator could serve a pro- or anti-inflammatory role at a given time or under given conditions. Thus, using data-driven models to suggest the time and context-dependent role of cytokines may be more informative than relying on an analysis with static, pre-assigned roles for cytokines. In a prior study, our data suggested that IP-10/CXCL10 initiates a low-level, resolvable inflammatory response in mice subjected to minor trauma alone. In contrast, MIG/CXCL9 drives a more robust and potentially unresolvable inflammatory response in the setting of the same minor trauma + hemorrhagic shock (44).

Several studies have demonstrated that both MIG/CXCL9 and IP-10/CXCL10 mRNA are elevated in experimental models of liver failure (81, 82), and circulating levels of both chemokines are implicated in chronic hepatitis C (83). Importantly, and supporting our hypothesis that IP-10/CXCL10 may drive a resolvable inflammatory response in PALF, Bone-Larson *et al* demonstrated that IP-10/CXCL10 is hepatoprotective in an experimental model of acute liver

injury (82). Both MIG/CXCL9 and IP-10/CXCL10 are also associated with IFN-γ signaling, a pathway that also influences liver regeneration.

Based upon these preliminary studies, we hypothesized that if IP-10/CXCL10 is stimulated initially, then this chemokine would both drive its own production and suppress that of MIG/CXCL9 and lead to self-resolving inflammation. In contrast, if MIG/CXCL9 is stimulated initially, then MIG/CXCL9 would drive its own production while suppressing that of IP-10/CXCL10, in turn leading to self-maintaining, or unresolvable inflammation. Based on DBN analysis, we found what we suspect to be a pattern of resolvable inflammation associated with SS and unresolvable inflammation associated with NS in our selected PALF cohort. Specifically, we find PALF SS and LTx participant's exhibit chemokines MIG/CXCL9 and IP-10/CXCL10, each of which exhibits feedback behavior and each of which appears to regulate the other. This chemokine switching network appears to drive a diverse inflammatory response that includes eotaxin, sIL-2rα, MCP-1, MIP-1α, MIP-1β, and nitric oxide (in spontaneous survivors) or eotaxin, sIL-2rα, IL-8, IL-10, MCP-1, and nitric oxide (LTx recipients). Accordingly, we interpret the inflammation networks in PALF SS and LTx participants as demonstrating the possibility of switching between inflammatory responses driven by IP-10/CXCL10 vs. inflammation driven by MIG/CXCL9, and ultimately manifesting in a pattern of resolvable inflammation. In contrast, PALF NS participants exhibited an inflammation network that suggests feedback behavior for MIG/CXCL9 but not for IP-10/CXCL10, driving the production of IL-6, IL-8, and nitric oxide and resulting in unresolvable inflammation.

There are several limitations to our study. This was a retrospective study, and the identified networks were not validated in a separate cohort of participants. The study cohort, as well as sampling time points, was heterogeneous, though the participants in the study cohort were representative of the larger PALF Study Group cohort, and the time frame of sampling was restricted to 7 days post-enrollment. Only a subset of inflammatory mediators was assayed, and, importantly, damage-associated molecular pattern molecules (e.g. HMGB1) were not assessed.

In conclusion, the present study suggests that the DBN-defined inflammatory networks might serve as powerful, new biomarkers for predicting outcomes in PALF, which represents a novel use of DBN inference methodology. These findings will be validated in a larger patient cohort with sampling time points extending to the outcome of death, discharge, or LTx if that outcome was beyond seven days. Despite a heterogeneous inflammatory response in individual PALF participants, our studies suggest a network-based analysis may have the potential to segregate spontaneous survivors and non-survivors with LTx recipients having a biomarker pattern more similar to spontaneous survivors than those of non-survivors. Our data also leave open the possibility that these chemokine-based, feedback-driven inflammatory switching mechanisms might actually mediate such outcomes. This consideration, in turn, suggests that it might be possible to identify subsets of PALF patients in whom specific immune-modulatory therapy might improve the likelihood of spontaneous survival.

2.4 INFLAMMATORY NETWORKS IN TRAUMA/HEMORRHAGIC SHOCK

In this section, we use DBNs to infer the networks of inflammatory mediators in Trauma/hemorrhagic shock (T/HS), another condition with an inflammatory etiology that is poorly understood.. T/HS is the most common cause of death for young people in the U.S. and costs over $400 billion annually(84). Most deaths from T/HS occur due to the Multiple Organ Dysfunction Syndrome (MODS), a poorly understood disease that is thought to be due, in part, to dysregulated inflammation (85-89). We used the Dynamic Bayesian Network (DBN) algorithm described in Section 2.2 to define key networks of post-T/HS acute inflammation in both mice subjected to experimental T/HS and human trauma patients with evidence of hemorrhage. Inflammatory mediators were assayed in the plasma by Luminex™, and the data were subjected to DBN analysis. This analysis suggested a core network that involves the cytokine IL-10, as well as the chemokines IP-10 and MIG in mouse T/HS. In contrast, the chemokines MIG and MCP-1 and IP-10 were inferred as the central nodes in human trauma patients. Both cases showed network motifs indicative of switching between distinct inflammatory profiles driven by chemokines, suggesting a common core network structure that may drive divergent responses.

2.4.1 Introduction

Trauma and hemorrhage, like infection, are insults that induce an acute inflammatory response involving a coordinated mobilization of numerous cells and molecules. The complex nature of the response to T/HS, with its many redundant and overlapping pathways and mediators, does not lend

itself to a simple reductionist analysis, especially when there is limited or no experimental constraints on this system. We hypothesize that these multiple mechanisms of inflammation, operating at different time scales, contribute to the complexity of the post-T/HS inflammatory response. Prior studies have focused primarily on either patterns of inflammatory mediators as biomarkers of a particular response, or measured these mediators in cells and/or tissues. However, inflammatory mediators can spill out into the systemic circulation especially when the inflammation is dysregulated, as is the case in T/HS (6, 88, 90, 91). Thus, we focused on time courses of circulating inflammatory mediators in order to infer the (dis)coordination among inflammatory mediators in response to T/HS. Moreover, in the case of human patients, the blood is an easily accessible compartment for sampling. Previous work by Mi et al shed mechanistic insight into the dynamic inflammatory response in T/HS in mice using statistical data-driven methods. In this study, we hypothesize causal networks of inflammatory mediators in mouse T/HS, as well as human trauma patients, inferred by Dynamic Bayesian Networks. Our results indicate that the inflammatory response to trauma, both with and without hemorrhage, may be directed by the interplay a set of key chemokines.

2.4.2 Methods

2.4.2.1 Mouse Model of Hemorrhagic Shock

This study was approved by the Institutional Animal Care and Use Committee of the University of Pittsburgh (protocol No. 1003645) and was conducted in accordance with the National Institutes of Health Guidelines for the Care and Treatment of Small Laboratory Animals. Fifty-four Male

C57BL/6 mice (Charles River Laboratories, Raleigh, NC) weighting 25–30 grams underwent surgical preparation under anesthesia with isoflurane and Nembutal (70 mg/K). Animals were either untreated or cannulated and divided into four groups (n = 6 mice per group), subjected to 1, 2, 3 or 4 h sham procedure (surgical cannulation trauma only; ST) or four groups of 1, 2, 3 and 4 h of HS in addition to this surgical cannulation trauma (ST + HS). Serum was collected from mice sacrificed at each time point. ST + HS was carried out using a hardware/software platform for computerized, closed-loop HS in mice that maintains the blood pressure at below normal at 25mm Hg (13).

Twenty cytokines and chemokines (basic fibroblastic growth factor [bFGF], granulocyte-macrophage colony stimulating factor [GM-CSF], interferon [IFN]-γ, IL-1α, IL-1β, IL-2, IL-4, IL-5, IL-6, IL-10, IL-12p40/p70, IL-13, IL-17, IP-10, Keratinocyte Chemoattractant (KC), monocyte chemotactic protein-1 [MCP-1], MIG, macrophage inflammatory protein-1α (CCL-3) [MIP-1α], TNF-α, and basic VEGF) were assessed in the serum using Luminex™ (MiraiBio, Alameda, CA) using the BioSource 20-plex™ mouse cytokine bead set (BioSource-Invitrogen, San Diego, CA) as per manufacturer's specifications. The nitric oxide reaction products NO_2^-/NO_3^- were assessed using the nitrate reductase kit (Cayman Chemical, San Diego, CA) as per manufacturer's specifications.

2.4.2.2 Human Trauma Patients – Hypotension Cohort

Human Trauma Patients: From a cohort of 484 blunt trauma survivors that were studied following IRB approval, 14 hypotensive patients (10 males and 4 females; age: 42.1±5.1; Injury Severity Score [ISS]:21.4±2.3) were matched with 14 normotensive patients (9 males and 5

females; age: 44.6±3.8;ISS: 22±2.4). Serial blood samples were obtained from all patients (3 samples within the first 24 h and then from days 1 to 5 post-injury). The human inflammatory MILLIPLEX ™ MAP Human Cytokine/Chemokine Panel-Premixed 26 Plex (Millipore Corporation, Billerica, MA) and Luminex™ 100 IS (Luminex, Austin, TX) was used to measure plasma levels of interleukin (IL)-1β, IL-1 receptor antagonist (IL-1Ra), IL-2, soluble IL-2 receptor-α (sIL-2Rα), IL-4, IL-5, IL-6, IL-7, IL-8, IL-10, IL-13, IL-15, IL-17, interferon (IFN)-γ, IFN-γ inducible protein (IP)-10, monokine induced by gamma interferon (MIG), macrophage inflammatory protein (MIP)-1α, MIP-1β, monocyte chemotactic protein (MCP)-1, granulocyte-macrophage colony stimulating factor (GM-CSF), Eotaxin, and tumor necrosis factor alpha (TNF-α). The Luminex™ system was used in accordance to manufacturer's instructions. NO_2^-/NO_3^- was measured using the nitrate reductase/Griess assay (Cayman Chemical Co., Ann Arbor, MI).

2.4.2.3 Network Inference

Networks were inferred using the Dynamic Bayesian Network algorithm detailed in Section 2.2. For mouse data, the input for the DBN algorithm was a single time course of mean values of inflammatory mediators. This was done because we did not sample the serum from each mouse serially, but rather collected it from different mice at each time point. In contrast, because we had serial sampling in human patients, we ran individual DBN inference procedures for each patient, and reported the consensus network determined by taking the mean of the adjacency matrix for all patients. That is, only edges that had an average marginal posterior probability greater than 0.5

across all patient networks were included in the final consensus network, with the thickness of edges representing the averaged marginal posterior probability for that edge.

2.4.3 Results

DBNs inferred from mice subjected to surgical trauma (ST) with and without hemorrhagic shock (HS) are shown in Figure 2.3. We define central nodes, highlighted in green, as nodes with out-degree greater than three. The network in ST portrays a response that seems to be driven mainly by IP-10 and MIG, with cross-interaction between them. In contrast, the ST+HS network has more than two central nodes: IP-10, IL-10, MIG, and FGF-B, with cross-interactions and feedback between several of them. When ranked by the sum of in and out degree, the highest ranking node was IL-10 in ST+HS and MIG in ST.

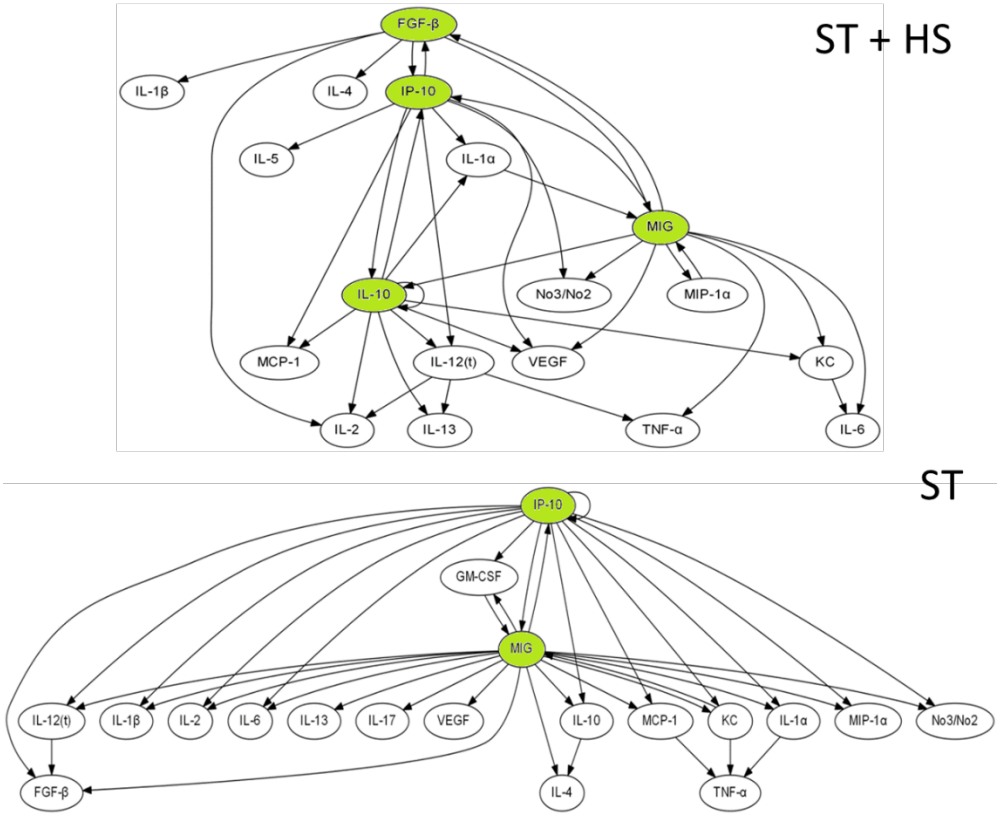

Figure 2.7 Inferred Networks for Mouse ST and ST+HS

In order to assess whether the results from our mouse model were clinically relevant, we repeated the DBN analysis on inflammatory mediators measured in human trauma patients. As an indicator for the presence of hemorrhagic shock, we chose to patients who sustained low blood pressure (hypotensive) within the first 24 hours versus those who had normal blood pressure (normotensive). The patient groups were matched for age, gender, and injury-severity in order to remove any influence of these factors on their inflammatory profiles. Once again we observe two central nodes with cross-interaction between them (Figure 2.7). However, instead of MIG and IP-10 as in the mouse study, we see the chemokines MIG, MCP-1 and IP-10 as the central nodes. In addition to differences in the overall set of mediators connected downstream of these central nodes, we note that several of the mediators common to both networks are connected to MCP-1 in

hypotensive but MIG in the normotensive groups (IL-Ra, IL-10, MIP-1β). This is reiterated when comparing the degree centrality scores, which reveal that MCP-1 is the highest ranked node in hypotensive whereas MIG is the highest ranked in normotensive. Importantly, we note that IL-6 was influenced by both MIG and MCP-1 in hypotensive patients but only MIG in normotensive patients.

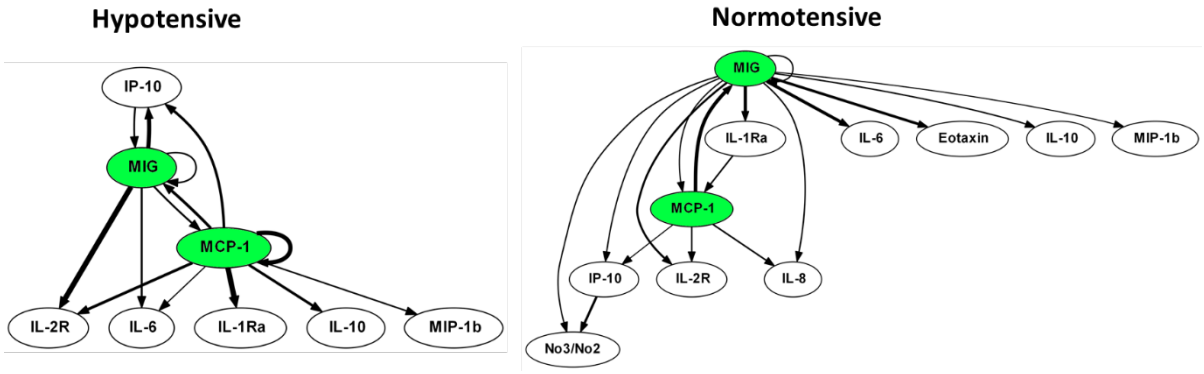

Figure 2.8 Comparison of Networks Inferred for Hypotensive and Normotensive patients

2.4.4 Discussion

Like many other diseases, T/HS has benefited from the systems view afforded by genomic and proteomic studies in the past decade (92-94). Data-driven analyses of these high dimensional data have yielded valuable insights into the pathophysiology of T/HS but have been largely limited to finding associations between sets of genes or pathways and phenotypic outcomes. In this work, we aimed at deriving more mechanistic insight into the interaction among inflammatory mediators as acute inflammation progresses by inferring directed networks from time course data. A previous study by Mi et al on the same mouse dataset studied herein had identified MIG, IP-10, and IL-12

as the best discriminants between ST and ST+HS using multivariate analysis (44). In our study, the aim was not to find discriminating factors but rather on discerning differences in the interaction among inflammatory mediators. These differences in network structure can provide mechanistic hypotheses to explain differences in the course of inflammation between the two conditions. In the study by Mi et al, the authors also inferred connectivity among inflammatory mediators using a technique termed Dynamic Network Analysis. This method is based on statistically significant elevation and linear correlation of mediators within particular time windows and therefore does not yield directed interactions like the networks inferred in this study. Regardless, the authors identified IP-10 as the central node in ST, and MIG, followed (in time) by KC, as the central nodes in ST+HS. Our DBN results suggest that MIG and IP-10 are central to both networks, but have different connections based on condition. In addition, our network suggests IL-10 has the most significant role in the mouse ST+HS network as measured by degree centrality but not in ST alone. This fits well with known inflammatory mechanisms in hemorrhagic shock – namely that hemorrhagic shock leads to an immediate catecholamine burst (95), and that these catecholamines directly induce expression of IL-10 (96, 97).

Our study in the mouse model of ST+HS was specifically designed to induce shock for 1-4 hours as that is a survivable time range for the mice. Thus, the inflammatory response to this insult is analogous to a survivable episode of ST+HS in humans. Accordingly, we analyzed the inflammatory response in human blunt trauma survivors with evidence of hemorrhage indicated by hypotension. Although there has been some controversy regarding correspondence between human and mouse inflammatory responses at the genomic level (98), we sought to determine

whether we could identify any similarities in network structure and interactions at the level of serum inflammatory mediators. The resulting networks for our human study were sparser than the mouse networks, although this is likely due in part to the differing method of calculating the consensus network (see Section 2.3.2.3). However, the role of chemokines as central mediators in the network remained consistent. This hypothesis is supported by the known central role of chemokines in acute inflammation (99, 100), including T/HS (101, 102). For a detailed discussion of chemokines as central mediators of the inflammatory response, see Section 2.5.

Taken together, our results indicate a novel role for cross-regulation among the chemokines MIG and IP-10 in mice and MIG, IP-10 and MCP-1 humans in directing the inflammatory response to trauma and hemorrhagic shock. In humans, a key difference in the networks of hypotensive and normotensive patients was in the addition of MCP-1 as an effector of IL-6. Indeed, we observed that MIG correlates with moderate levels of IL-6 whereas MCP-1 correlates with higher levels, suggesting that modulating the effect of MCP-1 on IL-6 may lessen the greater inflammation induced in the setting of T/HS over trauma alone.

2.5 SUMMARY OF ACUTE INFLAMMATION NETWORKS

As outlined in Chapter 1, acute inflammation leads to a series of events that involve the coordination of several cell types via secreted/released biomolecules, in order to respond appropriately to stress and restore the body to homeostasis. This coordination is disrupted in many diseases with an inflammatory etiology, leading either to overabundant or inadequate inflammation. Due to the multiple conflicting roles of many cytokines dependent on timing and

context, we sought to infer interactions agnostically from time course data. Our primary goal was to generate mechanistic hypotheses that relate differences in how these mediators interact, with the progression of inflammation in different settings. To this end, we studied inflammation in response to trauma/hemorrhagic shock in mice and humans, as well as the inflammatory response in pediatric acute liver failure. While both of these studies generated hypotheses regarding the differences between groups, we also observed a repeated occurrence of two to three central nodes, usually chemokines, with cross regulation between them. After surveying the results from numerous other *in vitro, in vivo,* and clinical settings of both sterile and infection-induced inflammation, we hypothesized that there is a conserved motif of MIG, IP-10, and MCP-1 three-way "switching" that may be responsible for directing the overall trend of the inflammatory response towards self-sustaining or resolving. In particular, we have observed similar networks in liver cells, which are a primary site of inflammatory activity during T/HS (11). DBNs inferred from in vitro measurements of both secreted and intracellular inflammatory mediators of mouse liver cells subjected to hypoxic stress identified MIG, IP-10, and MCP-1 as central nodes with varying connectivity depending on condition. Moreover, an extensive study of inflammation in multiple tissues in mouse models of infection and HS reiterated the central role for these three chemokines (unpublished data). The resulting central nodes of these studies, as ranked by degree centrality, are summarized in Table 2.2.

Table 2.2 Summary of Central Nodes in DBNs of Various Acute Inflammatory Settings

Study	Condition	CN1	CN2	CN3
In-Vitro Hypoxia	Hypoxia Sup + Lysates	IP-10	VEGF	
	Normoxia Sup + Lysates	MIG	MCP-1	IP-10*
Mouse Endotoxin	Plasma	KC	MCP-1	
	Liver	IP-10	MIG	
	All organ average	MIG	IP-10	KC
Mouse T/HS	ST + HS	IP-10	MIG	IL-10
	ST only	IP-10	MIG	
Human Trauma - Hypotensive	Hypotensive	MIG	MCP-1	
	Normotensive	MIG	MCP-1	
Human Trauma - Rheumatoid Arthritis	Trauma + RA	MIG	IL-2R	
	Trauma only	IP-10	MIG	MCP-1
Human Trauma - Nosocomial Infection	Trauma + Infection	MIG	MCP-1	
Human Trauma - SCI	Trauma + SCI	IP-10	MIG	MCP-1*
	Trauma only	MCP-1		
Human PALF	PALF Spontaneous Survivors	IP-10	MIG	
	PALF Non-Survivors	MIG	IP-10	
	PALF Transplanted	IP-10	MIG	

There are two broad classes of chemokines, the CC chemokines that contain two adjacent cysteine residues, and the CXC chemokines that have a single amino acid between the two cysteines. CC chemokines, of which CCL2/MCP-1 is the best studied, attract monocytes to the site of inflammation (103). In contrast, CXC chemokines like CXCL9/MIG and CXCL10/IP-10,

attract polymorphonuclear leukocytes like neutrophils, and have been linked to angiogenesis. CCL2/MCP-1 has only one receptor, CCR2, whereas CXCL9 and CXCL10 both share a receptor in CXCR3 and are also both inducible by IFN-gamma. Although their functions are thought to be redundant, CXCL9 and CXCL10 are expressed differentially in different cell types, and have been implicated individually in various diseases (104, 105).

While we observe a conserved chemokine cross-regulatory motif, the identity of downstream targets seems more specific to the particular inflammatory disease/setting. One exception is IL-6, which is always seen downstream of MIG and/or MCP-1. Indeed, a recent study from our group showed that IL-6 levels are significantly reduced in MCP-1 knockout liver cells and that high MCP-1 levels in human trauma patients correlate with high IL-6 levels (106). In addition, we found that MIG is associated with elevated but lower IL-6 (unpublished data). The assignment of induction versus suppression in the cross-regulatory interactions between chemokines is hypothesized based on our data that suggests that IP-10 and MIG have opposite effects, and supported by literature that indicates that chemokines down-regulate each other at the level of shared receptors (104, 107, 108). These distinctions of stimulatory versus inhibitory interactions may be learnt directly from the data using the method outlined in Section 2.2.1.1, or from iterative model refinement and validation as shown in Section 3.2.

Based on the aforementioned observations, we hypothesize that the course of inflammation in a particular setting is determined by the interplay of the three chemokines MIG, IP-10 and MCP-1, which act as a decision system that can lead to differential induction of IL-6, and subsequently, differential outcomes (Figure 2.9). We hypothesize that while MIG and MCP-1 have proinflammatory effects, IP-10 likely drives anti-inflammation leading to resolution (82). The

dynamic interplay of these key mediators may be responsible for the distinction between an appropriate pro-inflammatory response followed by anti-inflammatory activity and resolution, versus a self-perpetuating pro-inflammatory response that becomes dysregulated and excessive.

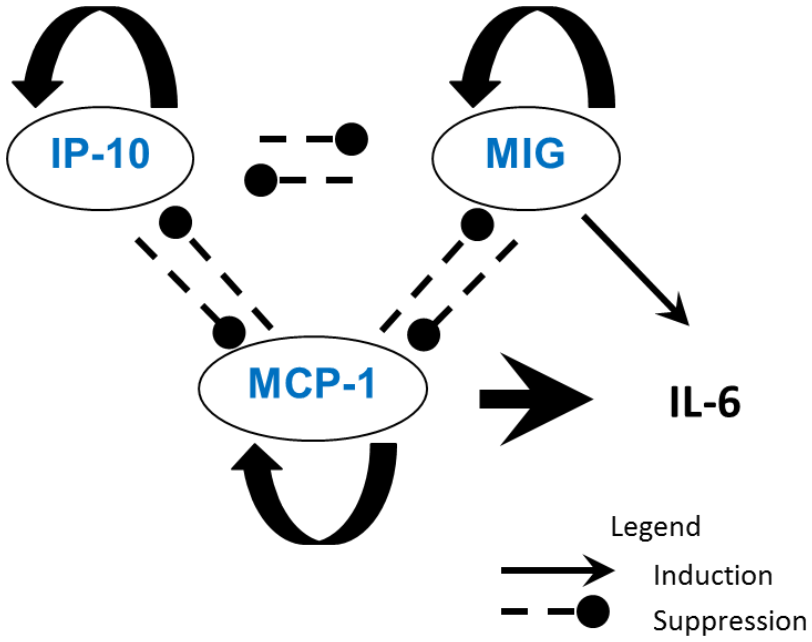

Figure 2.9 Hypothesized Conserved Chemokine Switching Network

3.0 MECHANISTIC MODELING OF INFLAMMATION

In the preceding chapter, we used data-driven modeling to decipher the complexity of multidimensional data. This is a necessary step in the comprehensive systems approach mentioned in Chapter 1 as it allows us to identify the essential features of a response. This is especially important when interpreting inflammatory mediator function. Although there is a depth of knowledge about particular canonical roles of inflammatory mediators, the specifics can vary greatly depending on tissue or even early versus later within the same compartment. It is evident that these functions are not necessarily uniform across time or samples (patients, animals etc.) even in highly controlled experimental systems as in the mouse model of T/HS discussed in Section 2.3. Network inference is therefore very valuable in informing causal mechanisms by which these biomolecules can interact. However, ultimately this inference is at most a hypothesis generator of mechanism that must be validated either by experimental perturbation and relearning, or by being encoded as a simulatable model whose predictions can be validated experimentally. The advantage of the latter, in addition to being able to perform *in silico* experiments, is that they also possess a rich set of tools to analyze the dynamical and steady state properties of the model. These analyses can shed further insight into the functional role of mediators and/or connectivity structures.

In this chapter, I present two complementary studies utilizing mechanistic modeling. Traditionally, mechanistic models are built from a knowledge base of biochemical reaction pathways discovered through decades of focused research. Although such models have more

supporting experimental evidence to justify their structure, the assumptions built into them are not always clear and are not necessarily reassessed as new biology is discovered. In the case of abstracted interactions among inflammatory mediators, where biochemical parameterization is not appropriate, we chose to develop a more qualitative model using logical rules and discrete states. In Section 3.1, I develop a logical model based on the consensus chemokine network topology hypothesized by DBNs (Section 2.5). This model helps specify the details of the interactions inferred by DBN, and also captures a number of interesting features of the data. In Section 3.2, we conduct a more detailed study of a particular well-characterized biochemical signaling pathway, where I combine modeling and experimental studies to identify a signaling pathway that leads to a complex dose and time response of TGF-B1 activation by NAD^+.

3.1 BOOLEAN MODEL OF CHEMOKINE SWITCHING MOTIF

In this study, I use manual model fitting to specify the label (activation or inhibition) as well as the mode of combination of interactions that best recapitulate population averaged clinical data for differently injured groups of patients. Despite being calibrated to the mean response, the model also captures differences in behaviors of subpopulations of different starting conditions within moderately and severely injured patients. Finally, I use a novel comparison of "time to reach steady state" in the model, to patient discharge rate of moderate versus severe injury. This work lends further support to the hypothesis that the chemokine switching motif (Figure 2.9) can account for and may drive the differences in trajectories in acute inflammation

3.1.1 Introduction

Traumatic injury is a significant cause of morbidity and mortality in patients, especially among young people (84, 109). In recent years, the outcomes landscape in blunt trauma has shifted from mortality to secondary complications such as multiple organ dysfunction syndrome (MODS) and nosocomial infection, leading to a prolonged length of stay (LOS) at the hospital (110). These complications can be attributed in large part to the pathophysiological inflammation and immune dysregulation elicited after trauma/hemorrhage (85-89). Trauma/hemorrhage induces an acute inflammatory response that occurs at multiple scales and involves the activation of signaling pathways that mobilize inflammatory cells and stimulate the secretion of chemokines, cytokines and damage-associated molecular pattern (DAMP) molecules. Numerous studies have investigated this response at the level of cellular mobilization, genomic pathway activation (93), and secreted mediators (90, 91). Analyzing inflammatory mediators is particularly informative as they constitute the communication medium for organizing the response among the various cell types. Thus, we can discern the overall coordination of the response, and consequently, its dysregulation, by analyzing the dynamics of these secreted inflammatory mediators.

Previous studies have either focused on association of dynamic patterns of inflammatory mediators with specific outcomes (91) or building predictive mechanistic models from prior biological knowledge/literature (12). In this study, we sought to identify the connectivity of inflammatory mediators directly from clinical data, and build a simulatable model that we could connect to clinical outcomes. Our aim was to go beyond the identification of patterns or associations with outcomes, but to identify a set of mediators and plausible mechanistic

interactions that can give rise to the observed inflammatory responses. We argue that the combination of data-driven and mechanistic insight can better inform potential therapeutic strategies. We inferred initial network connectivity from time-courses of serum inflammatory mediators using Dynamic Bayesian Networks (DBN) analysis (see Chapter 2), which identified a core motif of cross-regulating chemokines MIG, MCP-1 and IP-10. Building on the inferred network with biological mechanism and hypotheses, we constructed a logical model of this "chemokine switching" network, which we hypothesize represents the early control module that determines subsequent inflammatory trajectories. We calibrated our model to data from trauma patients with mild, moderate, and severe injury at the population level, and validated it by analyzing its performance on subpopulations with specific initial conditions. Importantly, we were able to connect differences in the time to resolve inflammation in the model to differences in LOS between moderate and severe injury groups.

3.1.2 Boolean Modeling Background

Mechanistic models can be classified according to the treatment of the variables as either continuous or discrete. However, continuous models, usually described by a set of differential equations, require parameterization of the kinetics of interactions. The interactions among inflammatory mediators that we study are abstracted interactions that function through several layers of signal transduction and gene regulation on different cells that ultimately leads to the production/activation of the target mediator. Thus, there are no measured biochemical parameters that define the rate or particular form of dependence between mediators. Discrete models, such as

Boolean modes (111-113), require little parameterization while providing a qualitative description of dynamics, and are thus well suited for such less-characterized systems.

In Boolean models, each node (variable) can have only two values: 0 (OFF), indicating a below-threshold level of activity that is unsufficient to affect downstream nodes, and 1 (ON) which indicates an above-threshold activity. The logical model is defined by rules that determine the value of an element in relation to values for its effectors at the previous time step. An example of a Boolean network with corresponding rules is shown in Figure 3.1 A-B. For instance A* = B OR C (following the convention of Albert et al (114)) indicates that the value for A at the present time t will be 1 if either B or C had value 1 in the previous time step, or 0 if both B and C had value 0 in the previous time step. It is not always clear whether interactions should integrate with AND or OR logic, and in the absence of experimental evidence, one may permute through several variants of the Boolean rules and compare the behavior of the resulting systems with real data to decide which is best.

A Boolean model may be simulated with either synchronous or asynchronous update algorithms. Synchronous models assume that all nodes are updated at the same time, whereas asynchronous models update nodes in variable order. While synchronous models are always deterministic, asynchronous models may be stochastic if the update order is chosen to be random (115, 116). The state of the whole system is expressed as a vector of individual node states, and by reporting the system state at each time step and mapping the allowed transitions between them, one can obtain a "state transition diagram". This diagram shows how the system evolves over time for all possible states. As an example, the state transition graphs for synchronous and random asynchronous update schemes are shown in Fig 3.1 C-D. The long term behavior of the system is described by attractors, which may either be fixed point steady state vectors or oscillatory

(complex attractors) (Figure 3.1 C-D nodes marked in yellow). Although fixed point attractors are common to synchronous and asynchronous techniques, it may be possible for complex attractors to exist in only one (generally synchronous). Boolean models have been successfully applied in the numerous settings of both gene regulation and signal transduction(117). In this study, we use a discrete logical model to qualitatively model the possible trajectories of inflammatory mediators with an emphasis on identifying different dynamics and/or steady states of the response.

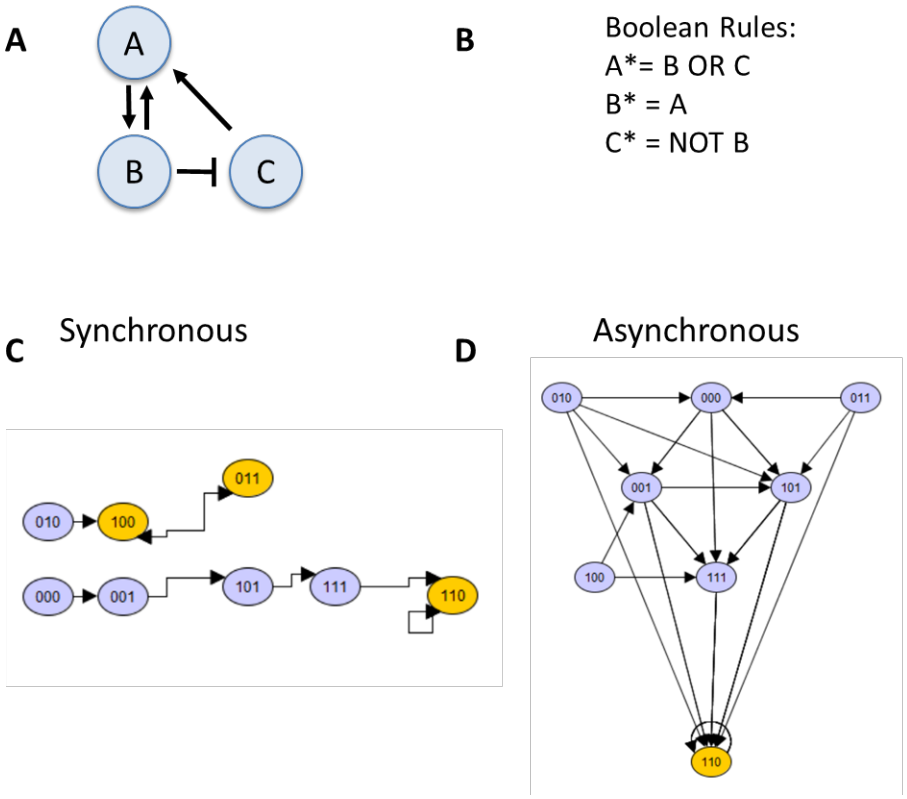

Figure 3.1 Example Boolean Network

3.1.3 Methodology

From a cohort of 484 blunt trauma survivors that were studied following IRB approval, 49 mildly injured, 49 moderately injured, and 49 severely injured patients were matched according to age

and gender distribution (Table 3.1). Serial blood samples were obtained from all patients (3 samples within the first 24 h and then from days 1 to 7 post-injury). The number and span of time points sampled for each patient varied, but all patients had at least three time points, all within the first 24 hours. Since we are focusing on how early events control the trajectory of inflammation, we include patients who don't have data for later time points, as the networks inferred will reflect the early events that we are focusing on. The methodology for inferring DBNs is detailed in Chapter 2 of this thesis.

Table 3.1 Demographics of human trauma patients

	Mild (n=47)	Moderate (n=47)	Severe (n=47)
Age	42 ±1.9	42 ±1.9	42 ±2.6
Gender	M=32 F=15	M=33 F=14	M=32 F=15
ICU LOS*	3.2 ±0.4	6.0 ±1.3	9.8 ±1.1
Total LOS*	9.7 ±1.2	11.1 ±0.9	17.8 ±1.6
Ventilation days*	1 ±0.3	3.3 ±1.5	6.1±0.9
ISS*	10.6 ±0.4	19.7 ±0.5	32.4 ±1.0

To study the properties of the core chemokine network motif, we started our logical model with only MIG, MCP-1 and IP-10 elements. We connected the model to injury severity as the

initiating event, and IL-6 as a key output cytokine in order to compare the inflammatory dynamics observed in different groups of trauma patients. The elements in the model were connected as inferred in the DBNs. Edges were assigned as stimulating or inhibiting based on plausible mechanisms upon reviewing the literature, and fine-tuned to reproduce observed cytokine trajectories. Logic rules that defined the combination of multiple inputs were chosen in a similar fashion.

We started all elements as strictly two-state Boolean variables, except injury severity which needed to have three states to represent mild, medium and severe injury. However, in order to reproduce the clinical data and avoid spurious oscillations, MCP-1, IP-10, and IL-6 were modified to have three states as well. Three-state elements were encoded by splitting their corresponding variables to "high" and "low" variables, the sum of which gives the final state for that element. Model simulations were run with synchronous updates and fixed injury severity but random initial conditions for all other variables, in order to mimic the variability of initial cytokine and chemokine values observed in the patient population. Since the initial states were specified as "random", we ran 1000 simulations to ensure that we covered all possible permutations of initial states. Results are presented as mean and standard deviation of the 1000 simulations. The model was encoded and run using Booleannet (114).

3.1.4 Results

We first selected three groups of trauma patients matched for age and gender distribution but differing in severity of injury (Table 3.1). As expected, outcomes were worse with increasing level

of injury. We then sought to compare the dynamic networks of inflammation across these groups. Network inference by DBN showed a consistent core motif across all three groups involving the chemokines MIG, MCP-1 and IP-10 with cross-regulation between them (Fig 3.2 A-C). The interactions among cytokines in our model are not reaction mechanisms but rather representative of effects that involve activation and recruitment of cells as well as the intracellular signaling and gene regulation leading to changes in expression/secretion of target cytokines. Accordingly, and due to the absence of quantitative data to parameterize a reaction network model, we chose to construct a logical model. In contrast to reaction network models that are most often constructed as systems of differential equations, logical models do not require quantitative parameters. In this approach, the network elements are represented with discrete variables, and interactions are defined by logical rules. The resulting model allows exploration of dynamical and steady state behavior while providing qualitative comparison to experimental data.

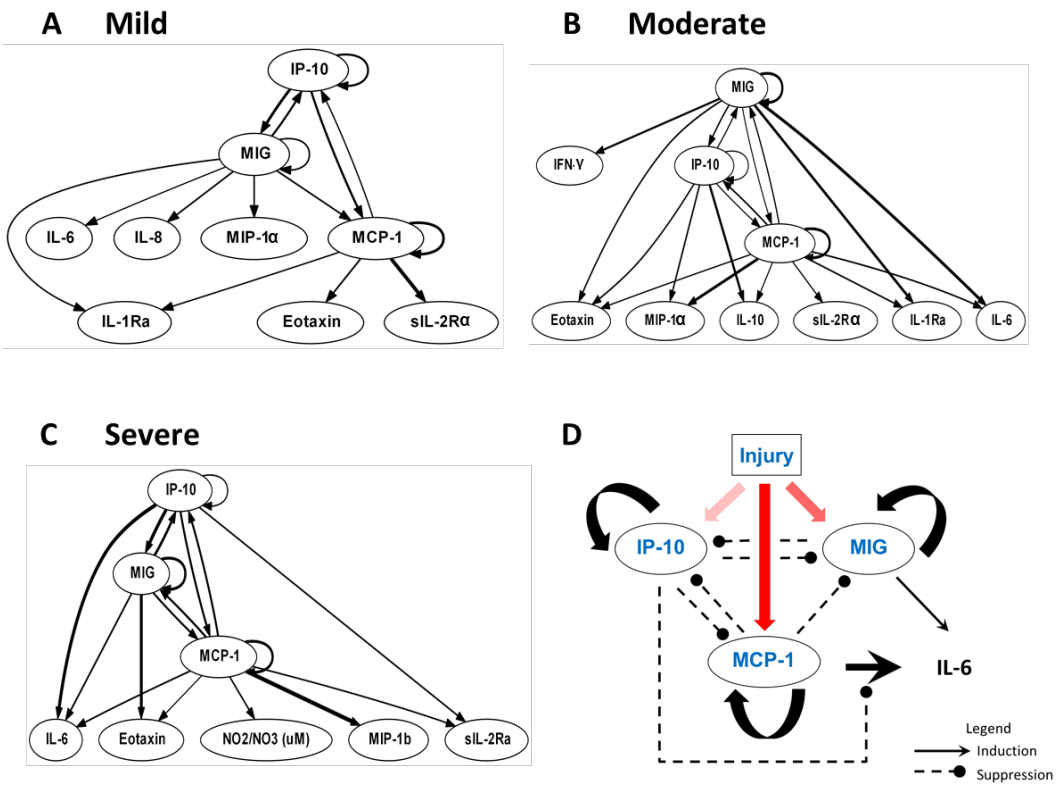

Figure 3.2 A-C **DBN for Mild, Moderate and Severe Injury.** D **Boolean model structure**

To understand the dynamics of this core network, we constructed a discrete logical model based on these interactions with the addition of injury as a stimulus element and IL-6 as a putative output cytokine (Fig 3.2 D). Previous studies have shown that these chemokines can be activated either directly by infection and injury or indirectly through other cytokines like IFN-gamma. Because the parameters are integrated out during DBN structure learning, we can only translate the directionality of the interactions but not the sign (activation or inhibition). When constructing the logical model, we initially labeled the sign based on plausible mechanism from the literature and our own hypotheses. The labels were then adjusted as needed in order to recapitulate the clinically observed trajectories of the model elements. A similar approach was employed to deduce

the logical rules governing combinations of interactions. Thus, the model was calibrated to reproduce the observed population behavior of moderately and severely injured patients.

The final set of rules for the Boolean model is given in *Appendix B.1*. Briefly, moderate injury induces IP-10 and MIG, while severe injury induces these as well as MCP-1. IP-10 has positive feedback on itself and both MIG and MCP-1 must be active (have value "1" or higher) to suppress IP-10. MCP-1 can be induced either by high injury alone, or itself, but high IP-10 suppresses this self-feedback. MCP-1 can reach high levels only in the combination of high injury, moderate MCP-1 and lack of high IP-10, i.e. self-feedback is not sufficient to reach high MCP-1 levels. Thus, the model rules clearly dictate that MCP-1 can only reach high levels in severe injury and also that as long is injury is severe, MCP-1 will remain at least at moderate levels even with high IP-10 (Figure 3.3A). MIG has self-feedback but is suppressed when both IP-10 is high and MCP-1 is active. IL-6 is activated by both MIG and MCP-1 but high IL-6 is induced only by MCP-1 and suppressed by high IP-10. When all elements are initialized to zero, they remain at zero (Figure 3.3B). When injury is set to moderate, IP-10 rises to high while all other variables remain at zero (Figure 3.3C). When injury is set to severe, IP-10 rises to high while both MCP-1 and then IL-6 rise to high before dropping back down to a moderate level at steady state (Figure 3.3D).

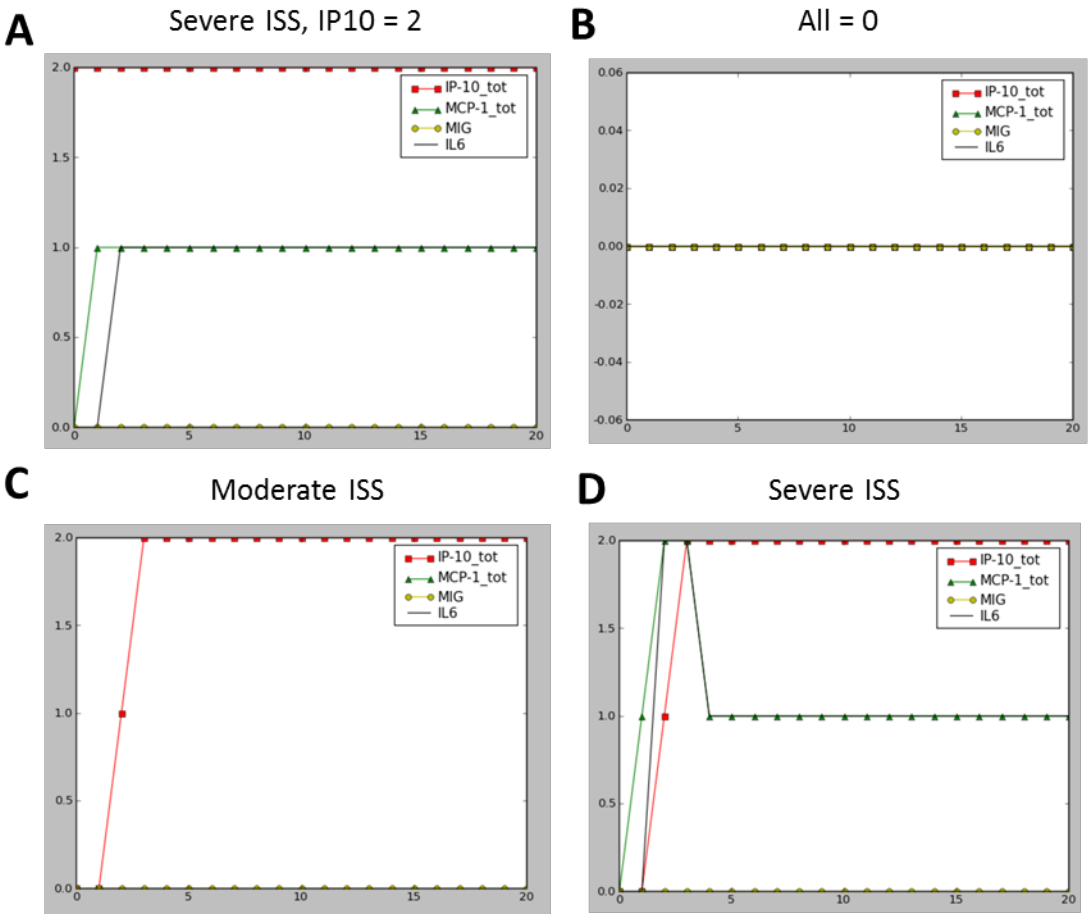

Figure 3.3 General behavior of model for different baseline initial conditions.

To mimic a population of patients starting with random baseline values of each of the cytokines, the model was next simulated with random initial conditions. Our simulations matched qualitatively with the clinical data, and importantly, were able to capture the key differences between MCP-1 and IL-6 trajectories of moderately and severely injured patients (Figure 3.5A-B vs 3.5A-B). In patients, IL-6 levels remained higher for up to day 3 in severely injured patients (Figure 3.5B) whereas they returned to near baseline values within the first 24 hours in moderately injured patients (Figure 3.5B). Correspondingly in the simulations, IL-6 reached a steady state at

low levels within the first 5 time-steps for moderate injury, whereas it spiked and maintained at higher levels until reaching steady state at 6 time-steps for the severe injury case. Notably, the IL-6 trajectory in the simulations maintained at a medium steady state whereas in the patients it did come down to baseline once again. For MCP-1 we observed a monotonic decrease to a lower level in moderately injured patients whereas there was a sharp spike and settling at a higher level for severely injured patients. Accordingly, the simulations for MCP-1 showed the same behavior. MIG and IP-10 trajectories did not differ qualitatively between moderate and severe injury groups and the simulations matched closely with them. However, the simulations for IP-10 showed a monotonic rise to a steady state high level whereas in the patients, there was an early dip and delayed rise.

In order to address the discrepancy in the IP-10 simulations, we hypothesized an additional node (labeled X) positioned upstream of IP-10 that may delay its induction by injury. We examined both spiky (Figure 3.6A) and sustained (Figure 3.6B) dynamics of element X and observed that the IP-10 trajectory corresponding to the latter most closely fit our clinical data (Figure 3.6C and Figure 3.6D vs Figure 3.6E). We compared this trajectory for element X to the other inflammatory mediators measured and found that it matched most closely to IFN-gamma, the putative inducer of IP-10.

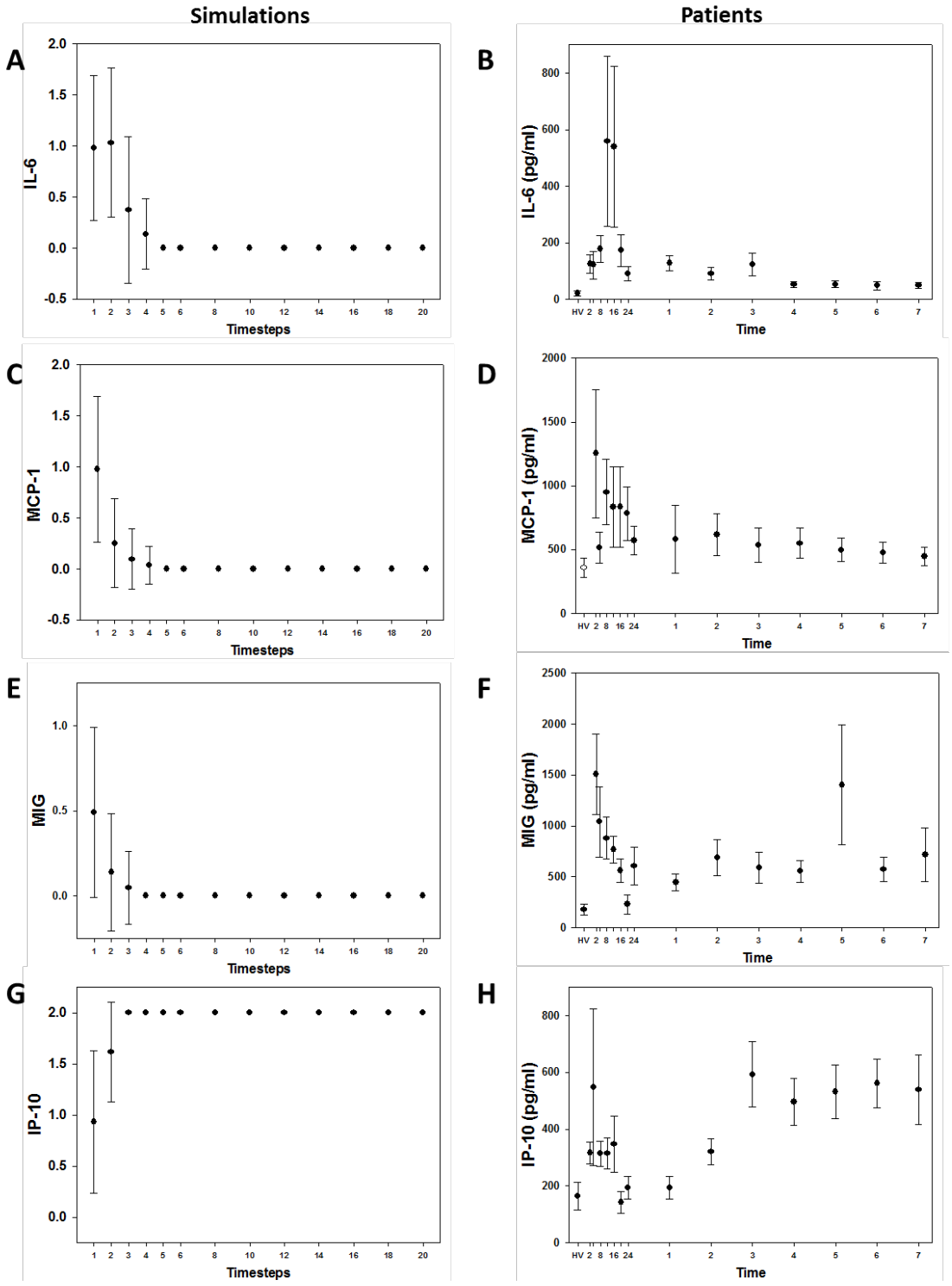

Figure 3.4 Cytokine trajectories for Moderate Injury – Patients vs Simulations

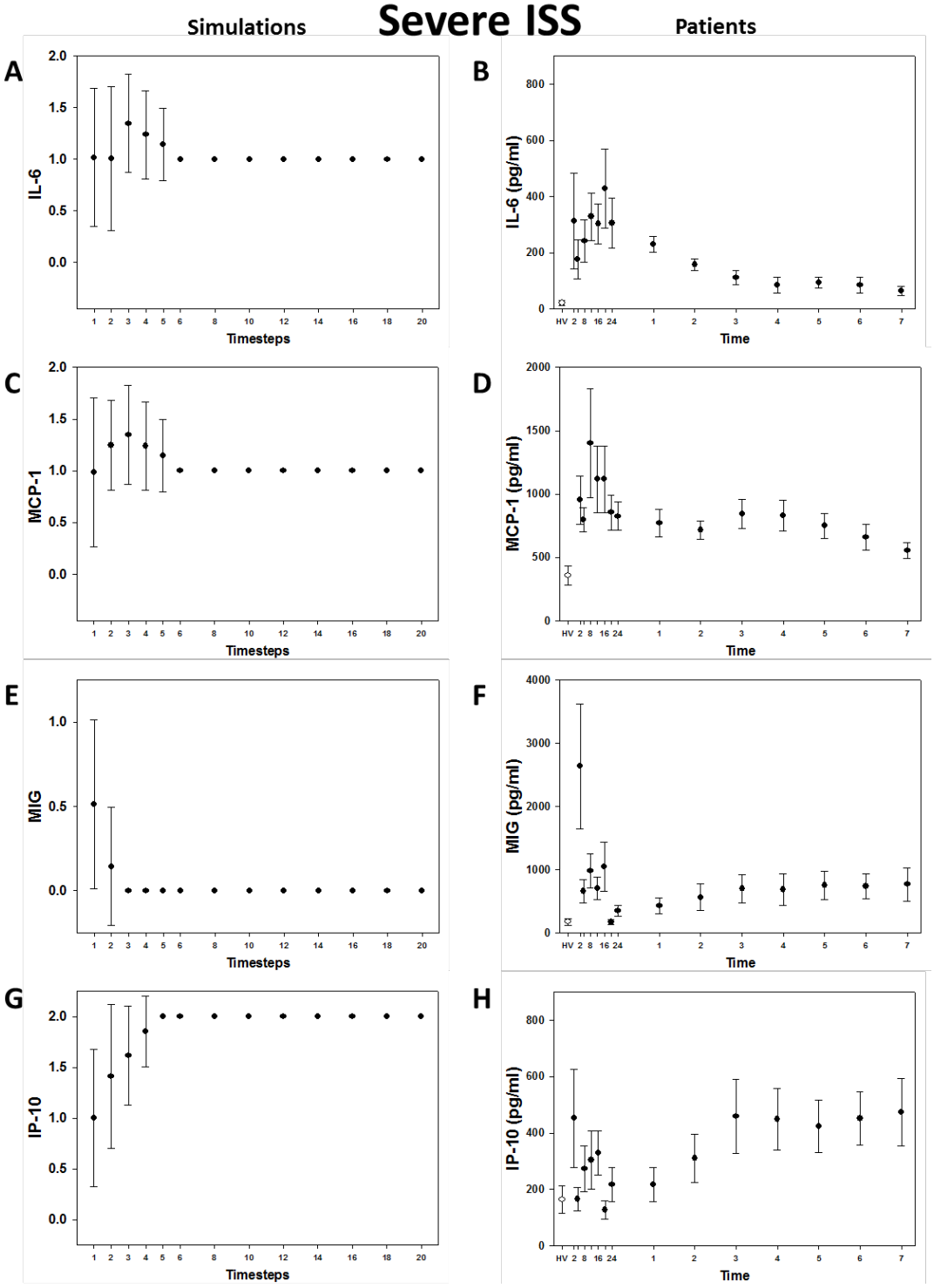

Figure 3.5 Cytokine trajectories for Severe Injury – Patients vs Simulations

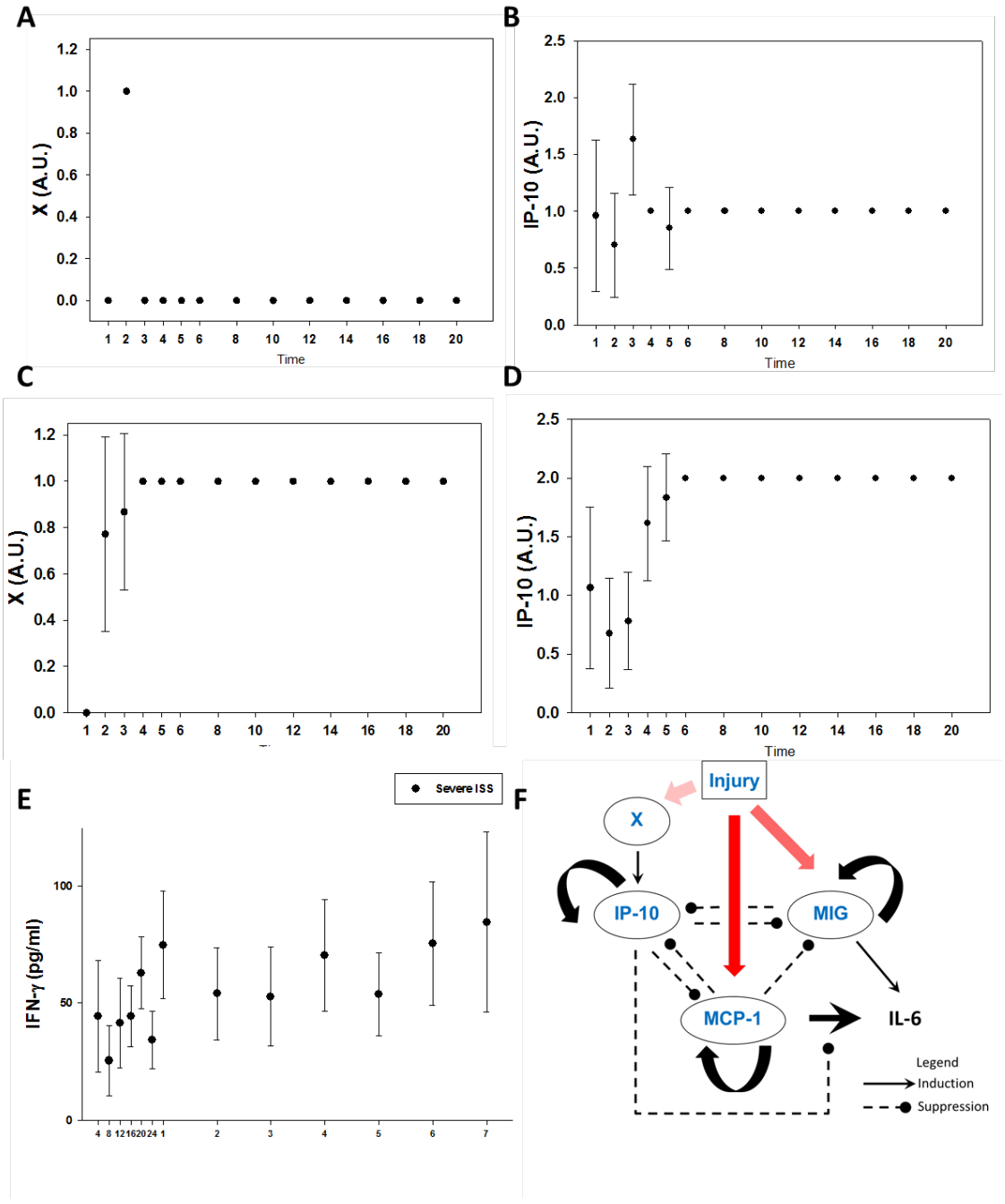

Figure 3.6 Addition of Node X Improves IP-10 Simulations

We next tested whether subpopulations with specific initial conditions also resulted in simulations that matched clinically observed cytokine trajectories. As the model was calibrated to overall population behavior with random initial conditions, we consider this a form of validation. A previous study from our group had shown that trauma patients segregated by MCP-1 levels show significant differences in outcomes. Therefore, we chose the threshold used in that study of MCP-1 levels lower than 1000 pg/ml to correspond to an initial condition of low MCP-1. We compared the responses of patients with low MCP-1 under moderate or severe injury and observed that MCP-1 levels were significantly higher in patients with severe injury compared to moderate injury ($P<0.05$, 2-way ANOVA, Figure 3.7B vs 3.7D). Correspondingly, model simulations showed that under moderate injury, MCP-1 levels remained at a lower level than under severe injury when starting with the same initial condition of MCP-1 low (Figure 3.7A vs Figure 3.7C).

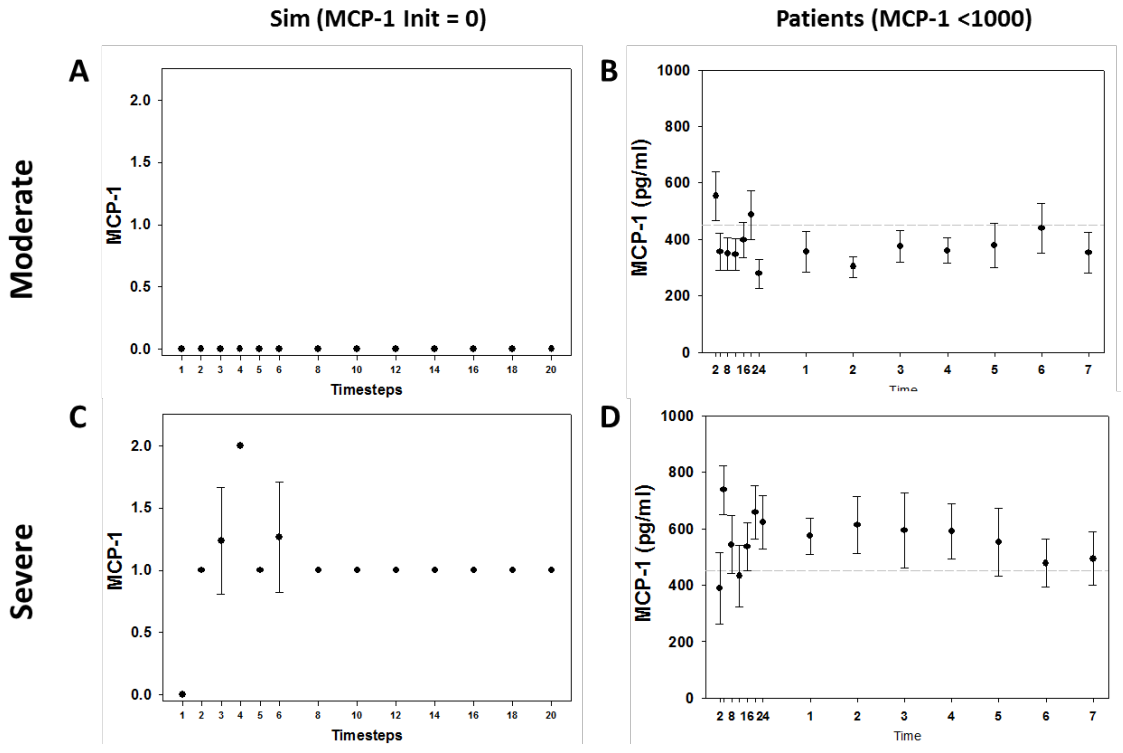

Figure 3.7 Model captures differences in Moderate vs Severe Injury Patients with low MCP-1

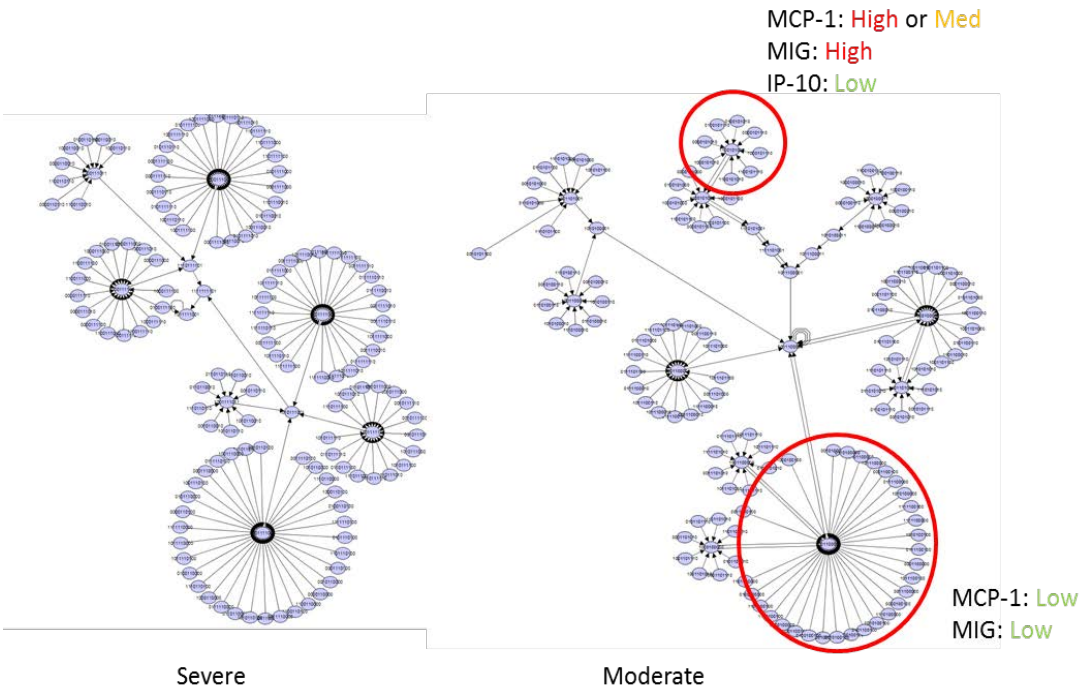

Figure 3.8 State transition graphs for Severe and Moderate Injury Simulations.

Although there was only one steady state for each injury severity, we investigated whether the time to reach that steady state varied depending on initial conditions by examining the state transition graphs for the logical model (Figure 3.8). Our simulations are deterministic, so there is only one path from each initial state to the final steady state. For severe injury, all initial states also take the same number of steps to reach the steady state. However for moderate injury, different clusters of initial states take varying number of steps to reach the steady state. We compared this behavior to patient discharge as a clinical metric analogous to reaching steady state (Figure 3.9). Although we did not observe a sharp time of discharge for severe injury patients as in the simulations, the model was able to capture the earlier discharge of moderate injury patients.

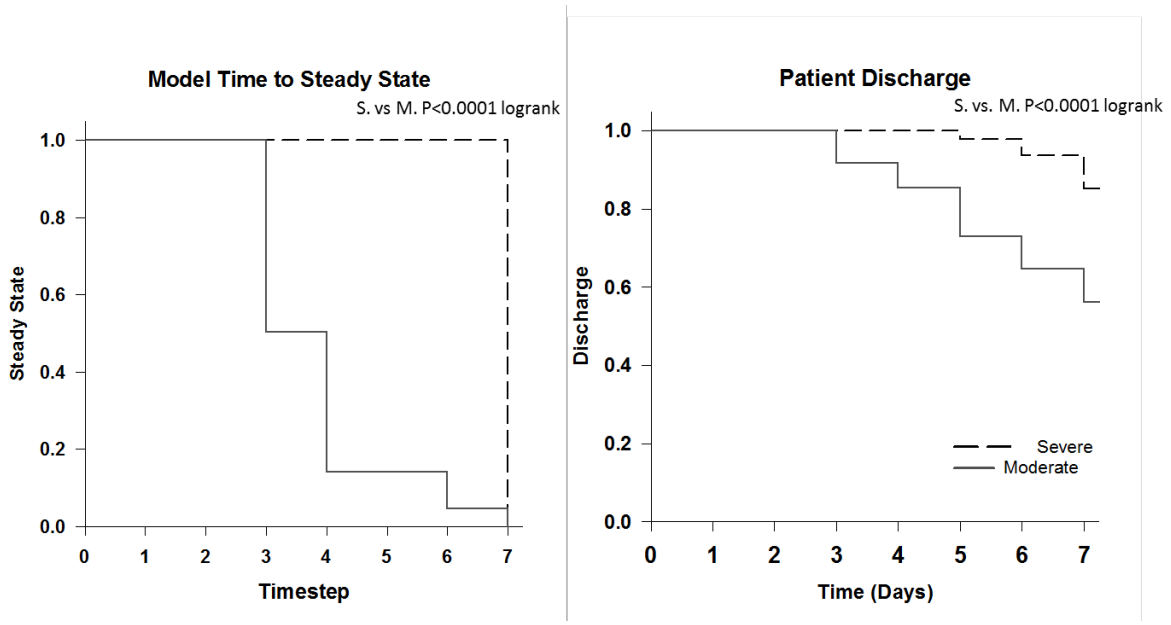

Figure 3.9 Model captures differences in Patient Discharge in Moderate vs Severe Injury Patients

3.1.5 Discussion

Most evidence suggests that either insufficient (7) or self-sustaining (118) inflammation drives the pathobiology of trauma/hemorrhage and subsequent processes such as nosocomial infection-induced sepsis. Acute inflammation due to traumatic injury represents a highly complex and coordinated response. We hypothesized that the coordination of inflammatory mediators early in the response dictates the subsequent trajectory and speed of resolution. By studying demographically matched groups of trauma patients with mild, moderate, or severe injury, we aimed to elucidate the mechanisms by which their corresponding inflammatory responses differed. Accordingly, we applied DBNs to infer the inflammatory networks across injury severity. Our results showed that over a broad range of ISS, the core chemokine motif persists. Interestingly, IL-

6 received more connections as severity of injury increased, i.e. for mild injury IL-6 only received input from MIG, whereas for moderate it was both MIG and MCP-1 and for severe it was MIG, MCP-1 and IP-10. In the absence of experimental perturbations to validate the model, we used trajectories of subgroups to show that the model can capture a range of dynamics that were observed in the patients instead of just the mean behavior that it was calibrated to.

Our most interesting result came from analysis of the state transition diagrams. These suggested that in the setting of moderate injury, initial conditions of the inflammatory mediators can determine how long it takes to reach the (resolving) steady state. In contrast, all trajectories reached steady state at the same time point under severe injury. This suggests that severity of injury may trump individual differences in baseline inflammatory mediators.

There are a number of limitations to this study. The proposed logical model is not the only network that can give rise to the observed data and therefore does not represent a unique solution. Since the network is relatively small, a more rigorous effort to quantify model uncertainty can be made by permuting through all possible Boolean functions based on the network topology (i.e. combinations of AND/OR/NOT logic) and measuring the output of these models compared to the patient data. Alternatively, one may use Probabilistic Boolean Networks to determine the robustness of the model behavior to varying the logical functions encoding interactions (119). In addition, although we are modeling resolution of inflammation, we are not modeling healing. We assume that injury is present throughout and therefore affects the activation of the chemokines equally throughout the time course. Also, resolution of inflammatory mediators as determined by steady state in the model does not necessarily correspond to discharge, as there are many other clinical factors besides inflammatory condition that determine discharge. More work needs to be

done to solidify the connection between the steady state of inflammatory molecules and patient discharge. Lastly, the choice of synchronous updates may not be appropriate for this case. We assume that the events leading to the activation or suppression of one cytokine on another all involve cell migration, signaling, and gene transcription and therefore operate over relatively long timescales and are therefore similar across each cytokine-cytokine interaction. However, it is possible that these cytokines interact in more direct ways as well that may be on faster timescales – indicating that interactions follow a particular order (rank order updates) or take into account stochastic effects (asynchronous updates). Indeed, there is evidence to suggest that the interaction among chemokines may be occurring at the level of competition for shared receptors, a relatively fast process (104, 107, 108). A more thorough characterization of the biochemistry of interactions among cytokines can inform the appropriate choice of update scheme and also help refine the logical rules in the model.

3.2 TRANSFORMING GROWTH FACTOR- Β1 REGULATION BY EXTRACELLULAR NAD^+

This section is taken from a paper published in Journal of Biological Chemistry (120). In this work, we characterized a novel mechanism of induction and activation of TGF-β1 by NAD^+. We characterized the signaling pathway by with NAD^+ mediates this induction through combined experiment and mathematical model refinement. My role in this study was to design and perform experiments in combination with differential equation model design, analysis and refinement in

order to investigate the mechanism for the complex dose and time dependent response of TGF-β1 activation and induction by NAD^+.

3.2.1 Introduction

Inflammation is a complex process in which various potent mechanisms that can control infection, injury, and proliferative diseases must be kept in check (8). Studies over the past decade have focused on the release of damage-associated molecular patterns (DAMPs) from cells, a class of molecules that signal a disruption of cellular homeostasis. Prototypically, these DAMPs are proteins or other cellular constituents that carry out housekeeping functions normally, but are released in settings of stress, inflammation, or injury. In turn, these agents stimulate, propagate, or potentiate both innate and adaptive immune responses (121). Recent studies have suggested that one such mediator may be β-nicotinamide adenine dinucleotide (NAD^+), a ubiquitous cellular constituent that is used by cells as an electron acceptor (or, in its reduced form, NADH, as an electron donor) in a wide variety of enzyme-catalyzed redox reactions. These actions of NAD^+ occur in multiple cell types secondary to the formation of cyclic adenosine dinucleotide ribose (cADPR) from NAD^+, with subsequent release of Ca^{2+} (122). Importantly, NAD^+ has been found to exert a profound anti-inflammatory activity that it appears to share with nicotinamide (123). The mechanisms by which these anti-inflammatory actions are carried out, however, remain poorly understood.

Transforming Growth Factor β1 (TGF-β1) is a cytokine that belongs to a family of three related isoforms, all of which exert crucial biological functions. Of these three isoforms, TGF-β1

is the most prominent in the control of inflammation and immunity (124). The numerous biological functions of all TGF-β's require a set of post-translational modifications termed "activation." The bioactive forms of all TGF-β's are 25 kDa homodimers produced from ~50 kDa monomers that dimerize to form the ~100 kDa TGF-β precursor. This precursor is cleaved intracellularly by furin proteases to yield the 25 kDa active TGF-β dimer, which remains associated with the remaining portion of its own pro-form, the latency-associated peptide (LAP, ~75 kDa). This complex is termed "latent TGF-β,"and is secreted in this form. Other proteins, such as latent TGF-β binding proteins (LTBP, which targets TGF-β's to the extracellular matrix) or α2 macroglobulin (which is associated with circulating TGF-β1) can bind to this complex, creating the so-called large latent complex. Latent TGF-β is activated by a process that involves dissociation and degradation of LAP by proteins (e.g. plasmin and transglutaminase), heat, chaotropic agents, acid, as well as oxygen and nitrogen free radicals. Though TGF-β1 can auto-induce its own expression at the mRNA level, the post-translational control of TGF-β1 through activation is arguably the most potent regulatory mechanism for this cytokine (125, 126).

As early as 1978, an "NAD^+-splitting enzyme" was reported in macrophages (127-129).Since cytokines, radiation, and free radicals can lead to the activation and increased expression of latent TGF-β1 in macrophages (130-133), we hypothesized that extracellular NAD^+ could exert a similar effect. We further hypothesized that the mechanism by which NAD^+ would act would involve the generation of cADPR from extracellular NAD^+. Finally, we hypothesized that cADPR would exert its effects via the stimulation of Ca^{2+}. In order to better understand the complex interplay among NAD^+, cADPR, Ca^{2+}, active and latent TGF-β1, we constructed both

statistical and mathematical models and validated some predictions from these models *in vitro*. These computational models also suggested the existence of as yet unknown mechanisms by which NAD^+ can augment TGF-β1.Taken together, our results demonstrate a novel pathway for TGF-β1 activation via NAD^+ and its metabolites, and highlight the utility of mathematical modeling for discovering novel biological mechanisms.

3.2.2 Methods

3.2.2.1 Cell culture and experimental treatments

RAW 264.7 mouse macrophage-like cells (American Type Culture Collection, Manassas, VA) and primary peritoneal macrophages isolated from C3H/HeJ (TLR4-mutant, n=8 animals) and C3H/HeOuJ (wild-type controls for C3H/HeJ, n=8 animals) mice (The Jackson Laboratory, Bar Harbor, ME) were cultured and plated in DMEM + 1% FBS containing L-glutamine and penicillin/ streptomycin. The FBS used was previously determined to have the lowest levels of TGF-β1 of various manufacturers and lots (data not shown), in order to minimize the exposure of cells to TGF-β1 that could auto-induce further expression of TGF-β1. The cells were cultured in 1% FBS since this was the lowest concentration of serum that allowed for cell proliferation while minimizing exposure to TGF-β1. The passage number was kept <18 for the same reason: as the passage number increased, the basal immunocytochemical expression of both active and latent TGF-β1 increased (data not shown). The cell culture and semi-quantitative immunocytochemical detection of active and latent TGF-β1 have been described previously (134). In brief, the cells were plated in eight-well Lab Tek™ Chamber Slide™ tissue culture plates (NalgeNunc

International, Rochester, NY), which allowed for several experimental conditions per well and also for immunocytochemistry at the end of the culture period. The cells were plated at a concentration of 2x105 cells/ml in 500 µL and were maintained in 5% CO_2 in a humidified atmosphere until adherent. The cells were then treated with either NAD^+ or 3-cADPR, in the presence or absence of other pharmacological agents, and analyzed for active/latent TGF- β1 as indicated. In those experiments where Ca^{2+} antagonists were used, the medium was removed before further treatment with the Ca^{2+} agonists or NAD^+ as indicated. For time-course experiments, the cells were treated with NAD^+ and were left to incubate at 37°C for 1, 2, 6, 8, 12, or 24 h and then processed for immunocytochemistry as described previously (134). Each treatment was carried in duplicate, in order to allow for the eventual parallel immunocytochemical detection of active and latent TGF- β1 (see below).

3.2.2.2 Immunocytochemistry

In previous studies on TGF-β1 activation in macrophages, we utilized dual immunofluorescence to detect active vs. latent TGF-β1 (132, 135). However, we found that NAD^+ caused macrophages to auto-fluorescence in a dose-dependent manner, and this artifactual effect confounded our ability to detect active and latent TGF-β1 (data not shown). Accordingly, we carried out separate immunostaining for active and latent TGF-β1 using the DAB method, as described previously (134). In brief, at the conclusion of the incubation period, the cells were fixed in 70% ethanol for 30 min. Endogenous peroxidases were inhibited using 0.3% hydrogen peroxide solution for 30 min. Non-specific antibody reactivity was blocked as follows. The wells that were stained for active TGF-β1 were blocked with 1.5% goat serum, while the wells stained for latent TGF-β1 were

blocked with 1.5% rabbit serum; all blocking was performed for 20 min. The cells were then incubated with primary antibody specific for either active TGF-β1 (chicken anti-human active TGF- β1) or latent TGF-β1 (goat anti-human latent TGF-β1) for 30 min. The cells were then incubated with secondary antibodies as follows. For wells being stained for active TGF-β1, the secondary antibody solution consisted of approximately 0.5% goat anti-chicken antibody, mixed with 1.5% goat serum and 1 mL PBS. For wells being stained for latent TGF-β1, the secondary antibody solution consisted of 0.5% rabbit anti-goat antibody mixed with 1.5% rabbit serum and 1 mL PBS. The incubation time for the secondary antibody was 30 min. The cells were then exposed to the ABC enzyme conjugate for 30 min, after which they were stained with a diaminobenzidene (DAB) brown stain for 90 sec. The cells were then incubated with a hematoxylin blue counterstain for 20 sec. The slides were then dehydrated and cleared in a series of graded ethanol solutions (one wash in 70%, two washes in 95%, and two washes in 100%), followed by one wash in xylene. The slides were then dried overnight and mounted with Permount™ (Fisher Scientific, Pittsburgh, PA).

3.2.2.3 Quantification of immunocytochemistry

Quantification of active/latent TGF-β1 immunostaining was carried out as described previously (134). In brief, three images from each well were captured using a Zeiss Axioskop 40 (Göttingen, Germany) equipped with a digital camera and Motic Image 2000® software. The images were captured at 400x magnification, and were analyzed using the Image J™ 1.35c freeware (NIH, Bethesda, MD) and the Color Inspector 3D plugin. Since the two primary colors in each picture

were brown and blue, data were gathered using a brown to blue ratio. Due to the DAB brown stain, the color brown indicated presence of TGF-β1, while the color blue, from the hematoxylin counter-stain, indicated the absence of TGF-β1. We used the histogram setting in Color Inspector 3D in order to cluster similar color values, thus simplifying the quantification process. We then determined different values to mean "blue" or "brown" and counted the percentage of the screen taken up by pixels that fell under the "blue" category or the "brown" category. The ratio of brown positive/blue positive cells in 2-3 fields per image was calculated utilizing the following formula:

Brown-to-blue ratio = (Sum 2-3 fields brown/Sum 2-3 fields blue) x 100 [%]

Each complete immunocytochemistry assessment was repeated at least three times/experiment and the mean brown positive/blue positive ratio was calculated. A higher brown-to-blue value indicates a higher cell-associated expression of either active or latent TGF-β1. In some experiments, the final values for active or latent TGF-β1 were determined as fold change (vs. non-treated control cells) ± SEM of at least three independent experiments as indicated.

3.2.2.4 Northern Blot analysis

Total RNA was isolated from treated and control RAW 264.7 cells using an UltraSpec™ RNA isolation reagent from Biotecx Laboratories, Inc. (Houston, TX). Northern blot analysis of TGF-β1 mRNA levels was carried out using a 1.6-kb TGF-β1 cDNA probe derived from the mouse full-length sequence (Image clone #3586216 from Invitrogen, Carlsbad, CA, Accession #BC013738) after Xba 1 and Sal 1 digestion as described previously (134). This probe cannot distinguish between active and latent TGF-β1.

3.2.2.5 Statistical analysis

All data are presented as means ± SEM of n number of independent experiments as shown in each Figure Legend. Unless otherwise indicated the data were analyzed by one-way analysis of variance (ANOVA) followed by a post hoc test (Student-Newman-Keuls Method) as appropriate using SigmaPlot for Windows Version 11.0 (Systat Software Inc., San Jose, CA).

3.2.2.6 Statistical model

A statistical model was generated from the dose-curve and time-course data. The responses of active and latent TGF-β1 could be explained by two independent variables, concentration of NAD^+ (values of 0, 10, 100 or 1000 μM) and time (values of 1, 2, 4, 6, 8, 12, or 24 h). At each (concentration, time) pairing, 5-7 independent observations (experimental repeats) were ultimately obtained; some outliers were omitted. These responses were modeled as a bivariate Gaussian vector, and the explanatory (independent) variables were interpreted as ordered factors. Orthogonal polynomial contrasts were used as columns of the factorial design matrix. Various possible model choices were explored, and second-degree polynomial fits with interactions provided a good explanation of the data. Specifically, we allowed linear and quadratic effects in concentration and time, as well as possible interactions between these effects.

3.2.2.7 Differential equation model

The system was modeled in Matlab® using ordinary differential equations (ODEs) with mass action kinetics for the following 7 variables: N (NAD^+), C (Ca^{2+}), Tl (Latent TGF-β1), Ta (Active TGF-β1), Tm (TGF-β1 mRNA) and X1 and X2 (unknown intermediaries). All variables were

presumed to have exponential decay rates. In addition, the following interactions were included in the ODEs:

- NAD^+ is consumed to produce Ca^{2+}
- Latent TGF-β1 is produced by translation from TGF-β1 mRNA and consumed by the Ca^{2+} catalyzed conversion to active TGF-β1
- Active TGF-β1 is produced by the Ca^{2+}-catalyzed conversion from latent TGF-β1, and is consumed by a threshold-dependent constant rate
- The variables X1 and X2 represent a conglomeration of the intermediary steps going from NAD^+ signaling to TGF-β1 mRNA induction
- X1 is produced according to a Hill function of NAD^+ and X2 is produced by X1
- TGF-β1 mRNA is subsequently produced by X2

The parameters of the model were estimated manually such that the latent TGF-β1 response becomes dose-dependent at approximately 12 h, as observed experimentally.

3.2.3 Results

3.2.3.1 NAD^+ increases the expression of active and latent TGF-β1 in RAW 264.7 macrophage-like cells

We first tested the hypothesis that treatment of macrophages with extracellular NAD^+ would lead to increased expression of both active and latent TGF-β1 in macrophages, utilizing the RAW 264.7 mouse macrophage-like cell line. Various studies have suggested that the activation of latent TGF-β1 is often best assessed immunocytochemically (132-134), and so we utilized this method initially. In prior studies (134), we have shown concordance between immunoblotting and this

immunocytochemistry-based method of differential detection of active vs. latent TGF-β1. As shown in Fig. 3.9, treatment with 10-1000 μM NAD^+ for 2 h led to a dose-dependent increase in immunocytochemically detectable latent (Panels B-D) and active (Panels F-H) TGF-β1 compared to control resting cells (Panels A and E).

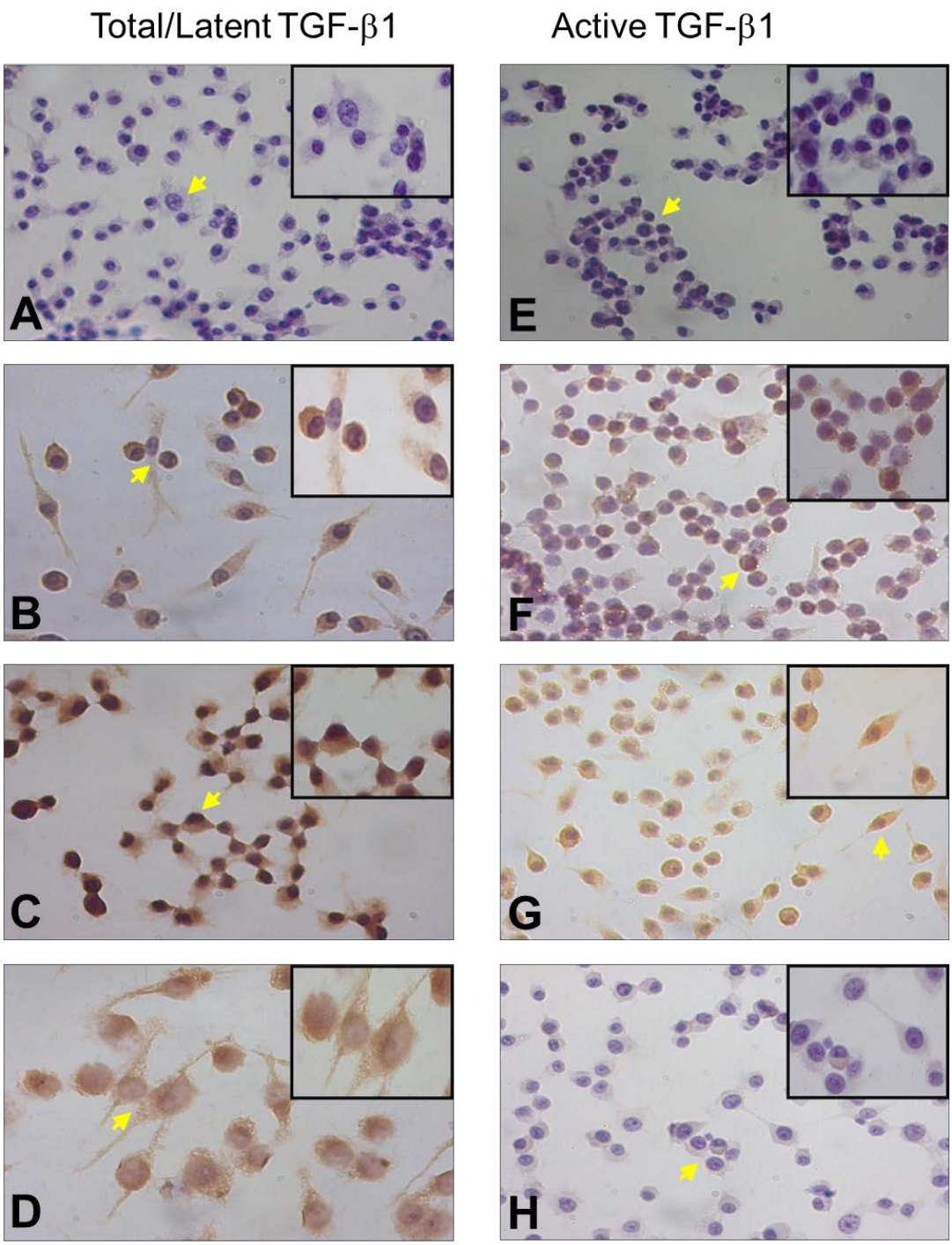

Figure 3.10 Increased expression of active and latent TGF-β1 protein induced by NAD+ in RAW 264.7 macrophage-like cells.

Mouse RAW 264.7 cells were either incubated with medium alone (Panels A and E) or were treated with 10, 100, or 1000 μM NAD^+ for 2 h (Panels B-D and F-H) as indicated, and subsequently immunostained for latent (Panels A-D) or active (Panels E-H) TGF- β1

3.2.3.2 NAD^+ and its extracellular metabolite cADPR increase the expression of active and latent TGF-β1 in primary mouse peritoneal macrophages

We next sought to confirm in primary macrophages the basic finding of NAD^+/cADPR-mediated increase in TGF-β1, and to determine whether or not the effect of NAD^+/cADPR was due to LPS contamination, again using our previously published immunocytochemical method coupled with image analysis and quantification (134).

As seen in Figure 3.10, treatment with either 100 μM NAD^+ or 10 nM of the stable cADPR analog 3-deaza-cADPR (136) for 1 h led to increased active (Figure 3.10A-B) and latent TGF-β1 (Figure 3.10C) in isolated peritoneal macrophages from both wild-type (C3H/HeOuJ) and LPS-hyporesponsive, TLR4-mutant (C3H/HeJ) mice at 1 h post-treatment. Moreover, there were no statistically significant differences between C3H/HeJ and C3H/HeOuJ macrophages with regard to expression of NAD^+/cADPR-induced active TGF-β1 (Figure 3.10B). Taken together, these results show that NAD^+ and 3-cADPR can induce and activate TGF-β1 in primary macrophages *in vitro*, and strongly suggest that LPS contamination is at most an extremely minor contributor to the effects of NAD^+ and 3-cADPR on TGF-β1.

3.2.3.3 The extracellular NAD^+ metabolite cADPR increases the expression of both active and latent TGF-β1 in RAW 264.7 macrophages

As seen in Figure 3.11A, treatment with 100 μM NAD^+ for 2 h led to increased active TGF-β1. To determine if this effect of NAD^+ depends on the prior conversion to cADPR (122), we treated RAW 264.7 cells with NAD^+ in the presence of the stable, cell-permeable cADPR antagonist 8-Br-cADPR (137). As seen in Figure 3.11A, 10 uM 8-Br-cADPR antagonized the effect of NAD^+

on both active and latent TGF-β1. We also observed a significant expression of active (but not latent) TGF-β1 induced by this dose of 8-Br-cADPR, which we hypothesize is due to an off-target effect of this compound.

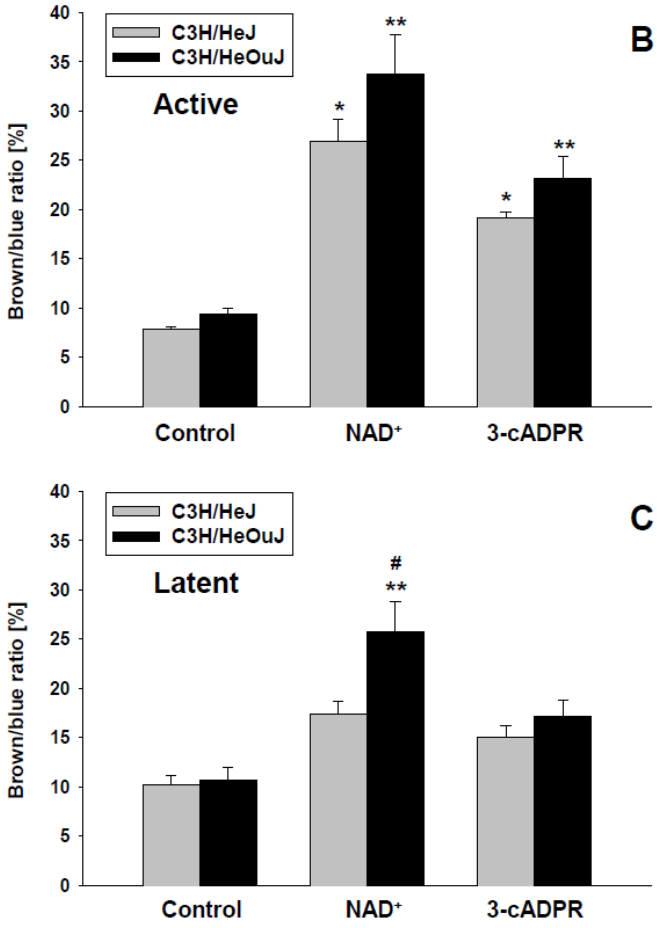

Figure 3.11 Increased expression of active and latent TGF-β1 protein induced by NAD+ and its extracellular cADPR in primary mouse peritoneal macrophages.
Isolated peritoneal macrophages from both wild-type (C3H/HeOuJ) and the TLR4-mutant (C3H/HeJ) mice were either incubated with medium alone (Control) or were treated with NAD+ (100 μM) or the cADPR analogue 3-cADPR (10 nM) for 1 h as indicated, and subsequently immunostained for active (Panels A-B) or latent (Panel C) TGF-β1. (Panel A: *P<0.05 vs. Ctrl HeJ, **P<0.05 vs. Ctrl HeOuJ; Panel B: *P<0.05 vs. Ctrl HeJ, **P<0.05 vs. Ctrl HeOuJ, #P=0.005 vs. NAD+ HeJ, analyzed by one-way ANOVA followed by Tukey test).

We next sought to further define the TGF-β1 response of RAW 264.7 cells to cADPR. As seen in Figure 3.12B, authentic cADPR (10 μM) led to increased expression of both active and latent TGF-β1. Similarly, the stable cADPR analog 3-deaza-cADPR (136) (which is much more stable than authentic cADPR) also led to increased expression of both active (Figure 3.12C) and latent TGF-β1 (Figure 3.12D) at concentrations of 1-50 nM.

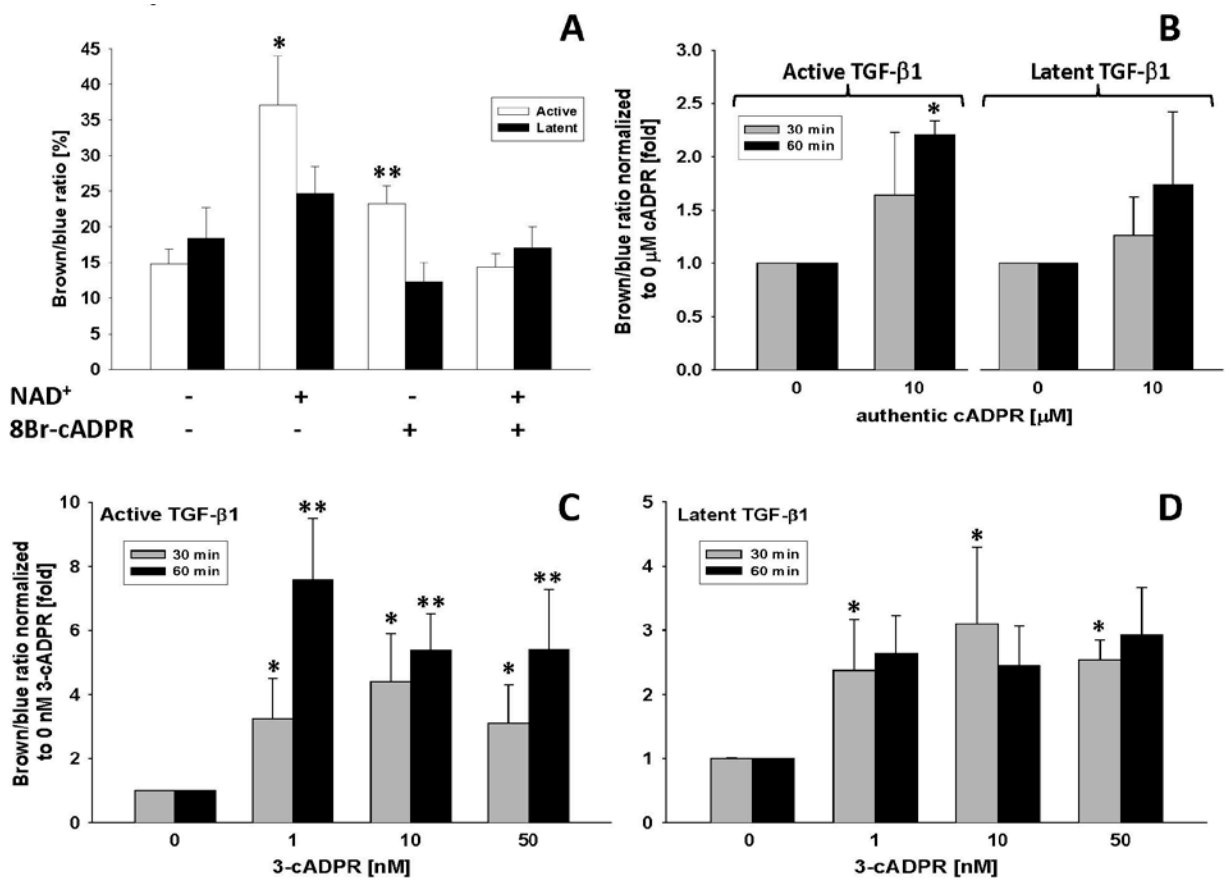

Figure 3.12 cADPR increases the expression of both active and latent TGF-β1.
(**A**) RAW 264.7 cells were treated with 100 μM NAD^+ for 2 h with or without 30 min pretreatment with 8Br-cADPR (10 μM) as indicated, and subsequently immunostained for active and latent TGF-β1 as described in the *Materials and Methods* (n=5, **P*<0.05 vs. Ctrl and NAD^++ 8Br-cADPR, ***P*<0.05 vs. Ctrl and NAD^+ + 8Br-cADPR for active TGF-β1). (**B-D)** RAW 264.7 cells were treated with 10 μM authentic cADPR (Panel **B**) or with 1, 10 and 50 nM 3-cADPR for 30 or 60 min (Panels **C-D**) as indicated, and subsequently immunostained for active or latent as described in the *Materials and Methods.* Panel **B:** n=3, **P*<0.001 vs. 0 μM at 60 min, analyzed by Student's t-test. Panel **C**: n=7, **P*<0.05 vs. 0 nM at 30 min, ***P*<0.05 vs. 0 nM at 60 min; Panel **D**: n=8, **P*<0.05 vs. 0 nM at 30 min).

3.2.3.4 The effects of NAD^+ and cADPR on TGF-β1 require Ca^{2+} mobilization, are mimicked by Ca^{2+} agonists, and are inhibited by Ca^{2+} antagonist

cADPR has been reported to lead to the release of Ca^{2+} from ryanodine-sensitive intracellular stores (122). Accordingly, we further probed this pathway in the response to NAD^+. We found that blocking Ca^{2+} with the Ca^{2+} chelator BAPTA (10 μM) inhibited the activation of TGF-β1 by 100 μM NAD^+ (Figure 3.13A) at 1 h and to a lesser degree at 3 h (Figure 3.13B). Furthermore, treatment with the cADPR analogue 3-cADPR (1 nM, Figure 3.14A), the Ca^{2+} agonists bradykinin (10 μM, Figure 3.14B) or ionomycin (1 μM, Figure 3.14C) for 1 h induced increased active and latent TGF-β1, an effect inhibited by pretreatment for 30 min with the Ca^{2+} chelator BAPTA. The involvement of Ca^{2+} mobilization in the activation of TGF-β1was further investigated using the L-type calcium channel blocker verapamil. We found that pretreatment of macrophages with 100 μM verapamil for 30 min resulted in a significant inhibition of NAD^+-induced activation of TGF-β1 (Figure 3.14D), though this drug had no effect on the immunostaining for latent TGF-β1.

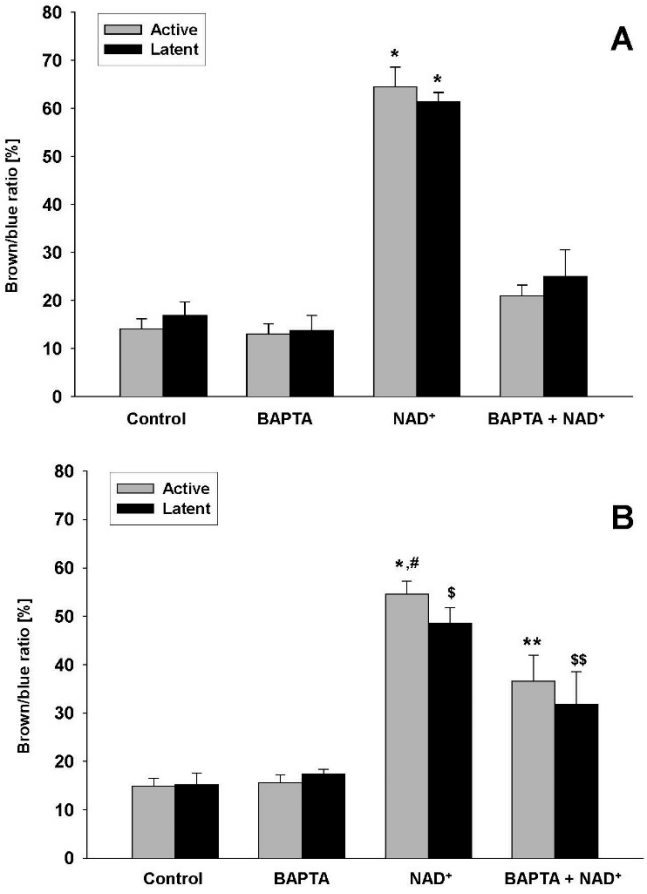

Figure 3.13 The effects of NAD^+ on TGF-β1 are inhibited by Ca^{2+} antagonism.
RAW 264.7 cells were pretreated with or without the Ca^{2+} chelator BAPTA (10 μM) for 30 min followed by incubation in media alone or media containing 100 μM NAD^+ for 1 h (Panel A) or 3 h (Panel B) as indicated. The cells were then immunostained for active and latent TGF-β1 as described in the *Materials and Methods (*Panel A: n=6, **P*<0.001 vs. Ctrl, BAPTA and BAPTA + NAD^+ for both active and latent TGF-β1; Panel B: n=6, **P*<0.001 vs. Ctrl and BAPTA, $^{\#}P$=0.001 vs. BAPTA + NAD^+, ***P*<0.001 vs. Ctrl and BAPTA for active TGF-β1; $^{\$}P$<0.05 vs. Ctrl, BAPTA and BAPTA + NAD^+, $^{\$\$}P$<0.05 vs. Ctrl and BAPTA for latent TGF-β1).

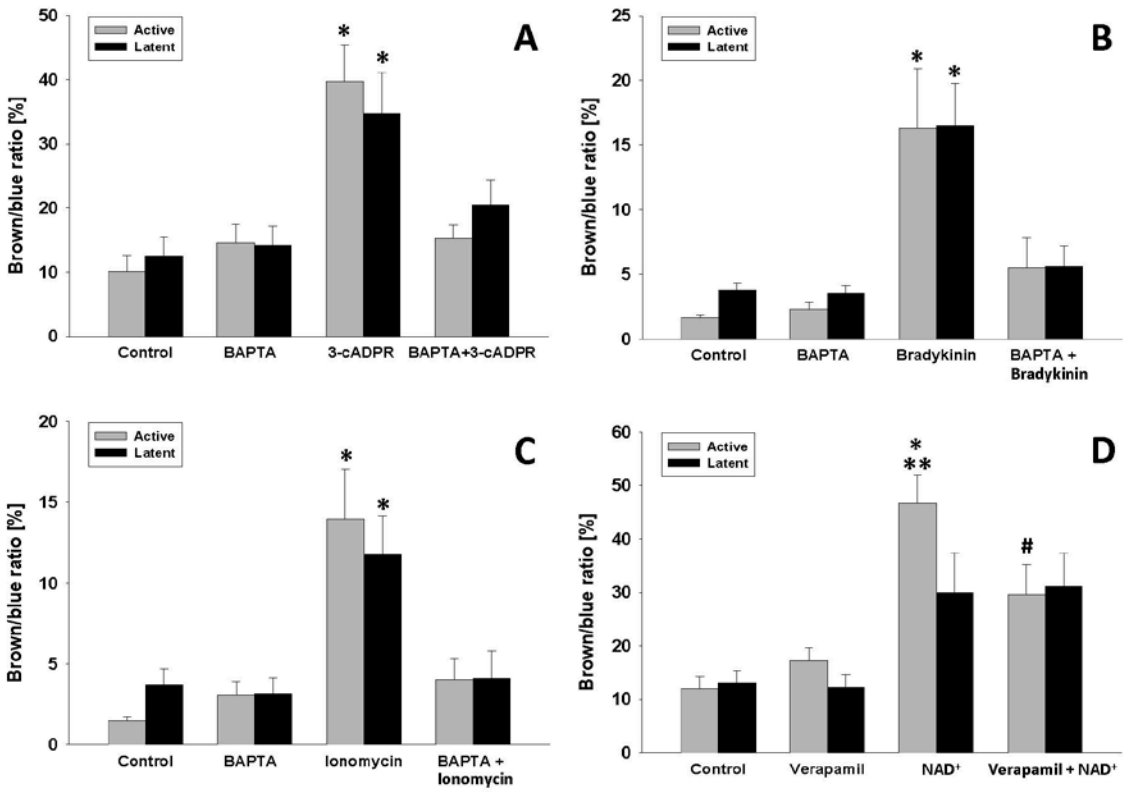

Figure 3.14 The effects of cADPR on TGF-β1 require Ca^{2+} mobilization, are mimicked by Ca^{2+} agonists, and are inhibited by Ca^{2+} antagonism.
RAW 264.7 cells were pretreated without or with the Ca^{2+} chelator BAPTA (5 μM Panel A or 10 μM Panels B and C) or the L-type calcium channel blocker verapamil (100 μM, Panel D) for 30 min followed by incubation in media alone or media containing 1 nM 3-cADPR (Panel A), 10 μM bradykinin (Panel B), 1μM ionomycin (Panel C) or 100 μM NAD^+ (Panel D) for 1 h as indicated. The cells were then immunostained for active and latent TGF-β1 as described in the *Materials and Method* (Panel A: n=12, **P*<0.05 vs. Ctrl, BAPTA and BAPTA + 3-cADPR for both active and latent TGF-β1; Panel B: n=6, **P*<0.05vs. Ctrl, BAPTA and BAPTA + bradykinin for both active and latent TGF-β1; Panel C: n=6, **P*<0.05 vs. Ctrl, BAPTA and BAPTA + ionomycin for both active and latent TGF-β1; Panel D: n=7, **P*<0.001 vs. Ctrl and verapamil, ***P*=0.015 vs. verapamil + NAD^+, $^{\#}P$=0.031 vs. Ctrl for active TGF-β1. One-way ANOVA for latent TGF-β1 resulted in an overall significance of *P*=0.02).

3.2.3.5 The effect of NAD^+ on active and latent TGF-β1 follows a complex dose and time course

We next carried out a detailed dose- and time-course study of the effects of NAD^+ on the immunocytochemically detectable expression of active (Figure 3.15A) and latent TGF-β1 (Figure 3.15D). This study suggested that the effect of NAD^+ on both active and latent TGF-β1 was complex and possibly biphasic. NAD^+ led to the activation of latent TGF-β1 at early time points

(1-2 h), which declined by 6 h and then appeared to rise again towards 24 h. The effect on latent (total) TGF-β1 was similar but shifted in time, with the peak effect of NAD^+ on latent TGF-β1 occurring at 6 h and then declining by 12 h. This study also suggested that the effect of NAD^+ on active TGF-β1 was dose-dependent from 10-1000 μM at late time points (8-24 h) post-stimulation, but peaked at 100 μM and declined at 1000 μM at early time points (1-6 h). The effects on NAD^+ on latent TGF-β1 were similar but again appeared to be shifted in time, with dose-dependent increases of latent TGF-β1 apparent at 1, 12, and 24 h but with a peak at 100 μM at 2-8 h.

3.2.3.6 Statistical and mathematical modeling of the complex effects of NAD^+/cADPR/Ca^{2+} on TGF-β1

To gain insight into the complex dose- and time-courses described above, the responses were modeled statistically (see Figure 3.15B,E) as a bivariate Gaussian vector (see *3.2.2.6*). The expected value of active TGF-β1 was modeled as

$$\mathbf{E(active\ TGF\text{-}\beta1) = 1.74 + 0.75Cl - 0.5Cq + 0.49Tq + 1.07CqTl - 0.8CqTq}$$

Upper bounds on the p-values of these coefficients based on t-tests and read from left to right are, respectively, 0.0001, 0.0001, 0.005, 0.025, 0.015, and 0.068. The model-based estimate for the variance was S^2=1.09 on 142 degrees of freedom. The R^2 was 0.233. The hypothesis that there are no effects whatsoever upon this response was rejected based on an F-test with F-value of 5.38 on 8 and 142 degrees of freedom and a p-value of 0.00000644. From this model, we concluded that active TGF-β1 is significantly influenced primarily by the concentration of NAD^+, which

manifests both linear and quadratic influence, by a quadratic effect of time, and by two significant concentration-time interactions.

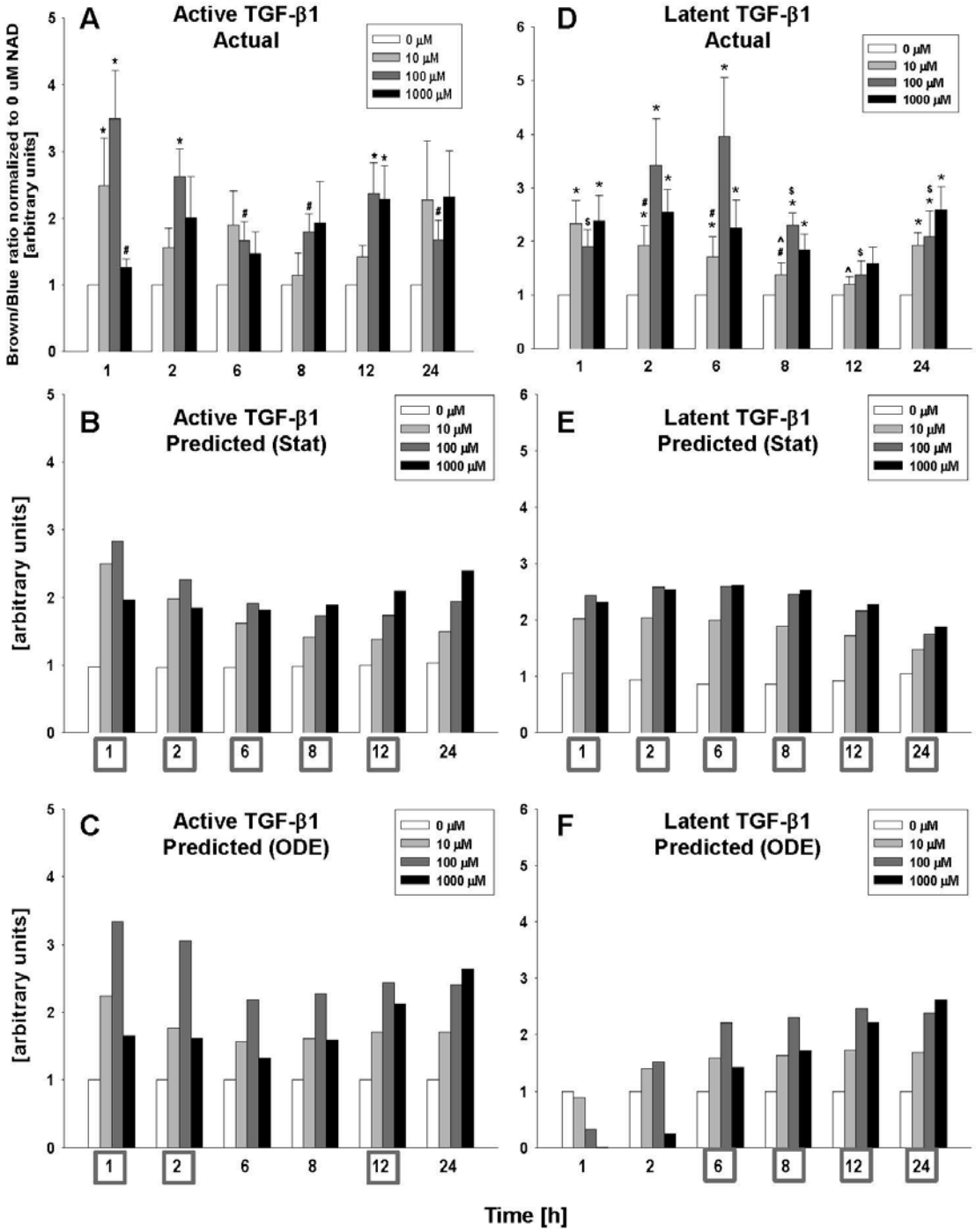

Figure 3.15 Complex dose- and time-course of the expression of active and latent TGF-β1 in RAW 264.7 cells treated with NAD^+.
RAW 264.7 cells were treated with 0, 10, 100, or 1000 μM NAD^+ for 0-24 h as indicated, and subsequently immunostained for active (Panel A) or latent (Panel D) TGF-β1. The results are mean ± SEM of 5-7 experiments. (Panel A: **P*<0.05 vs. 0 μM NAD^+, $^{\#}P$<0.05 vs. 100 μM NAD^+ at 1 h; Panel D: **P*<0.05 vs. 0 μM NAD^+, $^{\#}P$<0.05 vs. 100 μM NAD^+ at given time point, ^*P*<0.05 vs. 10 μM NAD^+ at 1 h, $^{\$}P$<0.05 vs. 100 μM NAD^+ at 6 h, analyzed by one-way ANOVA followed by the Fisher LSD method). Values generated by a Statistical model and a non-linear ODE model are shown in Panels B-C for active TGF-β1 and in Panels E-F for latent TGF-β1. Time-points in boxes (Panels B-F) represent good concordance with experimental data.

Dependence of latent TGF-β1 on NAD^+ was deemed to be simpler, in the sense that interactions between concentration and time were not required in the model. Indeed, in this case we obtained a purely linear dependence. The following equation describes the relationship between latent TGF-β1, NAD^+ concentration, and time:

$$\mathbf{E(\text{latent TGF-}\beta 1) = 1.85 + 0.97Cl - 0.5Cq - 0.35Tl}$$

The analogous p-values, read from left to right, are lower than the respective values of 0.0001, 0.0001, 0.005, and 0.108. The model-based S^2 is 1.08 on 142 degrees of freedom, with an R^2 of 0.238. The hypothesis of no effects of concentration and time upon latent is rejected based on an F-value of 5.554 on 8 and 142 degrees of freedom with a p-value of 0.000004051. This statistical model suggested that the effects of NAD^+ on TGF-β1 were nonlinear and this model was capable of predicting not only the levels of active (Figure 3.15B vs. 3.15A) and latent TGF-β1 (Figure 3.15E vs. 3.15D) but also the biphasic dose effect of NAD^+.

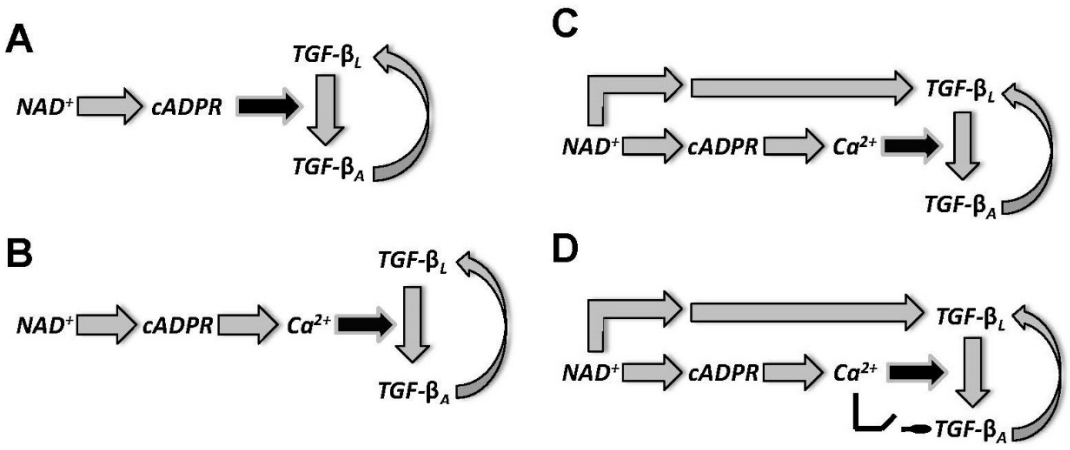

Figure 3.16 ODE Model Refinement.

In order to help define the mechanism by which NAD^+, cADPR, and Ca^{2+} led to the induction and activation of TGF-β1, we sought to create a mechanistic mathematical model of the presumptive interactions among these variables. Based on these data-driven modeling studies, we inferred that the effects of NAD^+ on TGF-β1 are non-linear. Accordingly, we created a non-linear ODE model of interactions we considered the most parsimonious and yet still capable of recapitulating the complex biological phenomena described above. Our initial ODE model included the interactions depicted in Figure 3.16B which shows NAD^+ signaling through cADPR and Ca^{2+} to activate TGF-β1, which can then auto-induce its own mRNA production. However, this initial model was unable to account for the apparent second rise in TGF-β1 observed at the later time-points in Figure 3.15A and 3.15D. Importantly, we sought to include a mechanism by which BAPTA could suppress the NAD^+-induced increase in both active and latent TGF-β1 at 1 h (Figure 3.14A), but to a lesser extent at 3 h (Figure 3.14B), arriving at the model depicted in Figure 3.16C. Simulations from this subsequent model were able to reproduce the experimentally

observed time-dependent response of TGF-β1. This model could account for the timing-based difference in the effect of BAPTA on NAD^+-induced active and latent TGF-β1, but could not recapitulate the attenuated response seen at high dose at the early time-points (Figure 3.15A,D). To explain this phenomenon, we hypothesized a threshold-dependent inhibitory effect of Ca^{2+} on TGF-β1 mRNA, which was included in our final model (Figure 3.16D), described by the following equations:

$$\frac{dN}{dt} = -k_1 N - k_{Nd} N$$

$$\frac{dC}{dt} = k_1 N - k_{Cd} C + \beta_C$$

$$\frac{dT_L}{dt} = -k_{Tld} T_L - k_{act} T_L C + k_{Tln} T_m$$

$$\frac{dT_A}{dt} = -k_{Tad} T_A + k_{act} T_L C$$

$$\frac{dX_1}{dt} = k_X \frac{N^{\propto}}{K^{\propto} + N^{\propto}} - k_{Xd} X_1$$

$$\frac{dX_2}{dt} = k_2 X_1 - k_{Xd} X_2$$

$$\frac{dT_m}{dt} = \beta_m + k_3 X_2 - k_{Tmd} T_m + k_{Tlp} T_A - \delta(C_{tot}, C_{thresh}) k_{neg} C$$

Parameter values for this model were estimated manually and are presented in Table I. An initial simulation was carried out with no NAD^+ input, and the resulting values were used as the initial conditions for each of the subsequent simulations with varying concentrations of NAD^+ input. This procedure allows the system to equilibrate to a steady state before making any perturbations, and corresponds to the culture of RAW 264.7 cells to allow for adherence (Figure 3.17).

Table 3.2 Description of parameter values used for the ODE model.

Parameter	Value	Description
k_1	30/hr	Rate of NAD^+ consumption to form cADPR
k_2	10/hr	Rate of formation of X_2
k_3	1/hr	Rate of formation of TGF-β 1 mRNA from X_2
k_{Nd}	1/hr	Degradation rate of NAD^+
k_{Cd}	1000/hr	Degradation rate of Ca^{2+}
k_{Tld}	56/hr	Degradation rate of Latent TGF-β1
k_{Tad}	12/hr	Degradation rate of Active TGF-β1
k_{Xd}	1.3/hr	Degradation rate of X_1 and X_2
k_{Tmd}	3.9/hr	Degradation rate of TGF-β1 mRNA
k_{act}	1500/Mhr	Rate of activation of TGF-β1
k_{Tln}	15/hr	Rate of translation of TGF-β1 mRNA
k_X	10/hr	Rate of formation of X_1
k_{neg}	4.5/Mhr	Rate of Ca^{2+} -mediated degradation of TGF-β1 mRNA
β_C	12/hr	Basal rate of Ca^{2+} production in cell
β_m	2/hr	Basal rate of TGF-β1 mRNA production in cell
α	1	Hill coefficient for X_1 production
C_{thresh}	1000	Threshold for activation of Ca^{2+} mediated inhibition

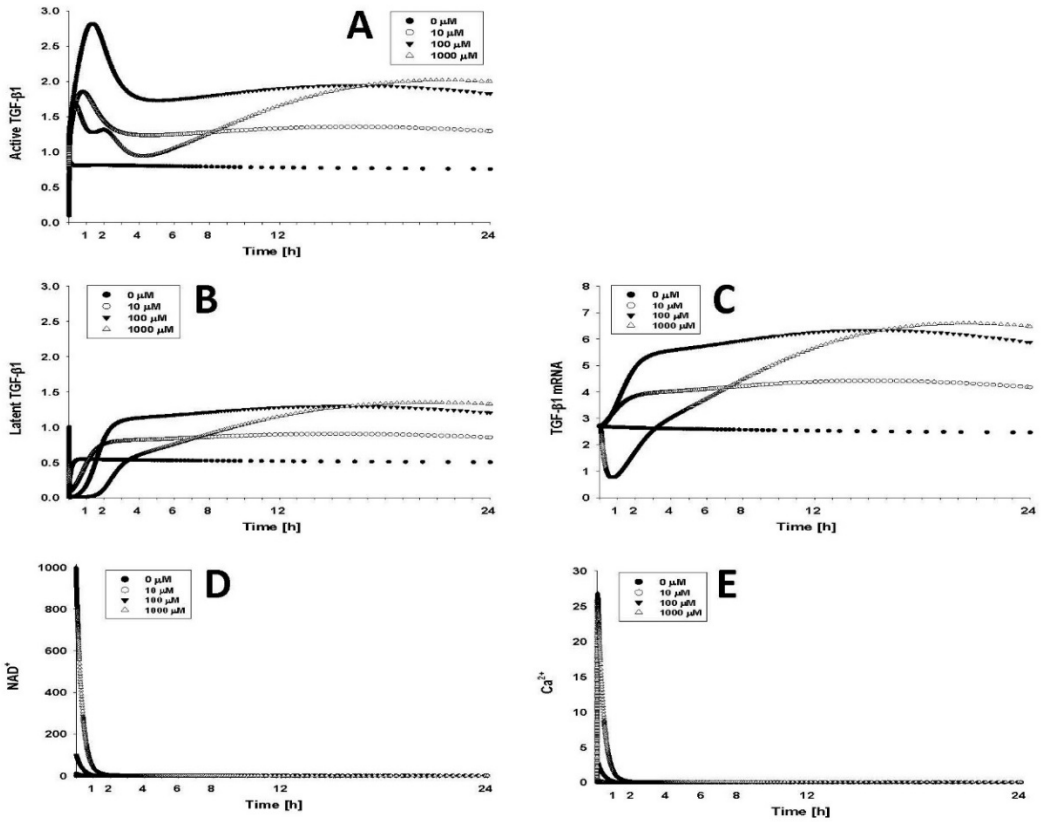

Figure 3.17 Full time courses for simulations of ODE model.

The ODE model simulations were generally in good concordance with experimental data for both active TGF-β1 (Figure 3.15C vs. 3.15A) and latent TGF-β1 (Figure 3.15F vs. 3.15D), although we observed a discrepancy at early time-points (1 and 2 h) for latent TGF-β1 (Figure 3.15 F vs.D).

We next attempted to validate the predictions of both the statistical and ODE models experimentally, at both the protein and mRNA levels. We first subjected RAW 264.7 cells to 10, 100, or 1000 μM NAD^+ for 16 h, a time point not used for the calibration of either model. As seen in Figure 3.18A-B, the statistical model was able to accurately predict the levels of active and latent TGF-β1. The ODE model was able to recapitulate the increase in active and latent TGF-β1 induced by 10 and 100 μM NAD^+, respectively, but was unable to capture the attenuated response to the 1000 μM NAD^+ dose observed at 16 h.

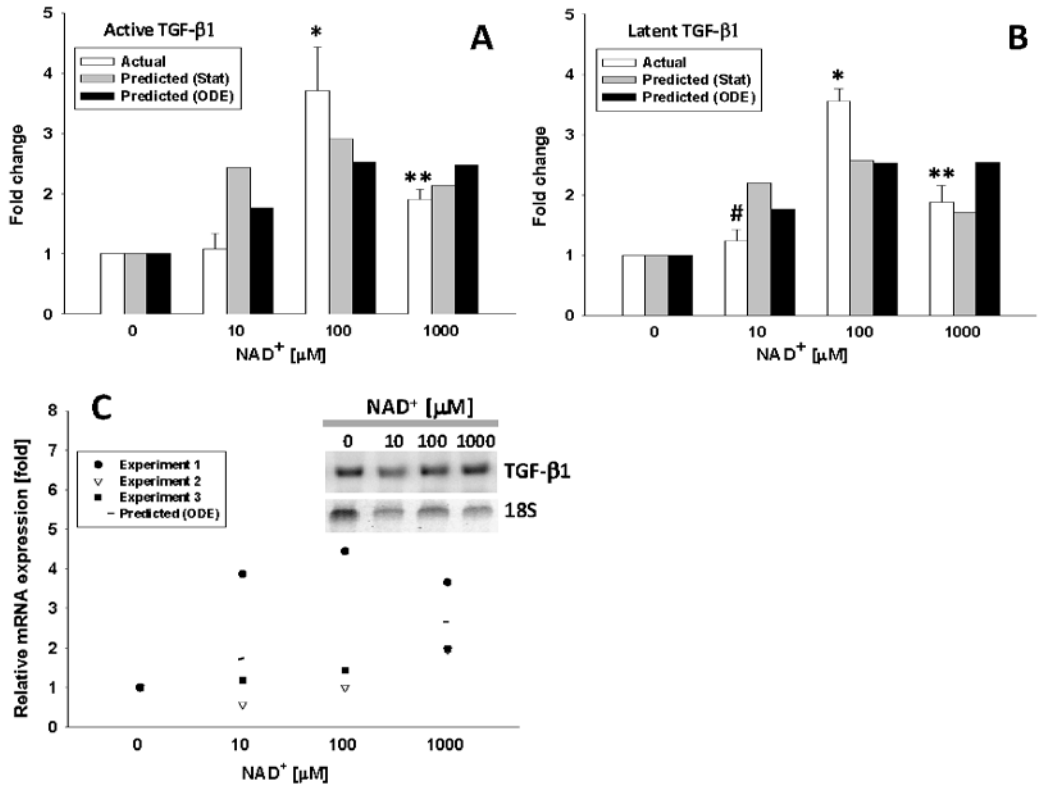

Figure 3.18 Validation of computational models of the effects of NAD^+ on active and latent TGF-β1.
The predictive capacity of the statistical model created with the data in **Fig. 3.13** was tested by treating RAW 264.7 cells with 0, 10, 100, or 1000 μM NAD^+ for 16 h (a time point not used in the construction of the model). The cultures were stained for the presence of active (Panel **A**) or latent (Panel **B**) TGF-β1. Open bars show actual data (Panel **A**: n=6, **P*<0.05 vs. 0, 10 and 1000 μM NAD^+, ***P*<0.05 vs. 0 and 10 μM NAD^+; Panel **B**: n=6, **P*<0.05 vs. 0, 10 and 1000 μM NAD^+, ***P*<0.05 vs. 0 and 10 μM NAD^+; $^{\#}P$<0.05 vs. 0 μM NAD^+). In both panels, gray bars show predictions using a statistical model and black bars show predictions using an ODE model as described in the *Materials and Methods*. Panel **C**: Total RNA was isolated from untreated (control) or RAW 264.7 cells treated with 10, 100, or 1000 μM NAD^+ for 21 h followed by Northern blotting and analysis for TGF-β1 mRNA as described in the *Materials and Methods*. The relative amount of mRNA is presented as the ratio of mRNA to 18S RNA

3.2.3.7 NAD^+ increases the expression of TGF-β1 mRNA in a manner predicted in silico

We next examined the effects of NAD^+ on TGF-β1 mRNA. TGF-β1 can auto-induce its own mRNA expression (125), and this auto-induction is presumably driven by exposure of cells to active TGF-β1. Since extracellular NAD^+ led to the activation of latent TGF-β1 protein and the increased expression of latent (total) TGF-β1 protein, we hypothesized that exposure to NAD^+ would lead to increased TGF-β1 mRNA as well. Moreover, since the maximal activation of TGF-

β1 by NAD^+ occurred at 1 h, whereas maximal NAD^+-stimulated latent TGF-β1 expression was seen at 6 h but persisted to 24 h, we examined the effects of NAD^+ on TGF-β1 mRNA at 21 h. As seen in Figure 3.18C, increased expression of TGF-β1 mRNA was observed with as little as 10 μM NAD^+, and persisted at levels of NAD^+ up to 1000 μM. As described in Figure 3.16B (see above), a mathematical model that invoked only the auto-induction of TGF-β1 was incapable of replicating the persistence of elevated TGF-β1 mRNA and protein at later time-points observed experimentally. In contrast, a mathematical model that included a hypothetical, Ca^{2+}-independent pathway acting at the level of TGF-β1 mRNA induction (Figure 3.16D) accurately predicted the experimental data on NAD^+-mediated TGF-β1 mRNA induction (Figure 3.18C).

3.2.4 Discussion

A large and growing class of DAMPs has emerged in over the past decade as pro-inflammatory endogenous cellular products that stimulate inflammation (e.g. the production of TNF-α when released in settings of cell stress or cell death) (121). Canonical DAMP's include high mobility group box-1 (HMGB1), S100A, uric acid, and heat shock protein-70 (HSP-70) (121). However, relatively little attention has been paid to endogenous anti-inflammatory compounds derived from cells, mediators that include adenosine (138), ubiquitin (139), and hemopexin (140). Herein, we have identified and partially characterized a novel pathway of TGF-β1 regulation by extracellular NAD+ in mouse macrophage-like cells, using combined biochemical and in silico methods (Figure 3.19), and our results suggest that NAD+ may be another member of this emerging group of anti-inflammatory DAMP's.

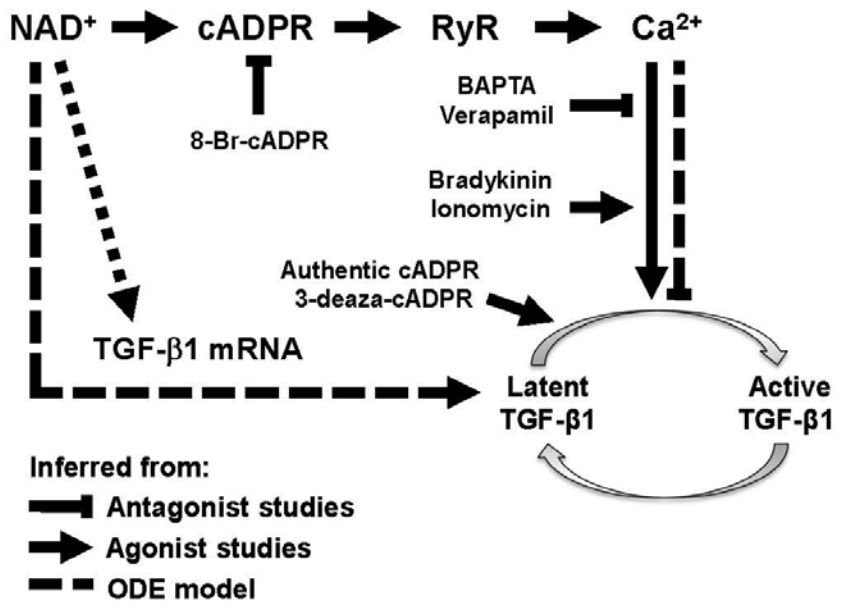

Figure 3.19 Mechanisms by which NAD^+ modulates TGF-β1.
Exposure to extracellular NAD^+ increases both the expression and activation of TGF-β1. NAD^+ signals through cADPR and Ca^{2+} to activate TGF-β1, which can then auto-induce its own mRNA production, leading to increased expression of latent TGF-β1 protein. The effect of NAD^+ depends on the prior conversion to cADPR, an effect antagonized by the cADPR antagonist 8-Br-cADPR. The effects of NAD^+ and cADPR require Ca^{2+} mobilization, are mimicked by Ca^{2+} agonists (Bradykinin, Ionomycin) and are inhibited by Ca^{2+} antagonists (BAPTA, Verapamil). Mechanistic mathematical modeling of the complex effects of NAD^+/cADPR/Ca^{2+} on TGF-β1 suggests a Ca^{2+}-independent pathway for NAD^+ signaling, as well as a slow mechanism for inhibition of TGF-β1 activation that is induced at high levels of Ca^{2+}.

Indeed, an emerging literature raises the possibility that NAD+ could be released by parenchymal cells in the setting of cellular stress or injury (122), and to exert various effects on inflammation. Granulocytes treated with NAD+ exhibited increased production of reactive oxygen species and other features consistent with activation (141). There is also extensive evidence that T-cell signaling is affected by NAD+, with ultimate effects on proliferation and apoptosis (142-148). Furthermore, several studies have shown that NAD+ can protect against inflammatory stress both in vitro and in vivo (149, 150), in part via reduced activity of the central inflammatory transcription factor NF-κB (manuscript in preparation). We have also found that treatment of endotoxemic mice with NAD+ could protect from lethality in the case of mice injected with high

dose LPS, and greatly reduced plasma TNF-α and NO2-/NO3- and elevated IL-10, in mice subjected to low-dose LPS (manuscript in preparation).

Based on these data, we hypothesized that NAD+, like other DAMPs, would have to act on nearby macrophages to induce classical anti-inflammatory cytokines. Given the long-recognized, potent, and generally localized effects of TGF-β1 in inflammatory settings (124), we hypothesized that one mechanism by which NAD+ could exert such potent effects would be via modulation of this cytokine.

The canonical signaling intermediary that controls the extracellular functions of NAD+ appears to be cADPR, which has been reported to lead to the release of Ca2+ from ryanodine-sensitive intracellular stores (122). In most models of extracellular signal transduction, NAD+ is converted to cADPR and nicotinamide by extracellular ADP-ribosyl cyclase (122). The cADPR then enters cells through either a CD38-dependent (151) or –independent (152) mechanisms. The resulting increase in intracellular cADPR concentration leads to binding of cADPR to ryanodine-sensitive calcium channels on endoplasmic reticulum (ER) membranes. This binding increases the probability that the channel will be in an open conformation, allowing the release of ER calcium stores to the cytoplasm (122).

While a role for extracellular cADPR in intracellular signaling events has been reported, there are other mechanisms through which extracellular NAD+ may act on cells. It has been proposed that extracellular NAD+ may modulate cellular responses by acting as a substrate for endogenous ADP-ribosyltransferases (ARTs) (153, 154). Five mammalian ARTs (ART1–5) have been identified (155). Interestingly, CD38 has also been shown to possess ADP-ribosyl transferase activity (156). The ARTs are structurally and functionally related to cholera and pertussis toxins,

which interfere with signal transduction in human host cells by ADP-ribosylating regulatory G-proteins (122). Several structurally unrelated inhibitors of ART were found to inhibit LPS-induced production of reactive oxygen intermediates and TNF-α by human mononuclear cells (157, 158).

Our results demonstrate that mouse macrophage-like cells treated with NAD+ exhibit elevated expression of both active and latent TGF-β1, with a biphasic time course that also depends on the specific concentration of NAD+. In an attempt to discern the mechanisms responsible for this complexity, we utilized both data-driven and mechanistic computational modeling. Complex, multidimensional features of inflammation and associated processes (e.g. apoptosis) have been elucidated using such computational methods, for example suggesting that the regulation of the transcription factor NF-κB involves oscillations in the expression of its inhibitor, IκB (159) and that signaling for apoptosis can be reduced to two principal components (51). An initial statistical analysis suggested that the interactions among NAD+, latent TGF-β1, and active TGF-β1 were non-linear. A series of non-linear mechanistic mathematical models of increasing complexity were generated in an attempt to determine the mechanisms responsible for these non-linear interactions. When combined with our biochemical data, our models suggested that NAD+ mediates its complex effects on TGF-β1 via cADPR, secondary to stimulation of Ca2+ fluxes. Our results do not rule out a role of ARTs in the effect of NAD+ on TGF-β1, however. In fact, the inability of our mechanistic mathematical model–which does not incorporate the ARTs- to fully predict the multiphasic behavior of TGF-β1 in response to NAD+ may suggest that we have not fully accounted for all the relevant biological mechanisms in modeling this process.

In our studies, we found that blocking Ca2+ with the Ca2+ chelator BAPTA inhibited the activation of TGF-β1 by NAD+ or cADPR, and that treatment with the Ca2+agonists ionomycin and bradykinin both induced increased expression as well as activation of TGF-β1. These studies suggest that modulation of Ca2+ is a central mechanism responsible for the elevation of TGF-β1. However, in multiple attempts, we could not reproducibly demonstrate Ca2+ fluxes in RAW 264.7 cells (data not shown). Interestingly, while many cell lines exhibit Ca2+ fluxes in response to extracellular NAD+ (160, 161), there are no published reports of ryanodine-sensitive Ca2+ flux measurements in RAW 264.7 cells. It is therefore unclear if the effects of NAD+ and cADPR require the activation of ryanodine-sensitive Ca2+ channels. Moreover, our data suggest that the effects of NAD+ on TGF-β1 requires L-type Ca2+ channels, though we have not defined the specific channels involved.

There are several limitations to our study. The first is that, though the main finding of NAD+/cADPR-induced induction of TGF-β1 was shown both in RAW264.7 cells and in primary macrophages, the detailed time- and dose-curve experiments were carried out only in the former. We note that the extensive time- and dose-curve studies performed over many repeats would have been extremely cumbersome in primary cells. Moreover, we expect to have observed much greater variability in the biological responses studied. Another limitation is the extensive use of semi-quantitative immunocytochemistry for these studies. Indeed, the expression of latent and active TGF-β1 can be assessed by various methods, including ELISA, cell-based bioactivity assays, Western blotting, and immunocytochemistry to detect cell-associated TGF-β1 (162). In our prior work establishing the utility of this assay (134), however, we showed the concordance between

this method and other methods of determining TGF-β1. Furthermore, prior studies had shown that TGF-β1 is predominantly cell-associated (132, 133, 163, 164).

In conclusion, our results thus point to NAD+ as one of a growing group of agents (proteases, plasmin, chaotropic agents, acid pH, radiation, and oxygen and nitrogen free radicals) (126) capable of activating TGF-β1, and have at least partially elucidated the novel biochemical pathway by which these effects on TGF-β1 occur. Our studies may further suggest that one mechanism by which anti-inflammatory DAMPs exert their actions is via activation of TGF-β1. Moreover, our studies highlight the utility of traditional biochemical/pharmacological studies coupled with computational modeling in defining novel biological mechanisms.

4.0 CONCLUSIONS

The overarching goal of this dissertation was to understand how a complex inflammatory response arises from the coordination of several inflammatory mediators. This involves quantitative measurements at a systemic level, data-driven modeling to extract meaningful mechanistic features of the response, and subsequent development of mechanistic models for simulation and analysis. The latter part is especially useful for connecting the results of high throughput data analysis back to the underlying functional biology as it relates to system behavior. The innate immune response is fascinatingly robust to a wide range of conditions, yet surprisingly susceptible to breakdown in diseases of acute inflammation. By following a comprehensive systems biology approach as outlined in Section 1.2, we hypothesized the identity of these control points and gained insights into directing their modulation for therapy.

The inflammatory response to biological stress is generally beneficial, but can lead to disease when over-exuberant or inadequate. The complex and often dual role of inflammation in health and disease has presented a major challenge to developing effective therapeutics and diagnostics. In this dissertation, we tackled this complexity by studying the interplay of molecular mediators of the acute inflammatory response. These mediators serve as a communication medium to coordinate the innate immune response among various cell types, but their functional roles often change depending on context and timing (8, 165). To address this complexity, we analyzed the concentrations of numerous inflammatory mediators across time using a flexible generalization of Dynamic Bayesian Networks. By allowing parameters of interactions to vary, this approach ensured that we captured interactions that may be nonlinear or inconsistent across time and therefore missed using standard approaches. In the setting of pediatric acute liver failure (PALF),

we identified key differences in the networks of patients that were survivors versus non-survivors when other analyses proved inconclusive. This work also showed that inflammatory networks can be used both as biomarkers and to generate mechanistic hypotheses for the progression of inflammation in PALF, a poorly understood disease. Similarly, we identified key mediators and differences in the inflammatory networks in trauma patients as well as a mouse model of trauma and hemorrhage. By comparing results from other *in vitro, in vivo,* and clinical settings, we identified a conserved network motif of cross-regulating chemokines that appears to broadly orchestrate the acute inflammatory response.

We were particularly interested in further studying the early regulation of inflammation in trauma. Therefore, to elaborate on the directed but abstracted chemokine network identified by DBN, we developed a logical model of these interactions calibrated to reproduce the averaged data of trauma patients with different injury severities. By comparing the dynamics resulting from different starting conditions, we showed that the clinically observed heterogeneity in individual inflammatory responses is a function of particular initial conditions. Interestingly, we were also able to show that heterogeneity in the time for simulations to reach steady state mapped well onto differences in patient discharge times of moderately vs. severely injured patients. The ability of this mechanistic model to capture both inflammatory trajectory and clinical outcome differences suggests that the hypothesized interactions represent an important point of control regulating the progression of acute inflammation.

Finally, we studied a particular pathway of interest in depth, namely the activation of TGF-β1 by NAD^+. Our work showed that the unusually complex dose and time-dependent response of TGF-β1 activation by NAD^+ could not be explained by a linear signal flow. We developed a differential equation model, and performed iterative experiments and model refinement to partially

identify the signaling pathway that leads to the observed complex response. This work established a model-guided mechanistic understanding for the previously unexplained anti-inflammatory effects of NAD^+.

The keystone of this work has been the ability to investigate both the topology and function of acute inflammatory circuits by connecting experiments with data-driven and mechanistic systems modeling. The next steps will involve iteration of targeted experiments to disrupt the chemokine network at varying points along the pathway, much like in our NAD^+ study, except extended across a multiplexed signal response measurement.

APPENDIX A

SUPPLEMENTARY INFORMATION FOR SECTION 2.3

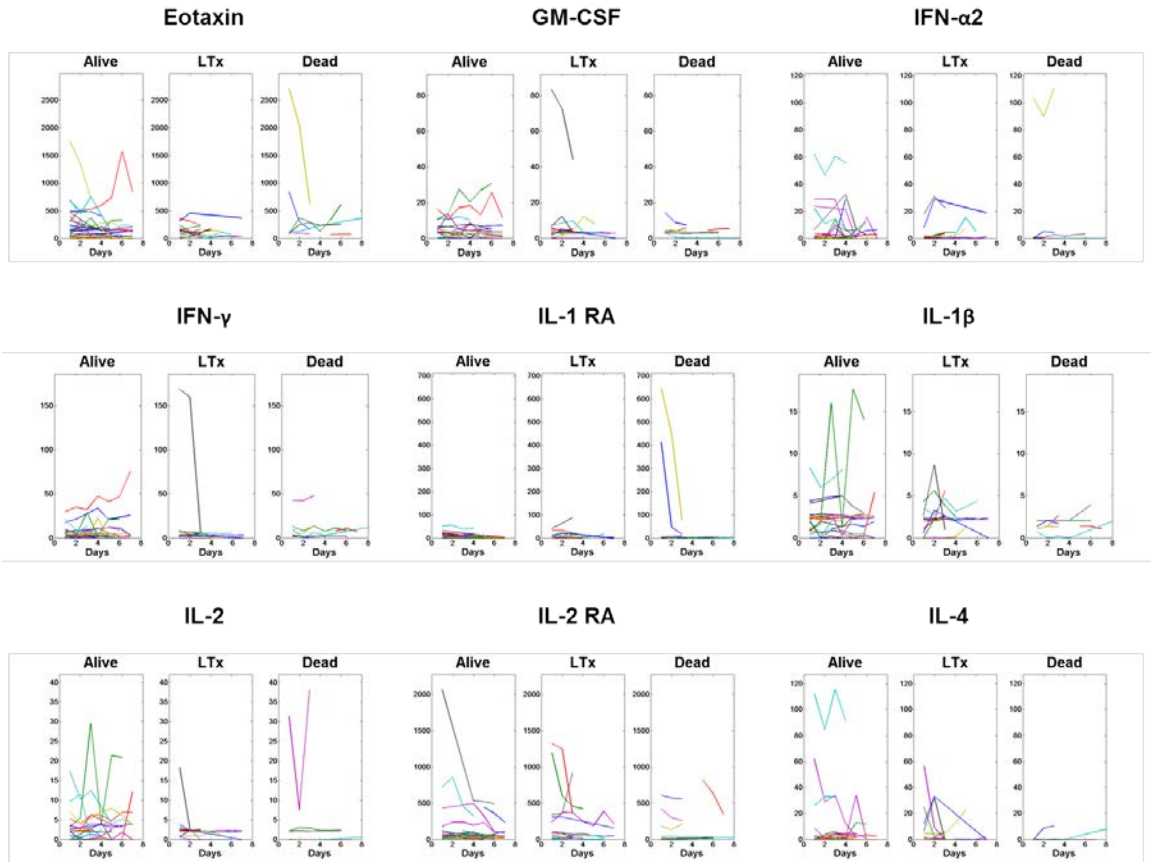

Figure A1.1

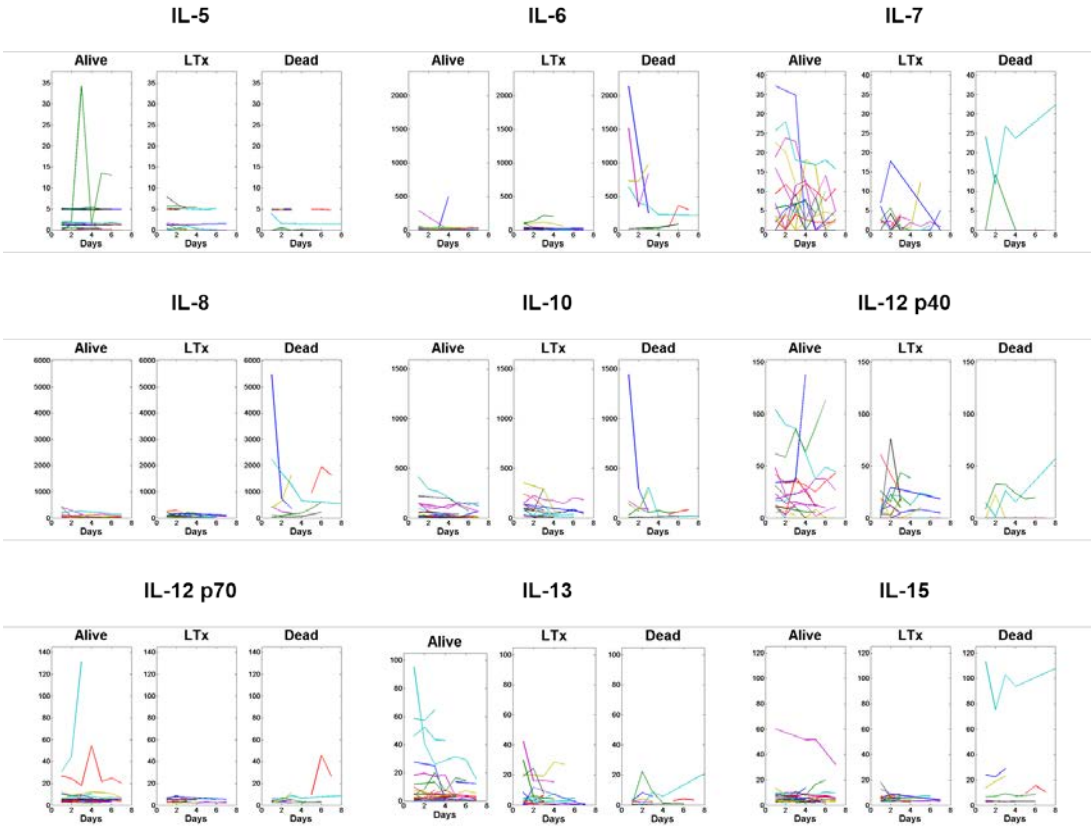
IL-5
Alive
LTx
Dead
IL-6
Alive
LTx
Dead
IL-7
Alive
LTx
Dead
IL-8
Alive
LTx
Dead
IL-10
Alive
LTx
Dead
IL-12 p40
Alive
LTx
Dead
IL-12 p70
Alive
LTx
Dead
IL-13
Alive
LTx
Dead
IL-15
Alive
LTx
Dead
Days

Figure A1.2

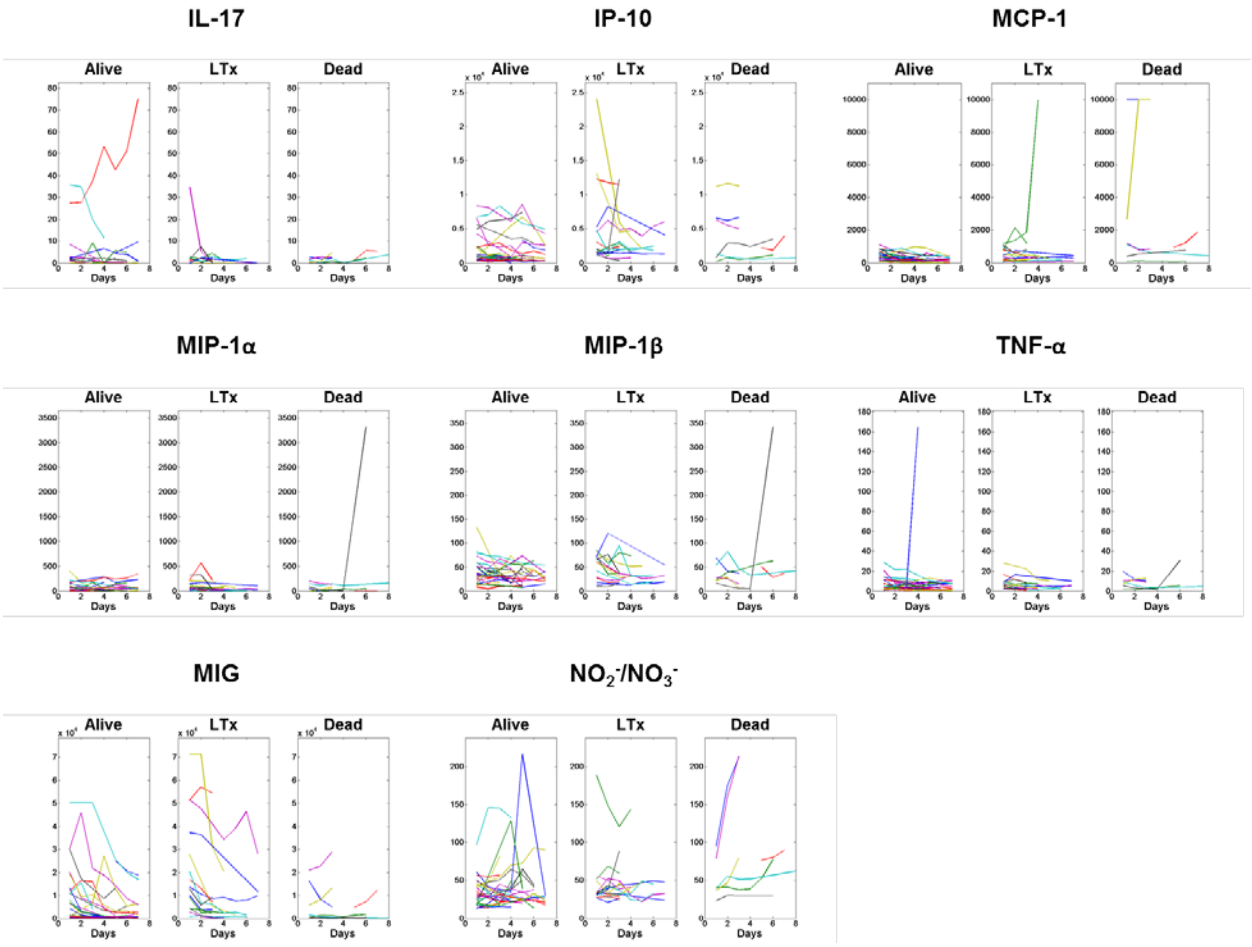

Figure A1.3

A.1 DETAILS OF PATIENT-SPECIFIC PRINCIPAL COMPONENT ANALYSIS

The goal of this analysis was to identify subsets of mediators that were most strongly correlated with the inflammatory response trajectory of a given PALF patient. To accomplish this, we utilized PCA to determine the dominance of each mediator relative to all other measured mediators that accounted for a given patient's inflammatory response during the seven days from which the

serum samples were taken. A minimum of 3 samples were available for cytokine analysis for each patient during the seven days following enrollment into the PALFSG. First, serum sample underwent cytokine measurements that were then normalized so that all cytokine levels were converted into the same range (from 0 to 1). Next, PCA was computed utilizing the normalized cytokine results derived from all samples that were collected for each patient. A PCA score was calculated for each cytokine, summarizing the relative degree to which that cytokine contributed to the inflammatory response for that patient over time. This was calculated by scaling each principal component's eigenvector by its respective eigenvalue and summing together the coefficients (loadings) that correspond to a given cytokine over all eigenvectors (sufficient to capture at least 95% of the variance in the data). These PCA scores taken together made up a patient's "inflammation barcode." This barcode was used to group patients using hierarchical clustering as described below. Resultant patient sub-groups were then cross-correlated with clinical outcomes: spontaneous survivor, non-survivor with native liver, or received liver transplant.

A.2 DETAILS OF HIERARCHICAL CLUSTERING ANALYSIS

The goal of this analysis was to highlight the natural variability, as well as any overlap, in inflammatory mediators from PALF patients that survived spontaneously without LTx, that died without receiving LTx, or that received LTx. Hierarchical clustering is a simple and unbiased method for segregating series of numerical values by similarity to each other. The limitation of this analysis is that the cluster must be built pairwise; since it is purely based on the similarity between the data, and the cluster may lack biological relevance(1). This analysis was performed

for all the inflammatory analytes – both unprocessed and following the patient-specific PCA described above – as published previously(2). Each row of the data matrix corresponds to either a single sample from patient (in raw data clustering) or a single patient's "inflammation barcode" derived from PCA clustering (see above), and each column corresponds to anti-inflammatory analyte (26 total: 25 cytokines/chemokines along with NO_2^-/NO_3^-). The magnitudes of these values were log-transformed and indicated by colors. The dendrogram (a branching diagram used to show relationships between members of a group) on the y-axis shows the similarities among samples according to their correlation measures (the correlation between the inflammatory mediators profiles) across all analyte values. The calculation is performed by using the Bioinformatics Toolbox in Matlab® 7.6.0, and the code for this algorithm has been made available publicly (2).

Luminex technology affords us the advantage of making many cytokine measurements from the same biological sample. Our dataset consists of 215 serum samples, each yielding 26 mediator measurements. We consider each set of mediator measurements belonging to the same serum sample to be a single point in 26-dimensional cytokine space. We used the Euclidean distance between these points in 26-dimensional space as the distance metric in our hierarchical clustering scheme. When clustering these raw data, we took each of the 215 points to be independent, even though several of them came from the same patient (median = 4 samples/ patient). Because each serum sample was independent, there was no guarantee that all samples from a given patient would cluster together. This led to the possibility that two measurements from the same patient could be assigned to different clusters. We examined the two clusters resulting from the first separation in the dendrogram, and found that samples from the same patient were rarely segregated into opposite clusters, For 32 out of 49 total patients, all serum samples clustered

together. Of the 17 remaining, there were only 4 patients whose data points were split equally between the two clusters. Of the 13 patients whose data were segregated unequally, only two patients had more than one data point in their minority cluster. Relabeling those points as each patient's majority cluster did not lead to a significantly different clustering (adjusted rand index was 0.59, where perfect agreement yields rand index = 1, no agreement = 0(3)). The resultant clusters also showed no strong correlation with clinical outcomes (adjusted rand index was 0.023). From this analysis, we concluded that unsupervised clustering of raw cytokine measurements was incapable of predicting clinical outcomes for these patients.

APPENDIX B

B.1 RULES FOR BOOLEAN MODEL

nodeX* = ISS

IP10_hi* = IP10

IP10* = nodeX and not (MCP1 and MIG)

MCP1* = ISS_hi or (MCP1 and not IP10_hi)

MCP1_hi* = ISS_hi and MCP1 and not IP10_hi

MIG* = ISS and MIG and not IP10_hi and not MCP1

IL6* = MIG or MCP1

IL6_hi* = MCP1 and not IP10_hi

BIBLIOGRAPHY

1. Medzhitov R. Origin and physiological roles of inflammation. Nature. 2008;454(7203):428-35.
2. Brown KL, Cosseau C, Gardy JL, Hancock RE. Complexities of targeting innate immunity to treat infection. Trends Immunol. 2007;28(6):260-6.
3. Marshall JC. Inflammation, coagulopathy, and the pathogenesis of multiple organ dysfunction syndrome. Crit Care Med. 2001;29(7 Suppl):S99-106.
4. Jarrar D, Chaudry IH, Wang P. Organ dysfunction following hemorrhage and sepsis: mechanisms and therapeutic approaches (Review). IntJMolMed. 1999;4(6):575-83.
5. Waxman K. Shock: ischemia, reperfusion, and inflammation. New Horiz. 1996;4(2):153-60.
6. Peitzman AB, Billiar TR, Harbrecht BG, Kelly E, Udekwu AO, Simmons RL. Hemorrhagic shock. CurrProblSurg. 1995;32(11):925-1002.
7. Namas R, Ghuma A, Torres A, Polanco P, Gomez H, Barclay D, et al. An adequately robust early TNF-α response is a hallmark of survival following trauma/hemorrhage. PLoS ONE. 2009;4(12):e8406.
8. Nathan C. Points of control in inflammation. Nature. 2002;420(6917):846-52.
9. Vodovotz Y, Csete M, Bartels J, Chang S, An G. Translational systems biology of inflammation. PLoSComputBiol. 2008;4:1-6.
10. Chow CC, Clermont G, Kumar R, Lagoa C, Tawadrous Z, Gallo D, et al. The acute inflammatory response in diverse shock states. Shock. 2005;24:74-84.
11. Lagoa CE, Bartels J, Baratt A, Tseng G, Clermont G, Fink MP, et al. The role of initial trauma in the host's response to injury and hemorrhage: Insights from a comparison of mathematical simulations and hepatic transcriptomic analysis. Shock. 2006;26:592-600.
12. Reynolds A, Rubin J, Clermont G, Day J, Vodovotz Y, Ermentrout GB. A reduced mathematical model of the acute inflammatory response: I. Derivation of model and analysis of anti-inflammation. JTheorBiol. 2006;242:220-36.
13. Torres A, Bentley T, Bartels J, Sarkar J, Barclay D, Namas R, et al. Mathematical modeling of post-hemorrhage inflammation in mice: Studies using a novel, computer-controlled, closed-loop hemorrhage apparatus. Shock. 2009;32:172-8.
14. Vodovotz Y, An G. Systems Biology and Inflammation. In: Yan Q, editor. Systems Biology in Drug Discovery and Development: Methods and Protocols. Totowa, NJ: Springer Science & Business Media; 2009. p. 181-201.
15. Mi Q, Li NYK, Ziraldo C, Ghuma A, Mikheev M, Squires R, et al. Translational systems biology of inflammation: Potential applications to personalized medicine. Personalized Medicine. 2010;7:549-59.
16. Chen GY, Nuñez G. Sterile inflammation: sensing and reacting to damage. Nat Rev Immunol. 2010;10(12):826-37.
17. Parker SJ, Watkins PE. Experimental models of gram-negative sepsis. BrJSurg. 2001;88(1):22-30.

18. Bellingan G. Inflammatory cell activation in sepsis. BrMedBull. 1999;55(1):12-29.
19. Jones AL, Selby P. Tumour necrosis factor: clinical relevance. Cancer Surv. 1989;8(4):817-36.
20. Cavaillon JM. Cytokines and macrophages. BiomedPharmacother. 1994;48(10):445-53.
21. Kox WJ, Volk T, Kox SN, Volk HD. Immunomodulatory therapies in sepsis. Intensive Care Med. 2000;26 Suppl 1:S124-S8.
22. Dinarello CA. Proinflammatory cytokines. Chest. 2000;118(2):503-8.
23. Pinsky MR. Sepsis: a pro- and anti-inflammatory disequilibrium syndrome. ContribNephrol. 2001(132):354-66.
24. Baugh JA, Bucala R. Mechanisms for modulating TNF alpha in immune and inflammatory disease. CurrOpinDrug DiscovDevel. 2001;4(5):635-50.
25. Chen G, Goeddel DV. TNF-R1 signaling: a beautiful pathway. Science. 2002;296(5573):1634-5.
26. An G, Nieman G, Vodovotz Y. Computational and systems biology in trauma and sepsis: Current state and future perspectives. IntJBurns Trauma. 2012;2:1-10.
27. Csete ME, Doyle JC. Reverse engineering of biological complexity. Science. 2002;295(5560):1664-9.
28. Vodovotz Y, Constantine G, Rubin J, Csete M, Voit EO, An G. Mechanistic simulations of inflammation: Current state and future prospects. MathBiosci. 2009;217:1-10.
29. Vodovotz Y, Constantine G, Faeder J, Mi Q, Rubin J, Sarkar J, et al. Translational systems approaches to the biology of inflammation and healing. ImmunopharmacolImmunotoxicol. 2010;32:181-95.
30. Mesarovic MD, Sreenath SN, Keene JD. Search for organising principles: understanding in systems biology. SystBiol(Stevenage). 2004;1(1):19-27.
31. Janes KA, Yaffe MB. Data-driven modelling of signal-transduction networks. NatRevMolCell Biol. 2006;7(11):820-8.
32. Kitano H. Systems biology: a brief overview. Science. 2002;295(5560):1662-4.
33. Arkin AP, Schaffer DV. Network news: innovations in 21st century systems biology. Cell. 2011;144(6):844-9.
34. Mac Nally R. Regression and model-building in conservation biology, biogeography and ecology: The distinction between GÇô and reconciliation of GÇô GÇÿpredictiveGÇÖ and GÇÿexplanatoryGÇÖ models. Biodiversity and Conservation. 2000;9(5):655-71.
35. Janes KA, Gaudet S, Albeck JG, Nielsen UB, Lauffenburger DA, Sorger PK. The Response of Human Epithelial Cells to TNF Involves an Inducible Autocrine Cascade. Cell. 2006;124(6):1225-39.
36. Angeli D, Ferrell JE, Sontag ED. Detection of multistability, bifurcations, and hysteresis in a large class of biological positive-feedback systems. Proceedings of the National Academy of Sciences of the United States of America. 2004;101(7):1822-7.
37. Reynolds A, Rubin J, Clermont G, Day J, Vodovotz Y, Bard Ermentrout G. A reduced mathematical model of the acute inflammatory response: I. Derivation of model and analysis of anti-inflammation. Journal of Theoretical Biology. 2006;242(1):220-36.
38. Bagci EZ, Vodovotz Y, Billiar TR, Ermentrout GB, Bahar I. Bistability in apoptosis: Roles of Bax, Bcl-2 and mitochondrial permeability transition pores. BiophysJ. 2006;90:1546-59.
39. Clermont G, Chow C, Kumar R, Vodovotz Y. Mathematical simulation of the innate immune response. Crit Care Med. 2001;29(Suppl):A111-A.

40. Marino S, Hogue IB, Ray CJ, Kirschner DE. A methodology for performing global uncertainty and sensitivity analysis in systems biology. Journal of Theoretical Biology. 2008;254(1):178-96.
41. Vodovotz Y, Constantine G, Faeder J, Mi Q, Rubin J, Bartels J, et al. Translational systems approaches to the biology of inflammation and healing. Immunopharmacol Immunotoxicol. 2010;32(2):181-95.
42. Mi Q, Li NYK, Ziraldo C, Ghuma A, Mikheev M, Squires R, et al. Translational systems biology of inflammation: Potential applications to personalized medicine. Personalized Medicine. 2010;7(5):549-59.
43. Grzegorczyk M, Husmeier D. Improvements in the reconstruction of time-varying gene regulatory networks: dynamic programming and regularization by information sharing among genes. Bioinformatics. 2011;27(5):693-9.
44. Mi Q, Constantine G, Ziraldo C, Solovyev A, Torres A, Namas R, et al. A dynamic view of trauma/hemorrhage-induced inflammation in mice: Principal drivers and networks. PLoS ONE. 2011;6:e19424.
45. Azhar N, Ziraldo C, Barclay D, Rudnick DA, Squires RH, Vodovotz Y. Analysis of serum inflammatory mediators identifies unique dynamic networks associated with death and spontaneous survival in pediatric acute liver failure. PLoS ONE. 2013;8(11).
46. Markowetz F, Spang R. Inferring cellular networks--a review. BMC bioinformatics. 2007;8 Suppl 6:S5.
47. Germain RN, Meier-Schellersheim M, Nita-Lazar A, Fraser ID. Systems Biology in Immunology: A Computational Modeling Perspective. AnnuRevImmunol. 2010.
48. Yosef N, Shalek AK, Gaublomme JT, Jin H, Lee Y, Awasthi A, et al. Dynamic regulatory network controlling TH17 cell differentiation. Nature. 2013;496(7446):461-8.
49. Nilsson R, Bajic VB, Suzuki H, di Bernardo D, Björkegren J, Katayama S, et al. Transcriptional network dynamics in macrophage activation. Genomics. 2006;88(2):133-42.
50. Kulbe H, Chakravarty P, Leinster DA, Charles KA, Kwong J, Thompson RG, et al. A dynamic inflammatory cytokine network in the human ovarian cancer microenvironment. Cancer research. 2012;72(1):66-75.
51. Janes KA, Albeck JG, Gaudet S, Sorger PK, Lauffenburger DA, Yaffe MB. A systems model of signaling identifies a molecular basis set for cytokine-induced apoptosis. Science. 2005;310(5754):1646-53.
52. Sachs K, Perez O, Pe'er D, Lauffenburger DA, Nolan GP. Causal protein-signaling networks derived from multiparameter single-cell data. Science. 2005;308(5721):523-9.
53. Murphy K. An introduction to graphical models. A Brief Introduction to Graphical Models and Bayesian Networks. 2001;10.
54. Koller D, Friedman N. Probabilistic graphical models: principles and techniques: MIT press; 2009.
55. Edwards D. Introduction to graphical modelling: Springer; 2000.
56. Needham CJ, Bradford JR, Bulpitt AJ, Westhead DR. A primer on learning in Bayesian networks for computational biology. PLoS Comput Biol. 2007;3(8):e129.
57. Murphy KP. Dynamic bayesian networks: representation, inference and learning: University of California, Berkeley; 2002.
58. Heckerman D, Geiger D, editors. Learning Bayesian networks: a unification for discrete and Gaussian domains. Proceedings of the Eleventh conference on Uncertainty in artificial intelligence; 1995: Morgan Kaufmann Publishers Inc.

59. Bansal M, Della Gatta G, Di Bernardo D. Inference of gene regulatory networks and compound mode of action from time course gene expression profiles. Bioinformatics. 2006;22(7):815-22.
60. Yu J, Smith VA, Wang PP, Hartemink AJ, Jarvis ED. Advances to Bayesian network inference for generating causal networks from observational biological data. Bioinformatics. 2004;20(18):3594-603.
61. Squires Jr RH, Shneider BL, Bucuvalas J, Alonso E, Sokol RJ, Narkewicz MR, et al. Acute liver failure in children: The first 348 patients in the pediatric acute liver failure study group. Journal of Pediatrics. 2006;148(5):652-8.e2.
62. Squires Jr RH. Acute liver failure in children. Seminars in Liver Disease. 2008;28(2):153-66.
63. Narkewicz MR, Olio DD, Karpen SJ, Murray KF, Schwarz K, Yazigi N, et al. Pattern of diagnostic evaluation for the causes of pediatric acute liver failure: An opportunity for quality improvement. Journal of Pediatrics. 2009;155(6):801-6.e1.
64. Lee WM. Acute liver failure. NEnglJMed. 1993;329(25):1862-72.
65. Brown KE, Tisdale J, Barrett AJ, Dunbar CE, Young NS. Hepatitis-associated aplastic anemia. NEnglJMed. 1997;336(15):1059-64.
66. Rolando N, Harvey F, Brahm J, Philpott-Howard J, Alexander G, Gimson A, et al. Prospective study of bacterial infection in acute liver failure: an analysis of fifty patients. Hepatology. 1990;11(1):49-53.
67. Bucuvalas J, Yazigi N, Narkewicz MR, Ng V, Lopez MJ. Immunophenotype predicts outcome in pediatric acute liver failure. J Pediatr Gastroenterol Nutr. 2012.
68. Bishop CM. Pattern recognition and machine learning: springer New York; 2006.
69. Jolliffe I. Principal component analysis: Wiley Online Library; 2005.
70. Poynard T, Morra R, Ingiliz P, Imbert-Bismut F, Thabut D, Messous D, et al. Chapter 4 Biomarkers Of Liver Fibrosis. Advances in Clinical Chemistry. 2008;46:131-60.
71. Tacke F, Hammerich L, Heymann F. Role of IL-17 and Th17 cells in liver diseases. Clinical and Developmental Immunology. 2011;2011.
72. Sattar N. Biomarkers for diabetes prediction, pathogenesis or pharmacotherapy guidance? Past, present and future possibilities. Diabetic Medicine. 2012;29(1):5-13.
73. Chan T, Gu F. Early diagnosis of sepsis using serum biomarkers. Expert Review of Molecular Diagnostics. 2011;11(5):487-96.
74. Halim SA, Newby LK, Ohman EM. Biomarkers in cardiovascular clinical trials: Past, present, future. Clinical Chemistry. 2012;58(1):45-53.
75. Chung KF. Inflammatory biomarkers in severe asthma. Current Opinion in Pulmonary Medicine. 2012;18(1):35-41.
76. Sekiyama KD, Yoshiba M, Thomson AW. Circulating proinflammatory cytokines (IL-1β, TNF-α, and IL-6) and IL-1 receptor antagonist (IL-1Ra) in fulminant hepatic failure and acute hepatitis. Clinical and Experimental Immunology. 1994;98(1):71-7.
77. Gupta RK, Yadav SK, Rangan M, Rathore RKS, Thomas MA, Prasad KN, et al. Serum proinflammatory cytokines correlate with diffusion tensor imaging derived metrics and 1H-MR spectroscopy in patients with acute liver failure. Metabolic Brain Disease. 2010;25(3):355-61.
78. Srivastava A, Yadav SK, Borkar VV, Yadav A, Yachha SK, Thomas MA, et al. Serial evaluation of children with ALF with advanced MRI, serum proinflammatory cytokines, thiamine, and cognition assessment. Journal of Pediatric Gastroenterology and Nutrition. 2012;55(5):580-6.

79. Vodovotz Y. Translational systems biology of inflammation and healing. WoundRepair Regen. 2010;18(1):3-7.
80. Namas R, Zamora R, Namas R, An G, Doyle J, Dick TE, et al. Sepsis: Something old, something new, and a systems view. Journal of Critical Care. 2012;27(3):314.e1-.e11.
81. Koniaris LG, Zimmers-Koniaris T, Hsiao EC, Chavin K, Sitzmann JV, Farber JM. Cytokine-responsive gene-2/IFN-inducible protein-10 expression in multiple models of liver and bile duct injury suggests a role in tissue regeneration. Journal of Immunology. 2001;167(1):399-406.
82. Bone-Larson CL, Hogaboam CM, Evanhoff H, Strieter RM, Kunkel SL. IFN-γ-inducible protein-10 (CXCL10) is hepatoprotective during acute liver injury through the induction of CXCR2 on hepatocytes. Journal of Immunology. 2001;167(12):7077-83.
83. Larrubia JR, Benito-Martínez S, Calvino M, Sanz-de-Villalobos E, Parra-Cid T. Role of chemokines and their receptors in viral persistence and liver damage during chronic hepatitis C virus infection. World Journal of Gastroenterology. 2008;14(47):7149-59.
84. Patton GC, Coffey C, Sawyer SM, Viner RM, Haller DM, Bose K, et al. Global patterns of mortality in young people: a systematic analysis of population health data. Lancet. 2009;374(9693):881-92.
85. Rose S, Marzi I. Mediators in polytrauma--pathophysiological significance and clinical relevance. Langenbecks ArchSurg. 1998;383(3-4):199-208.
86. Catania RA, Chaudry IH. Immunological consequences of trauma and shock. AnnAcad MedSingapore. 1999;28(1):120-32.
87. Aller MA, Arias JL, Nava MP, Arias J. Posttraumatic inflammation is a complex response based on the pathological expression of the nervous, immune, and endocrine functional systems. ExpBiolMed(Maywood). 2004;229(2):170-81.
88. Hardaway RM. Traumatic shock. MilMed. 2006;171(4):278-9.
89. Jawa RS, Kulaylat MN, Baumann H, Dayton MT. What is new in cytokine research related to trauma/critical care. J Intensive Care Med. 2006;21(2):63-85.
90. Lenz A, Franklin GA, Cheadle WG. Systemic inflammation after trauma. Injury. 2007;38(12):1336-45.
91. DeLong WG, Jr., Born CT. Cytokines in patients with polytrauma. ClinOrthopRelat Res. 2004(422):57-65.
92. Calvano SE, Xiao W, Richards DR, Felciano RM, Baker HV, Cho RJ, et al. A network-based analysis of systemic inflammation in humans. Nature. 2005;437:1032-7.
93. Xiao W, Mindrinos MN, Seok J, Cuschieri J, Cuenca AG, Gao H, et al. A genomic storm in critically injured humans. JExpMed. 2011;208(13):2581-90.
94. Warren HS, Elson CM, Hayden DL, Schoenfeld DA, Cobb JP, Maier RV, et al. A genomic score prognostic of outcome in trauma patients. MolMed. 2009;15(7-8):220-7.
95. Le Tulzo Y, Shenkar R, Kaneko D, Moine P, Fantuzzi G, Dinarello CA, et al. Hemorrhage increases cytokine expression in lung mononuclear cells in mice: involvement of catecholamines in nuclear factor-kappaB regulation and cytokine expression. J ClinInvest. 1997;99(7):1516-24.
96. Platzer C, Docke W, Volk H, Prosch S. Catecholamines trigger IL-10 release in acute systemic stress reaction by direct stimulation of its promoter/enhancer activity in monocytic cells. J Neuroimmunol. 2000;105(1):31-8.
97. Riese U, Brenner S, Docke WD, Prosch S, Reinke P, Oppert M, et al. Catecholamines induce IL-10 release in patients suffering from acute myocardial infarction by transactivating its promoter in monocytic but not in T-cells. MolCell Biochem. 2000;212(1-2):45-50.

98. Seok J, Warren HS, Cuenca AG, Mindrinos MN, Baker HV, Xu W, et al. Genomic responses in mouse models poorly mimic human inflammatory diseases. Proceedings of the National Academy of Sciences. 2013;110(9):3507-12.
99. Jin T, Xu X, Hereld D. Chemotaxis, chemokine receptors and human disease. Cytokine. 2008;44(1):1-8.
100. Viola A, Luster AD. Chemokines and their receptors: drug targets in immunity and inflammation. AnnuRevPharmacolToxicol. 2008;48:171-97.
101. Lomas JL, Chung CS, Grutkoski PS, LeBlanc BW, Lavigne L, Reichner J, et al. Differential effects of macrophage inflammatory chemokine-2 and keratinocyte-derived chemokine on hemorrhage-induced neutrophil priming for lung inflammation: assessment by adoptive cells transfer in mice. Shock. 2003;19(4):358-65.
102. Frink M, Hsieh YC, Hsieh CH, Pape HC, Choudhry MA, Schwacha MG, et al. Keratinocyte-derived chemokine plays a critical role in the induction of systemic inflammation and tissue damage after trauma-hemorrhage. Shock. 2007;28(5):576-81.
103. Charo IF, Ransohoff RM. The many roles of chemokines and chemokine receptors in inflammation. New England Journal of Medicine. 2006;354(6):610-21.
104. Giegold O, Ogrissek N, Richter C, Schroder M, Herrero San Juan M, Pfeilschifter JM, et al. CXCL9 causes heterologous desensitization of CXCL12-mediated memory T lymphocyte activation. J Immunol. 2013;190(7):3696-705.
105. Menke J, Zeller GC, Kikawada E, Means TK, Huang XR, Lan HY, et al. CXCL9, but not CXCL10, promotes CXCR3-dependent immune-mediated kidney disease. Journal of the American Society of Nephrology. 2008;19(6):1177-89.
106. Ziraldo C, Vodovotz Y, Namas RA, Almahmoud K, Tapias V, Mi Q, et al. Central role for MCP-1/CCL2 in injury-induced inflammation revealed by in vitro, in silico, and clinical studies. PLoS ONE. 2013;8(12).
107. Richardson RM, Ali H, Tomhave ED, Haribabu B, Snyderman R. Cross-desensitization of chemoattractant receptors occurs at multiple levels. Evidence for a role for inhibition of phospholipase C activity. The Journal of biological chemistry. 1995;270(46):27829-33.
108. Paust HJ, Turner JE, Riedel JH, Disteldorf E, Peters A, Schmidt T, et al. Chemokines play a critical role in the cross-regulation of Th1 and Th17 immune responses in murine crescentic glomerulonephritis. Kidney international. 2012;82(1):72-83.
109. World Health Organization report: Young People: Health Risks and Solutions. 2011 2011. Report No.
110. Berg RJ, Okoye O, Teixeira PG, Inaba K, Demetriades D. The double jeopardy of blunt thoracoabdominal trauma. Archives of surgery. 2012;147(6):498-504.
111. Kauffman SA. The origins of order: Self-organization and selection in evolution: Oxford university press; 1993.
112. Glass L, Kauffman SA. The logical analysis of continuous, non-linear biochemical control networks. Journal of theoretical Biology. 1973;39(1):103-29.
113. Kauffman SA. Metabolic stability and epigenesis in randomly constructed genetic nets. Journal of theoretical biology. 1969;22(3):437-67.
114. Albert I, Thakar J, Li S, Zhang R, Albert R. Boolean network simulations for life scientists. Source Code BiolMed. 2008;3:16.
115. Chaves M, Sontag ED, Albert R. Methods of robustness analysis for Boolean models of gene control networks. IEE Proceedings-Systems Biology. 2006;153(4):154-67.

116. Harvey I, Bossomaier T, editors. Time out of joint: Attractors in asynchronous random boolean networks. Proceedings of the Fourth European Conference on Artificial Life; 1997: MIT Press, Cambridge.
117. Saadatpour A, Albert R. Boolean modeling of biological regulatory networks: a methodology tutorial. Methods. 2013;62(1):3-12.
118. Neunaber C, Zeckey C, Andruszkow H, Frink M, Mommsen P, Krettek C, et al. Immunomodulation in polytrauma and polymicrobial sepsis - where do we stand? Recent Pat InflammAllergy Drug Discov. 2011;5(1):17-25.
119. Shmulevich I, Dougherty ER, Kim S, Zhang W. Probabilistic Boolean networks: a rule-based uncertainty model for gene regulatory networks. Bioinformatics. 2002;18(2):261-74.
120. Zamora R, Azhar N, Namas R, Metukuri MR, Clermont T, Gladstone C, et al. Identification of a novel pathway of transforming growth factor-beta1 regulation by extracellular NAD+ in mouse macrophages: in vitro and in silico studies. The Journal of biological chemistry. 2012;287(37):31003-14.
121. Matzinger P. The danger model: a renewed sense of self. Science. 2002;296(5566):301-5.
122. Koch-Nolte F, Fischer S, Haag F, Ziegler M. Compartmentation of NAD+-dependent signalling. FEBS Lett. 2011;585(11):1651-6.
123. Namazi MR. Nicotinamide: a potential addition to the anti-psoriatic weaponry. FASEB J. 2003;17(11):1377-9.
124. Wahl SM. TGF-beta in the evolution and resolution of inflammatory and immune processes. Introduction. MicrobesInfect. 1999;1(15):1247-9.
125. Vodovotz Y, Barcellos-Hoff MH. Direct and Indirect Modulation of the Inducible Nitric Oxide Synthase by Nitric Oxide: Feedback Mechanisms in Inflammation. In: Salvemini D, Billiar TR, Vodovotz Y, editors. Nitric Oxide and Inflammation. Progress in Inflammation Research. Basel: Birkhauser-Verlag; 2001. p. 41-58.
126. Annes JP, Munger JS, Rifkin DB. Making sense of latent TGFbeta activation. JCell Sci. 2003;116(Pt 2):217-24.
127. Artman M, Seeley RJ. Nicotinamide adenine dinucleotide splitting enzyme: a characteristic of the mouse macrophage. Science. 1978;202(4374):1293-5.
128. Artman M, Seeley RJ. Nicotinamide adenine dinucleotide splitting enzyme: a plasma membrane protein of murine macrophages. ArchBiochemBiophys. 1979;195(1):121-7.
129. Artman M, Seeley RJ. Nicotinamide adenine dinucleotide-splitting enzyme in normal, elicited and activated peritoneal macrophages of the mouse. JReticuloendothelSoc. 1979;25(5):479-87.
130. Twardzik DR, Mikovits JA, Ranchalis JE, Purchio AF, Ellingsworth L, Ruscetti FW. τ-Interferon-induced activation of latent transforming growth factor-Beta by human monocytes. AnnNY AcadSci. 1990;593:276-84.
131. Barcellos-Hoff MH, Dix TA. Redox mediated activation of latent transforming growth factor-β1. MolEndocrinol. 1996;10:1077-83.
132. Chong H, Vodovotz Y, Cox GW, Barcellos-Hoff MH. Immunocytochemical detection of latent TGF-β activation in cultured macrophages. JCellPhysiol. 1999;178:275-83.
133. Vodovotz Y, Chesler L, Chong H, Kim SJ, Simpson JT, DeGraff W, et al. Regulation of transforming growth factor-β1 by nitric oxide. Cancer Res. 1999;59:2142-9.
134. Metukuri MR, Namas R, Gladstone C, Clermont T, Jefferson B, Barclay D, et al. Activation of latent transforming growth factor-beta1 by nitric oxide in macrophages: role of soluble guanylate cyclase and MAP kinases. WoundRepair Regen. 2009;17(4):578-88.

135. Vodovotz Y, Chesler L, Chong H, Kim SJ, Simpson JT, DeGraff W, et al. Regulation of transforming growth factor β1 by nitric oxide. Cancer Research. 1999;59(9):2142-9.
136. Wong L, Aarhus R, Lee HC, Walseth TF. Cyclic 3-deaza-adenosine diphosphoribose: a potent and stable analog of cyclic ADP-ribose. BiochimBiophysActa. 1999;1472(3):555-64.
137. Sethi JK, Empson RM, Bailey VC, Potter BV, Galione A. 7-Deaza-8-bromo-cyclic ADP-ribose, the first membrane-permeant, hydrolysis-resistant cyclic ADP-ribose antagonist. JBiolChem. 1997;272(26):16358-63.
138. Ramakers BP, Riksen NP, van der Hoeven JG, Smits P, Pickkers P. Modulation of innate immunity by adenosine receptor stimulation. Shock. 2011;36(3):208-15.
139. Majetschak M. Extracellular ubiquitin: immune modulator and endogenous opponent of damage-associated molecular pattern molecules. JLeukocBiol. 2011;89(2):205-19.
140. Fink MP. Editorial: Hemopexin: newest member of the anti-inflammatory mediator club. JLeukocBiol. 2009;86(2):203-4.
141. Bruzzone S, Moreschi I, Guida L, Usai C, Zocchi E, DE Flora A. Extracellular NAD+ regulates intracellular calcium levels and induces activation of human granulocytes. BiochemJ. 2006;393(Pt 3):697-704.
142. Nowicki M, Landon C, Sugawara S, Dennert G. Nicotinamide and 3-aminobenzamide interfere with receptor-mediated transmembrane signaling in murine cytotoxic T cells: independence of Golgi reorientation from calcium mobilization and inositol phosphate generation. Cell Immunol. 1991;132(1):115-26.
143. Wang J, Nemoto E, Kots AY, Kaslow HR, Dennert G. Regulation of cytotoxic T cells by ecto-nicotinamide adenine dinucleotide (NAD) correlates with cell surface GPI-anchored/arginine ADP-ribosyltransferase. JImmunol. 1994;153(9):4048-58.
144. Wang J, Nemoto E, Dennert G. Regulation of CTL by ecto-nictinamide adenine dinucleotide (NAD) involves ADP-ribosylation of a p56lck-associated protein. JImmunol. 1996;156(8):2819-27.
145. Wang J, Nemoto E, Dennert G. Regulation of cytotoxic T cell functions by a GPI-anchored ecto-ADP-ribosyltransferase. AdvExpMedBiol. 1997;419:191-201.
146. Okamoto S, Azhipa O, Yu Y, Russo E, Dennert G. Expression of ADP-ribosyltransferase on normal T lymphocytes and effects of nicotinamide adenine dinucleotide on their function. JImmunol. 1998;160(9):4190-8.
147. Liu ZX, Azhipa O, Okamoto S, Govindarajan S, Dennert G. Extracellular nicotinamide adenine dinucleotide induces T cell apoptosis in vivo and in vitro. JImmunol. 2001;167(9):4942-7.
148. Aswad F, Kawamura H, Dennert G. High sensitivity of CD4+CD25+ regulatory T cells to extracellular metabolites nicotinamide adenine dinucleotide and ATP: a role for P2X7 receptors. JImmunol. 2005;175(5):3075-83.
149. Khan AU, Delude RL, Han YY, Sappington PL, Han X, Carcillo JA, et al. Liposomal NAD(+) prevents diminished O(2) consumption by immunostimulated Caco-2 cells. AmJ Physiol Lung Cell MolPhysiol. 2002;282(5):L1082-L91.
150. Han X, Uchiyama T, Sappington PL, Yaguchi A, Yang R, Fink MP, et al. NAD+ ameliorates inflammation-induced epithelial barrier dysfunction in cultured enterocytes and mouse ileal mucosa. JPharmacolExpTher. 2003;307(2):443-9.
151. Franco L, Guida L, Bruzzone S, Zocchi E, Usai C, De Flora A. The transmembrane glycoprotein CD38 is a catalytically active transporter responsible for generation and influx of the second messenger cyclic ADP-ribose across membranes. FASEB Journal. 1998;12(14):1507-20.

152. Franco L, Zocchi E, Usai C, Guida L, Bruzzone S, Costa A, et al. Paracrine roles of NAD+ and cyclic ADP-ribose in increasing intracellular calcium and enhancing cell proliferation of 3T3 fibroblasts. JBiolChem. 2001;276(24):21642-8.
153. Maehama T, Nishina H, Hoshino SI, Kanaho Y, Katada T. NAD+-dependent ADP-ribosylation of T lymphocyte alloantigen RT6.1 reversibly proceeding in intact rat lymphocytes. Journal of Biological Chemistry. 1995;270(39):22747-51.
154. Rigby MR, Bortell R, Stevens LA, Moss J, Kanaitsuka T, Shigeta H, et al. Rat RT6.2 and Mouse Rt6 locus 1 are NAD+:arginine ADP ribosyltransferases with Auto-ADP ribosylation activity. Journal of Immunology. 1996;156(11):4259-65.
155. Okazaki IJ, Moss J. Glycosylphosphatidylinositol-anchored and secretory isoforms of mono- ADP-ribosyltransferases. Journal of Biological Chemistry. 1998;273(37):23617-20.
156. Grimaldi JC, Balasubramanian S, Kabra NH, Shanafelt A, Bazan JF, Zurawski G, et al. CD38-mediated ribosylation of proteins. Journal of Immunology. 1995;155(2):811-7.
157. Hauschildt S, Ulmer AJ, Flad HD, Heyden T, Heine H. ADP-ribosylation: role in LPS-induced phosphorylation of two cytosolic proteins (p36/38) in monocytes. Progress in clinical and biological research. 1998;397:147-55.
158. Lührmann A, Thölke J, Behn I, Schumann J, Tiegs G, Hauschildt S. Immunomodulating properties of the antibiotic novobiocin in human monocytes. Antimicrobial Agents and Chemotherapy. 1998;42(8):1911-6.
159. Hoffmann A, Levchenko A, Scott ML, Baltimore D. The IκB-NFκB signaling module: Temporal control and selective gene activation. Science. 2002;298:1241-5.
160. Romanello M, Padoan M, Franco L, Veronesi V, Moro L, D'Andrea P. Extracellular NAD+ induces calcium signaling and apoptosis in human osteoblastic cells. Biochemical and Biophysical Research Communications. 2001;285(5):1226-31.
161. Looms DK, Tritsaris K, Nauntofte B, Dissing S. Nitric oxide and cGMP activate Ca2+-release processes in rat parotid acinar cells. BiochemJ. 2001;355(Pt 1):87-95.
162. Zamora R, Vodovotz Y. Transforming Growth Factor-β in Critical Illness. Crit Care Med. 2005;33:S478-S81.
163. Barcellos-Hoff MH, Ehrhart EJ, Kalia M, Jirtle R, Flanders K, Tsang ML-S. Immunohistochemical detection of active transforming growth factor-β *in situ* using engineered tissue. AmJPathol. 1995;147:1228-37.
164. Ehrhart EJ, Carroll A, Segarini P, Tsang ML-S, Barcellos-Hoff MH. Latent transforming growth factor-β activation *in situ*: Quantitative and functional evidence following low dose irradiation. FASEB J. 1997;11:991-1002.
165. Nathan C, Sporn M. Cytokines in context. JCell Biol. 1991;113:981-.